

NORTHWESTERN UNIVERSITY

Synaptic Dysfunction Mediated by Mutant LRRK2 in Parkinson's Disease Pathogenesis

A DISSERTATION

SUBMITTED TO THE GRADUATE SCHOOL  
IN PARTIAL FULFILLMENT OF THE REQUIREMENTS

for the degree

DOCTOR OF PHILOSOPHY

Field of

Northwestern University Interdepartmental Neuroscience Program (NUIN)

By

Maria Bac Ai Nguyen

EVANSTON, ILLINOIS

March 2019

© Copyright by Maria Bac Ai Nguyen 2018

All Rights Reserved

## ABSTRACT

Identifying key molecular mechanisms and targets for therapeutic development in sporadic neurodegenerative diseases has been challenging. Therefore, in-depth investigation of genetic forms of disease can provide valuable insight into pathogenic disease mechanisms. The discovery of genetic forms of Parkinson's disease (PD) has highlighted the importance of the autophagy/lysosomal and mitochondrial/oxidative stress pathways in disease pathogenesis. However, recently identified PD-linked and risk genes, including *DNAJC6* (auxilin), *SYNJ1* (synaptojanin 1), and *SH3GL2* (endophilin A1), have also highlighted disruptions in synaptic vesicle endocytosis as a significant contributor to disease pathogenesis. Additionally, the roles of other PD genes such as *LRRK2*, *PRKN* (parkin), and *VPS35* in the regulation of synaptic vesicle endocytosis are beginning to emerge. Here, we will discuss the recent work on the contribution of dysfunctional synaptic vesicle endocytosis to midbrain dopaminergic neurons' selective vulnerability and highlight pathways that mediate the interplay between mitochondrial, lysosomal, and synaptic dysfunction in the pathogenesis of PD.

Although defects in synaptic vesicle endocytosis have implicated synaptic dysfunction in PD pathogenesis, how synaptic dysfunction contributes to the vulnerability of human dopaminergic neurons has not been previously explored. We demonstrate that the commonly mutated, PD-linked leucine-rich repeat kinase 2 (*LRRK2*) mediates the phosphorylation of auxilin in its clathrin-binding domain at position Ser627. Kinase activity-dependent *LRRK2* phosphorylation of auxilin led to differential auxilin binding to clathrin resulting in disrupted synaptic vesicle endocytosis and decreased synaptic vesicle density in *LRRK2* patient-derived dopaminergic neurons. Moreover, impaired synaptic vesicle endocytosis contributed to the accumulation of oxidized dopamine that in turn mediated pathogenic effects such as decreased

glucocerebrosidase activity and increased  $\alpha$ Synuclein levels in mutant LRRK2 neurons. Importantly, these pathogenic phenotypes were partially attenuated by restoring wild-type auxilin function in mutant LRRK2 dopaminergic neurons. Together, this work suggests that mutant LRRK2 disrupts synaptic vesicle endocytosis leading to altered dopamine metabolism and dopamine-mediated toxic effects in patient-derived dopaminergic neurons and highlights the importance of synaptic dysfunction in the pathogenesis of Parkinson's disease.

## ACKNOWLEDGEMENTS

I have been truly blessed to undertake my graduate student training with Dr. Dimitri Krainc whose unyielding support and constructive advising have challenged me not just as a scientist but as a person. In him, I have found a lasting mentorship that will survive well beyond my time in his lab. This work would not have been possible without the support of past and current members of the Krainc lab who have trained me rigorously in new scientific techniques and thoughtfully discuss my hypotheses and data. I am especially grateful for Dr. Yvette C. Wong and Dr. Daniel Ysselstein who mentored me during my final years in graduate school. Their patience and useful advice have helped me both scientifically and professionally. I am also thankful to Drs. Lena Burbulla, Myung Jong Kim, Katarina Trajkovic, Pingping Song, Michael Schwake, Judith Blanz, and Hyunkyung Jeong for their helpful technical advice and guidance throughout my laboratory work. Dr. Jeffrey N. Savas and Dr. Joseph Mazzulli have guided me through specific data analyses in later stages of my project. Thank you to my fellow graduate student, Clarissa Valdez-Bhanvadia, for going through this challenging journey by my side.

I am especially thankful for my thesis committee members, Dr. Richard J. Miller, Dr. D. James Surmeier, and Dr. Gabriela Caraveo-Piso, who have all been extremely helpful in facilitating conversations to guide my thesis work and future career goals.

Lastly, heartfelt thanks to my loving parents, Rose Hong Van and Joseph Tai Ty Nguyen, family, and friends for their endless love and support in my pursuit of higher education.

This work was supported by 2T32AG020506 (to M.N.) and National Institutes of Health grants

R01 NS076054 and R37 NS096241 (to D.K.).

**LIST OF ABBREVIATIONS**

215A	GSK2578215A
2IN1	LRRK2-in-1
4-MU	4-methylumbelliferyl $\beta$ -glucopyranoside
ANK	ankyrin
ANOVA	analysis of variance
AP-2	adaptor protein 2
$\alpha$ Syn	$\alpha$ Synuclein (protein)
ATP	adenosine triphosphate
BCA	bicinchoninic acid (assay)
BSA	bovine serum albumin
CBE	conduritol B epoxide
CCV	clathrin-coated vesicle
cDNA	complementary deoxyribonucleotide
CLTC HC	clathrin heavy-chain
COR	C-terminal of Ras
DA	dopamine
DeltaCN	normalized difference in cross-correlation scores
DMEM	Dulbecco's Modified Eagle's Medium
DMSO	dimethyl sulfoxide
DNA	deoxyribonucleotide
<i>DNAJC6</i>	auxilin

DOC	deoxycholate
DOPAC	3,4-dihydroxy-phenylacetic acid
EDTA	ethylene diamine tetraacetic acid
EGFR	epidermal growth factor receptor
EGTA	ethylene glycol tetraacetic acid
FBS	fetal bovine serum
FDR	false discovery rates
<i>GAK</i>	cyclin-G associated kinase
<i>GBAI</i>	glucocerebrosidase (gene)
GAPDH	glyceraldehyde 3-phosphate dehydrogenase
GCase	glucocerebrosidase (protein)
GDP	guanosine diphosphate
GTP	guanosine triphosphate
GWAS	genome-wide association studies
HBSS	Hank's balanced salt solution
HEK	human embryonic kidney (cells)
HEPES	N-2-hydroxyethylpiperazine-N'-2-ethanesulfonic acid
HRP	horseradish peroxidase
iPSC	induced pluripotent stem cells
LRR	leucine-rich repeat
<i>LRKK2</i>	leucine-rich repeat kinase 2
MAO	monoamine oxidase
MCU	mitochondrial calcium uniporter
MOI	multiplicity of infection

mRNA	messenger ribonucleic acid
MS	mass spectrometry
NAc	nucleus accumbens
nIRF	near infrared fluorescence
PBS	phosphate buffered saline
PD	Parkinson's disease
p.p.m.	parts per million
<i>PRKN</i>	parkin
PSM	peptide/spectrum matches
PTEN	phosphatase and tensin
PVDF	polyvinylidene fluoride
Rab	Ras-associated binding (protein)
RIPA	radioimmunoprecipitation (lysis buffer)
ROC	Ras of Complex
ROS	reactive oxygen species
RPM	revolutions per minute
SDS	sodium didocyl sulfate
SDS-PAGE	sodium dodecyl sulfate polyacrylamide gel electrophoresis
SEM	standard error mean
<i>SH3GL2</i>	endophilin A1
shRNA	short hairpin ribonucleic acid
SNc	substantia nigra pars compacta
<i>SNCA</i>	$\alpha$ Synuclein (gene)
SNP	single nucleotide polymorphism

SVE	synaptic vesicle endocytosis
<i>SYNJI</i>	synaptojanin 1
TBST	Tris-buffered saline, with Tween
TCA	trichloroacetic acid
TEM	transmission electron microscopy
TH	tyrosine hydroxylase
vATPase	vacuolar ATPase
<i>VPS35</i>	vacuolar protein sorting-associated protein 35
VTA	ventral tegmental area
WT	wild-type
Xcorr	cross-correlation score

**DEDICATION**

To my grandparents,

Daminh Nguyen Van Ky and Joseph Pham Ngoc Khanh

Maria Do Thi Mau and Theresa Nguyen Thi Ngoc

## TABLE OF CONTENTS

ABSTRACT.....	3
ACKNOWLEDGEMENTS.....	5
LIST OF ABBREVIATIONS.....	6
ILLUSTRATIONS .....	12
TABLES .....	14
 CHAPTERS	
1. Chapter 1. Introduction .....	15
2. Chapter 2. LRRK2 phosphorylation of auxilin alters its function.....	29
Summary	
Methods	
Results	
Conclusions	
3. Chapter 3. Synaptic dysfunction in LRRK2 patient-derived neurons .....	52
Summary	
Methods	
Results	
Conclusions	
4. Chapter 4. Discussion .....	77
REFERENCES .....	86
CIRRICULUM VITAE .....	102

## ILLUSTRATIONS

<b>Figure 1.</b> Recently identified Parkinson’s disease genes play a role in synaptic vesicle endocytosis .....	20
<b>Figure 2.</b> Schematic diagram of leucine-rich repeat kinase 2 (LRRK2) domains .....	23
<b>Figure 3.</b> LRRK2 and auxilin colocalize in the presynaptic compartment.....	39
<b>Figure 4.</b> LRRK2 phosphorylates auxilin in its clathrin-binding domain at Ser627 .....	41
<b>Figure 5.</b> Mutant LRRK2 overexpression increases auxilin phosphorylation state.....	42
<b>Figure 6.</b> LRRK2 mediates phosphorylation of auxilin at Ser627.....	43
<b>Figure 7.</b> LRRK2 mediated regulation of auxilin alters its association with clathrin.....	47
<b>Figure 8.</b> Functional analyses of additional LRRK2-mediated phosphosites.....	49
<b>Figure 9.</b> Pluripotency marker expression in healthy controls and mutant LRRK2 induced pluripotent stem cells.....	61
<b>Figure 10.</b> G-band karyotyping analysis and Sanger sequencing results for reprogrammed cell lines.....	62
<b>Figure 11.</b> Dopaminergic neurons from patients with LRRK2-linked PD exhibit decreased levels of SVE proteins .....	64
<b>Figure 12.</b> Synaptic abnormalities in mutant LRRK2 dopaminergic neurons.....	65
<b>Figure 13.</b> LRRK2 R1441C/G dopaminergic neurons display increased levels of oxidized DA, $\alpha$ Syn accumulation, and decreased GCase activity.....	67
<b>Figure 14.</b> Tyrosine hydroxylase levels from iPSC-derived dopaminergic neurons .....	68
<b>Figure 15.</b> LRRK2 G2019S dopaminergic neurons display increased levels of oxidized DA, $\alpha$ Syn accumulation, and decreased GCase activity.....	68

<b>Figure 16.</b> Overexpression of phosphomutant auxilin does not attenuate increased oxidized DA levels in mutant LRRK2 neurons .....	70
<b>Figure 17.</b> Overexpression of wild-type auxilin reduces oxidized DA and attenuates downstream phenotypes in mutant LRRK2 neurons.....	71
<b>Figure 18.</b> Synaptic protein expression following wild-type auxilin transduction in human dopaminergic neurons .....	72
<b>Figure 19.</b> Lentiviral shRNA-mediated auxilin knockdown leads to the accumulation of oxidized DA in control dopaminergic neurons .....	73
<b>Figure 20.</b> Summary diagram highlighting LRRK2's involvement in synaptic dysfunction and Parkinson's disease pathogenesis .....	75
<b>Figure 21.</b> Deficits in synaptic vesicle endocytosis potentially mediate dopaminergic neurodegeneration through intersections with mitochondrial and lysosomal dysfunction .....	82

**TABLES**

<b>Table 1.</b> Additional mass spectrometry information on peptide coverage and spectral counts .....	46
<b>Table 2.</b> Additional mass spectrometry information on spectra count for auxilin Ser627 phosphosite .....	46

## CHAPTER 1.

### INTRODUCTION

#### *Parkinson's disease (PD)*

It is estimated that over 10 million people worldwide live with Parkinson's disease (PD) (Tysnes & Storstein, 2017). In the United States alone, about 1 million people are afflicted, making it the second most common neurodegenerative disease affecting the aging population (Marras et al., 2018). PD is characterized by the loss of A9 midbrain dopaminergic neurons in the substantia nigra pars compacta (SNc) and the appearance of  $\alpha$ Synuclein ( $\alpha$ Syn) inclusions termed Lewy bodies throughout the brain (Tysnes & Storstein, 2017). A9 midbrain dopaminergic neurons are distinct from other dopaminergic neuronal subtypes, such as those located in the ventral tegmental area (VTA) and nucleus accumbens (NAc), in that they produce large amounts of neuromelanin, a dark polymer pigment, and a key pathological marker of PD is the loss of black pigmentation in the SNc (Fedorow et al., 2005). Dopaminergic neurons of the SNc play an important role in the regulation of voluntary movements and degeneration of these neurons leads to the development of cardinal motor symptoms of PD, including resting tremors, slowed movement (bradykinesia), and rigidity (Tysnes & Storstein, 2017).

The discovery of genetic forms of PD has highlighted the importance of the autophagy/lysosomal and mitochondrial/oxidative stress pathways in disease pathogenesis. In addition, recently identified PD-linked and risk genes, including *DNAJC6* (auxilin), *SYNJ1* (synaptojanin 1), and *SH3GL2* (endophilin A1), have also highlighted disruptions in synaptic vesicle endocytosis as a significant contributor to disease pathogenesis. However, how these pathways converge in PD pathogenesis remains to be explored.

### ***Genetics of Parkinson's disease***

*SNCA*, encoding  $\alpha$ Synuclein ( $\alpha$ Syn), was the first gene to be discovered and linked to PD through autosomal dominant inheritance (Byers et al., 2011; Chartier-Harlin et al., 2004; Polymeropoulos et al., 1997). Mutations in or multiplication of *SNCA* led to aberrant protein function and several studies have shown that  $\alpha$ Syn accumulation negatively affects several cellular pathways, including vesicle trafficking, lysosomal, and mitochondrial function (Cooper et al., 2006; Devi, Raghavendran, Prabhu, Avadhani, & Anandatheerthavarada, 2008; Mazzulli et al., 2011). Mutations in *PRKN* (parkin) are the most common among autosomal recessive PD (Kitada et al., 1998). Parkin has E3 ubiquitin ligase activity and plays a role in maintaining mitochondrial integrity along with *PINK1* (Y. Chen & Dorn, 2013; Narendra et al., 2010; Yoshii, Kishi, Ishihara, & Mizushima, 2011). PINK1 is located across both inner and outer mitochondrial membranes and interacts with parkin to mediate autophagy of damaged mitochondria (Y. Chen & Dorn, 2013; Narendra et al., 2010), otherwise known as mitophagy. Mutations in PINK1 or parkin impair the clearance of dysfunctional mitochondria leading to the accumulation of reactive oxygen species (ROS) and cellular oxidative stress (Barodia, Creed, & Goldberg, 2017; Blesa, Trigo-Damas, Quiroga-Varela, & Jackson-Lewis, 2015; Wang, Nartiss, Steipe, McQuibban, & Kim, 2012; B. Xiao et al., 2017). In response to increased oxidative stress, DJ-1, a mainly cytosolic redox sensor with antioxidant function, translocates to mitochondria where it may act in parallel with the PINK1/parkin pathway to induce mitophagy (Thomas et al., 2011), although the exact mechanism is still unknown. Loss of function mutations in *DJ-1* cause early-onset PD and increased fragmented mitochondria have been reported in DJ-1 mutant models (McCoy & Cookson, 2011; X. Wang et al., 2012). Altogether, there is strong genetic evidence implicating loss of mitochondrial function, decreased clearance of damaged mitochondria through mitophagy, as well

as an accumulation of reactive oxygen species (ROS) leading to oxidative stress as cellular mechanisms that go awry in PD.

Mutations in *ATP13A2* result in Kufor-Rakeb syndrome, an early-onset form of PD along with dementia (Crosiers et al., 2011; Di Fonzo et al., 2007). *ATP13A2* gives rise to a lysosomal P-type ATPase that belongs to a family of transporters (van Veen et al., 2014). Although its substrates are still being identified, studies suggest that ATP13A2 transport function is necessary for maintaining lysosomal function (Tsunemi & Krainc, 2014). Loss of ATP13A2 function results in decreased lysosomal degradative capacity that is attenuated with overexpression of the protein (Dehay et al., 2012; Tsunemi & Krainc, 2014). *GBA1*, which encodes the lysosomal hydrolase, glucocerebrosidase (GCase), is the most common risk factor for PD (Crosiers et al., 2016; Goker-Alpan et al., 2006; Hernandez, Reed, & Singleton, 2016). Reduced GCase activity was also shown to be involved in conjunction with accumulated  $\alpha$ Syn in a toxic positive feedback loop that further impaired lysosomal function (Mazzulli et al., 2011). Moreover, *SCARB2* was also identified as a susceptibility factor in PD development and this gene encodes the lysosomal membrane protein, LIMP2, which is responsible for trafficking GCase to the lysosome (Alcalay et al., 2016; Do et al., 2011; Hopfner et al., 2013; Rothaug et al., 2014). Taken together, aberrations in these genes have highlighted the role of lysosomal dysfunction in the development of PD.

The collective identification of several genetic forms and risk factors of PD has strongly implicated mitochondrial and lysosomal dysfunction as key cellular processes that are involved in PD pathogenesis. In addition, multiple PD-linked genes involved in synaptic vesicle endocytosis (SVE) have recently been identified. These include mutations in *DNAJC6* (auxilin) and *SYNJ1* (synaptojanin 1) which were initially described in atypical parkinsonism patients (Edvardson et al., 2012; Kirola, Behari, Shishir, & Thelma, 2016; Koroglu, Baysal, Cetinkaya, Karasoy, & Tolun, 2013; Krebs et al., 2013; Olgiati et al., 2014; Olgiati et al., 2016; Quadri et al., 2013).

Homozygosity mapping of two patients with juvenile parkinsonism revealed a deleterious splice site mutation c.801-2, A>G in *DNAJC6* which led to a significant decrease in mRNA levels (Edvardson et al., 2012). A separate study found a patient with a *DNAJC6* homozygous truncating mutation, Q734X, leading to ~20% loss of the C-terminus including its functional J-domain responsible for binding its interaction partner hsc70 (Koroglu et al., 2013). Thus far, these mutations have linked *DNAJC6* to juvenile cases of atypical parkinsonism. However, recent investigations reported additional *DNAJC6* mutations, R927G and T741T, linked to early-onset PD cases (Olgiati et al., 2016). These mutations resulted in lowered auxilin expression and were predicted to decrease its overall function (Olgiati et al., 2016).

In addition, R258Q and R459P mutations in *SYNJ1* were recently reported in several independent studies to be associated with juvenile or early-onset PD (Kirola et al., 2016; Krebs et al., 2013; Olgiati et al., 2014; Quadri et al., 2013). These mutations are located in the Sac1 domain of synaptojanin 1 and impair its phosphatase activity (Kirola et al., 2016; Krebs et al., 2013). Interestingly, synaptojanin 1 haploinsufficiency led to delayed SVE in mouse midbrain dopaminergic but not cortical neurons suggesting that loss of synaptojanin 1 function could, in part, contribute to dopaminergic neuron vulnerability in PD pathogenesis (Pan et al., 2017). Lastly, *SH3GL2* (endophilin A1) was identified in a PD risk locus of a large-scale genome-wide association study (GWAS) meta-analysis, linking yet another gene involved in SVE regulation to PD (Chang et al., 2017). Collectively, these synaptic endocytic genes implicate defective SVE as a contributor to degeneration of midbrain dopaminergic neurons in patients.

### ***Synaptic dysfunction in Parkinson's disease***

Synaptic vesicle endocytosis (SVE) is the regeneration of synaptic vesicles from the plasma membrane following neurotransmission (Saheki & De Camilli, 2012). SVE begins with

the recruitment of clathrin by adaptor proteins such as adaptor protein 2 (AP-2) to the cytoplasmic surface of the plasma membrane (Cousin & Robinson, 2001; Cremona et al., 1999; Saheki & De Camilli, 2012). This adaptor protein regulates cargo sorting to ensure that the proper proteins are internalized along with the vesicle. Next, membrane benders such as endophilin A1 insert into the plasma membrane through the BAR domain and begin to mold and direct the invagination of the nascently forming vesicle (**Figure 1**) (Pechstein et al., 2015; Saheki & De Camilli, 2012). As the vesicle takes on a round and uniform shape, endophilin A1 subsequently interacts with dynamin and recruits synaptojanin 1 to the membrane interface (Hill, van Der Kaay, Downes, & Smythe, 2001; Milosevic et al., 2011; Saheki & De Camilli, 2012; Schuske et al., 2003; W. Song & Zinsmaier, 2003; Sundborger et al., 2011; Verstreken et al., 2003). Through its GTPase activity, dynamin stimulates the fission of the CCV from the plasma membrane (Ferguson et al., 2007). Once the CCV is free, synaptojanin 1 uses its phosphatase function to dephosphorylate membrane lipids (Krebs et al., 2013; Saheki & De Camilli, 2012). These dephosphorylation events release AP-2 and allow auxilin to bind the CCV through its PTEN-like and clathrin-binding domains (Guan, Dai, Harrison, & Kirchhausen, 2010; Rapoport, Boll, Yu, Bocking, & Kirchhausen, 2008; Saheki & De Camilli, 2012). Auxilin is a co-factor for hsc70 and its J-domain is responsible for recruitment of the ATPase to stimulate clathrin-coat removal (Eisenberg & Greene, 2007; Greener et al., 2001; Ma et al., 2002; Saheki & De Camilli, 2012). Once the CCV is uncoated, the nascent vesicle is then packaged with neurotransmitters and quickly transported to different synaptic vesicle pools in anticipation of the next neuronal stimulation.

Other modes for synaptic vesicle retrieval have also been well-described including kiss-and-run and several variations of bulk endocytosis such as ultrafast and activity-dependent bulk endocytosis (Cousin, 2017; Milosevic, 2018; Saheki & De Camilli, 2012). These mechanisms are initially clathrin-independent and happen on a much faster timescale and have also been found to

be regulated by proteins like dynamin, endophilin A1, and synaptojanin 1 (Watanabe et al., 2018; Y. Wu et al., 2014).

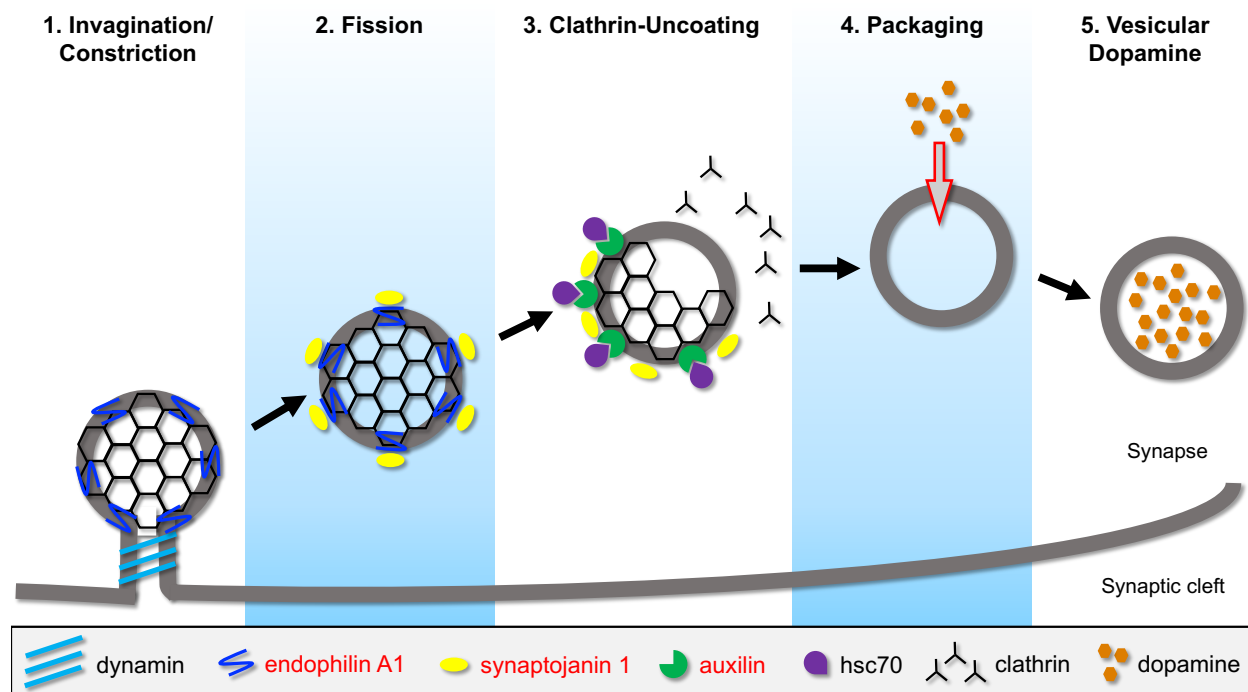


**Figure 1. Recently identified Parkinson's disease genes play a role in synaptic vesicle endocytosis.** The regeneration of synaptic vesicles following neurotransmission involves the concerted effort of different synaptic proteins recently linked to or identified as a risk factor for Parkinson's disease (indicated in red in the figure legend) **1. Invagination/Constriction:** Following the recruitment of adaptor and clathrin-coat proteins to the plasma membrane, endophilin A1 regulates the curvature of the emerging vesicle. Endophilin A1 is also responsible for recruitment of dynamin to the neck of the clathrin-coated vesicle (CCV). **2. Fission:** Dynamin then constricts the neck and mediates CCV fission from the plasma membrane. Endophilin A1 also recruits synaptojanin 1, whose phosphatase activity dephosphorylates synaptic vesicle membrane lipids to release adaptor proteins allowing auxilin to bind to the CCV. **3. Clathrin-Uncoating:** Auxilin is a cofactor for hsc70, which simulates the removal of the clathrin-coat through its ATPase activity. **4. Packaging:** Once the clathrin-coat is fully removed, dopamine can now be packaged into the nascent vesicle. **5. Vesicular Dopamine:** Dopamine sequestration inside the vesicle prevents it from becoming elevated and oxidized in the cytosol.

Animal knockout mouse models of *DNAJC6*, *SYNJ1*, and *SH3GL2* have all exhibited endocytic defects at the synapse, highlighting the importance of proper SVE control in maintaining axon terminal integrity (Cao, Milosevic, Giovedi, & De Camilli, 2014; Kim et al., 2002; Milosevic et al., 2011; Yim et al., 2010). It was previously reported that the presynaptic compartment of auxilin knockout mice displayed characteristics of defective SVE including reduced synaptic

vesicle density and increased CCVs and membraneless clathrin cages (Hirst et al., 2008; Yim et al., 2010). Interestingly, follow-up studies found that embryonic mouse lethality resulting from genetic ablation of both *GAK*, an auxilin homolog and PD risk gene, and *DNAJC6* could be rescued by overexpression of the GAK C-terminal fragment carrying both the clathrin-binding and J domains (Park et al., 2015). Although GAK and auxilin have redundant clathrin-uncoating actions in the cell, this data suggests that GAK overexpression can potentially mitigate auxilin dysfunction in PD. Furthermore, lack of auxilin in *Drosophila* led to specific age-related locomotor deficits and accelerated  $\alpha$ Syn-mediated dopaminergic neuron loss in this model (L. Song et al., 2017). This result implies that nigral neurons are more sensitive to loss of auxilin function. Consistent with previous reports, the synapses of *SYNJI* R258Q knock-in mice revealed drastic endocytic defects and higher levels of endocytic intermediates such as CCVs (Cao et al., 2017). Additionally, dystrophic axon terminals were observed in the dorsal striatum of these mice which is the site of SNc dopaminergic neuron projections in the brain (Cao et al., 2017). Moreover, auxilin and parkin (*PRKN*), protein levels were reported to be elevated in synaptotagmin 1 mutant mice (Cao et al., 2017). Endophilin A1 knockout mouse models also exhibited elevated parkin levels, as well as accumulated CCVs, highlighting a potential functional connection between these SVE proteins and parkin (Cao et al., 2014).

The regeneration of synaptic vesicles through SVE is essential to sustain neurotransmission and is therefore a highly regulated process. SVE is controlled by a large group of structurally distinct proteins termed dephosphins, which are regulated through phosphorylation–dephosphorylation events (Cousin & Robinson, 2001). Under basal conditions, SVE proteins are constitutively phosphorylated, which inhibits them from associating with other proteins in the endocytic pathway (Cousin & Robinson, 2001). When the neuron is stimulated,  $\text{Ca}^{2+}$  influx activates the  $\text{Ca}^{2+}$ -dependent calcineurin activity, which rapidly dephosphorylates endocytic

proteins to enable their interaction and recruitment to endocytic sites (Cottrell et al., 2016; Cousin & Robinson, 2001; X. S. Wu et al., 2014). SVE protein inactivation through rephosphorylation occurs on a much slower timescale in a stepwise progression. This process has been shown to be mediated in part by Cdk5 and Minibrain kinase (C. K. Chen et al., 2014; Lee, Wenk, Kim, Nairn, & De Camilli, 2004; Tan et al., 2003). However, there remains a significant gap in our knowledge of other possible protein kinases which are responsible for proper control of SVE. In this work, we explored the role of LRRK2 kinase in the regulation of synaptic function and its relevance in PD pathogenesis.

### ***Role of leucine-rich repeat kinase 2 (LRRK2) in Parkinson's disease pathogenesis***

In 2004, a familial mutation that presented as classical PD across four generations was successfully mapped to a locus on chromosome 12 (Funayama et al., 2002; Zimprich et al., 2004). This locus contained the coding sequence for leucine-rich repeat kinase 2 (LRRK2), a protein with both serine/threonine kinase and GTPase activity. On average, patients experienced disease onset in or near the fifth decade of life and Lewy body deposits could be observed upon autopsy of patient brains, indicating that mutations in LRRK2 led to classical PD phenotypes.

LRRK2 has a central catalytic core consisting of the Ras of Complex (ROC), C-terminal of ROC (COR), and kinase domains. The most common mutations, G2019S and R1441C/G/H, map to its kinase and GTPase domains, respectively (**Figure 2**). LRRK2 is unique in that patient carriers account for nearly 5% of all familial PD cases, and about 2% of sporadic cases (Di Fonzo et al., 2005; Gilks et al., 2005), the highest among any other gene described for PD. In some patient populations such as Ashkenazi Jews or North African Arabs, the incidence of PD development among LRRK2 mutation carriers is as high as 40% (Lesage et al., 2006; Ozelius et al., 2006). Furthermore, LRRK2 patients present with all classical phenotypes seen in sporadic patients,

making LRRK2 a relevant protein that could help to identify key cellular pathways that go awry in PD pathogenesis.

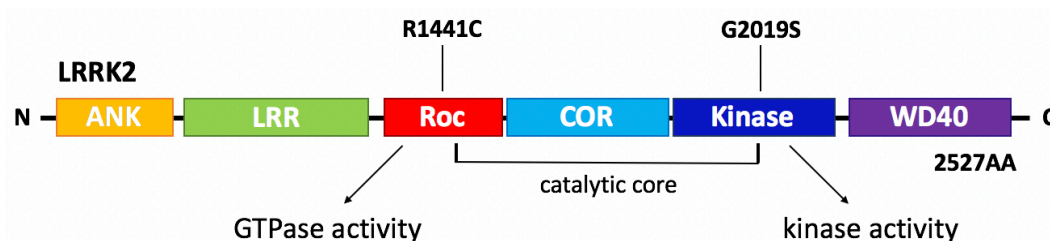


**Figure 2. Schematic diagram of leucine-rich repeat kinase 2 (LRRK2) domains.** LRRK2 is a large multi-domain protein that is about 280 kDa in size. It contains a central catalytic core comprised of the Ras of Complex (ROC), C-terminal of ROC (COR), and kinase domains. These domains are responsible for mediating the dual GTPase and kinase function of LRRK2. The most common pathogenic LRRK2 mutations G2019S and R1441C/G/H affect the kinase and GTPase domains, respectively. LRRK2 also contains the ankyrin (ANK), leucine-rich repeat (LRR), WD40 interaction domains which allow it to associate with a range of proteins.

LRRK2 is a large multi-domain protein which allows it to interact with and regulate many different proteins. The most common mutation, G2019S, is located within the binding pocket of the kinase domain (**Figure 2**) (Webber et al., 2011). Several functional studies have shown that this mutation leads to an increase in kinase activity (Greggio, 2012; Ray et al., 2014; Webber et al., 2011; West et al., 2007). The second most common mutation, R1441C/G/H, results in loss of ROC domain GTPase function by reducing GTP cycling and favoring its binding to GTP (**Figure 2**) (Lewis et al., 2007; West et al., 2007). Follow-up studies also showed that intact GTPase activity is necessary to regulate kinase activity and therefore mutations perturbing this function have recently been shown to increase kinase function, as well (Greggio, 2012; Steger et al., 2016; West et al., 2007). Interestingly, the R1441C/G/H mutation was also shown to lead to a higher occurrence of autophosphorylation mediated by its own kinase domain (Sheng et al., 2012; Webber et al., 2011). Taken together, these results implicate important cross regulatory events between the different catalytic domains of LRRK2. Aside from the central catalytic core, LRRK2 also has leucine-rich repeat (LRR), ankyrin (ANK), and WD40 domains (**Figure 2**), which mediate its

interaction with a wide-range of proteins. Based on the identified interaction partners of LRRK2 so far, roles for this protein have been described in vesicular trafficking, mitochondrial maintenance, and autophagy to the lysosome.

LRRK2 is mainly a cytosolic protein, but through its interaction domains, it can be localized to vesicular membranes (Biskup et al., 2006). A recent large-scale phosphoproteomics study on LRRK2 identified a small subset of Rab GTPases as substrates for LRRK2 kinase activity (Steger et al., 2016). Rab GTPases are the main regulators of vesicular trafficking to and from prominent cellular structures like the trans-Golgi network, endosomes, lysosomes, as well as the plasma membrane (Hutagalung & Novick, 2011). In addition, an independent study identified Rab5b as a LRRK2 substrate (Shin et al., 2008; Yun et al., 2015). This GTPase is localized to early endosomes where it mediates clathrin-mediated endocytosis and synaptic vesicle recycling in neurons (Shin et al., 2008).

In addition to Rab5b, LRRK2 has also been implicated in Rab7 function (Gomez-Suaga et al., 2014). LRRK2 mutants were shown to delay endosomal trafficking to the lysosome using the classical epidermal growth factor receptor (EGFR)-mediated degradative pathway assay (Gomez-Suaga et al., 2014). This study found that mutant LRRK2 regulation of Rab7 ultimately impaired its function and that deficits could be perturbed by overexpressing an active form of Rab7 (Gomez-Suaga et al., 2014). In addition, Rab7-dependent lysosome-mitochondria contacts were recently reported (Wong, Ysselstein, & Krainc, 2018), suggesting that LRRK2 may be further involved in regulating dynamic inter-organelle contacts. Both mitochondria and lysosomes have been previously linked to  $\text{Ca}^{2+}$  buffering in the cell which is important for maintaining A9 midbrain dopaminergic neurons pacemaking function (Guzman, Sanchez-Padilla, Chan, & Surmeier, 2009). Interestingly, LRRK2 mutant overexpression led to an increase in mitochondrial calcium uniporter (MCU) levels which resulted in increased  $\text{Ca}^{2+}$  flux into the mitochondria (Verma et al., 2017). As

high levels of  $\text{Ca}^{2+}$  store in mitochondria have been shown to lead to its impairment (Zaichick, McGrath, & Caraveo, 2017), this further implicates mutant LRRK2 in mitochondrial dysfunction.

While the discovery of mutations in *DNAJC6* and *SYNJ1* directly implicate synaptic dysfunction in PD pathogenesis, recent studies suggest that other PD genes including *LRRK2* and *VPS35* may also be potential regulators of SVE. Normal LRRK2 serine/threonine kinase activity is critical for proper SVE, as chemical inhibition of LRRK2 was shown to delay endocytosis (Arranz et al., 2015). In addition, LRRK2 mutant mice displayed an accumulation of CCVs and decreased synaptic vesicle density in dopaminergic terminals (Xiong et al., 2018). Many synaptic interacting partners and substrates have been described for LRRK2, but those specifically involved in SVE regulation have only recently been identified. Dynamin, which mediates the fission of CCVs from the plasma membrane, was identified as a LRRK2 interactor, highlighting a potential role for LRRK2 in the regulation of dynamin GTPase activity (Stafa et al., 2014). Moreover, LRRK2 was shown to phosphorylate endophilin A1 at positions T73 and S75 located in its BAR domain (Matta et al., 2012). Subsequent investigations confirmed that LRRK2-mediated phosphorylation of endophilin A1 at S75 acted as a critical switch in mediating endophilin A1 function at the synapse (Ambroso, Hegde, & Langen, 2014). Recent synaptic proteomic analysis of *LRRK2* mutant knock-in *Drosophila* models have also identified synaptojanin 1 as a LRRK2 kinase substrate (Islam et al., 2016). LRRK2 phosphorylates synaptojanin 1 at positions T1131 and T1205 located in its proline-rich sequence recognition domain resulting in defective synaptojanin 1–endophilin A1 interaction (Islam et al., 2016; Pan et al., 2017). Interestingly, another study found that phosphorylation of synaptojanin 1 at S1029 mediates the regeneration of distinct synaptic vesicle pools, suggesting that phosphorylation–dephosphorylation events of different residues can result in protein involvement in separate parts of SVE (Geng, Wang, Lee, Chen, & Chang, 2016). Importantly, we recently identified auxilin as a novel substrate for LRRK2

kinase activity in iPSC-derived dopaminergic neurons (Nguyen & Krainc, 2018). We found that S627, located in auxilin's clathrin-binding domain, is a LRRK2-mediated phosphorylation site and that dephosphorylation of this site led to increased auxilin association with clathrin (Nguyen & Krainc, 2018). Thus, LRRK2 kinase activity regulates several aspects of SVE, which could be exacerbated by LRRK2 disease-linked mutations, leading to downstream toxic effects that contribute to the degeneration of dopaminergic neurons.

LRRK2 has also been functionally linked to *VPS35*, a PD-linked gene that encodes a major component of the retromer complex involved in the recycling of proteins from the endosome/lysosome to the trans-Golgi network and from the endosome to the plasma membrane (Burd & Cullen, 2014; Follett et al., 2014). PD-associated mutations in *VPS35*, which display decreased function, functionally elevate wild-type LRRK2 kinase activity (Mir et al., 2018). Additionally, loss of the *Drosophila* homolog *VPS35* leads to deficits in synaptic vesicle recycling involving LRRK2 which could be rescued upon *VPS35* or LRRK2 overexpression (Inoshita et al., 2017). Taken together, these studies reveal the existence of multiple layers of SVE regulation modulated by PD-linked genes previously implicated in mitochondrial and lysosomal dysfunction. These studies also suggest that the more common PD-linked gene, LRRK2, may mediate the convergence of these dysfunctional pathways in the process of neurodegeneration.

## Conclusions

In-depth investigation of genes linked to PD provides valuable mechanistic insight into pathogenesis for therapeutic development. In particular, recently identified mutations in *DNAJC6* (auxilin) and *SYNJ1* (synaptojanin 1) in patients with juvenile and early-onset atypical parkinsonism further strengthened the importance of synaptic dysfunction in PD pathogenesis (Edvardson et al., 2012; Kirola et al., 2016; Koroglu et al., 2013; Krebs et al., 2013; Olgiati et al.,

2016; Quadri et al., 2013), as both genes are involved in clathrin-dependent synaptic vesicle endocytosis which replenishes synaptic vesicles following neuronal activity. Moreover, LRRK2, the most commonly mutated protein in familial and sporadic PD, has also been implicated in synaptic function (Biskup et al., 2006; Di Fonzo et al., 2005; Gilks et al., 2005). Pathogenic PD-linked mutations in LRRK2, R1441C/H/G and G2019S, perturb its kinase activity which is important for SVE and neurotransmission (Arranz et al., 2015; Henry et al., 2015; Hinkle et al., 2012; Tong et al., 2009; Webber et al., 2011; West et al., 2007), and several SVE proteins including synaptojanin 1 and endophilin A1 are LRRK2 kinase substrates (Ambroso et al., 2014; Islam et al., 2016; Matta et al., 2012; Pan et al., 2017), suggesting that LRRK2 globally regulates SVE via its kinase activity.

Synaptic vesicle pools can be regenerated at the axon terminal through clathrin-mediated SVE, a process tightly controlled by phospho-regulated proteins (Cousin & Robinson, 2001; Saheki & De Camilli, 2012). This pathway initiates when clathrin is recruited to the plasma membrane via AP-2 (**Figure 1**). A new clathrin-coated vesicle then invaginates from the plasma membrane through the concerted effort of endophilin A1 and synaptojanin 1 and is subsequently cleaved off by dynamin 1. Following fission, auxilin binds and recruits hsc70 to remove the clathrin lattice thereby producing a synaptic vesicle that can be packaged with neurotransmitters. Importantly, loss of individual SVE proteins leads to similar synaptic defects, including increased retention of clathrin-coated vesicles and decreased synaptic vesicle density (Cao et al., 2014; Ferguson et al., 2007; Kim et al., 2002; Milosevic et al., 2011; Yim et al., 2010). We hypothesized that defective SVE in SNc dopaminergic neurons could ultimately lead to increased cytosolic dopamine (DA) due to inefficient DA packaging, which can be rapidly oxidized to drive downstream toxic effects and subsequent nigrostriatal neurodegeneration (Lotharius & Brundin,

2002). Previously, we have shown that one consequence of increased oxidized DA is the accumulation of  $\alpha$ Syn, a major component of Lewy bodies in PD (Burbulla et al., 2017).

However, the connection between synaptic dysfunction and DA-mediated toxic effects has not been previously examined in patient-derived dopaminergic neurons. In this study, we demonstrated that LRRK2 and auxilin interact and that LRRK2 kinase activity mediates auxilin phosphorylation in its clathrin-binding domain at Ser627 to regulate auxilin's binding to clathrin during SVE (Nguyen & Krainc, 2018), suggesting that LRRK2 and auxilin functionally interact in mediating synaptic dysregulation in dopaminergic neurons. As mutant LRRK2 has also been previously linked to mitochondrial and lysosomal dysregulation (Gomez-Suaga et al., 2014; Verma et al., 2017), our studies further suggest that LRRK2 may mediate the convergence of these pathways in PD pathogenesis.

## CHAPTER 2.

### LRRK2 PHOSPHORYLATION OF AUXILIN ALTERS ITS FUNCTION

#### Summary

LRRK2 has been previously determined to be an important regulator of synaptic function through its localization and interaction with proteins involved in both endocytosis and exocytosis (Ambroso et al., 2014; Arranz et al., 2015; Belluzzi et al., 2016; Islam et al., 2016). However, the emergence of genome wide association study (GWAS) hits and familial, juvenile or early-onset Parkinson's disease (PD) cases have linked synaptic genes particularly involved in clathrin-mediated synaptic vesicle endocytosis (SVE) as important mediators of PD pathogenesis (Chang et al., 2017; Edvardson et al., 2012; Kirola et al., 2016; Koroglu et al., 2013; Krebs et al., 2013; Olgiati et al., 2014; Olgiati et al., 2016; Quadri et al., 2013). These genes *SH3GL2*, *SYNJ1*, and *DNAJC6* encode endophilin A1, synaptojanin 1, and auxilin, respectively. These synaptic proteins are heavily enriched in neurons and have distinct roles in SVE to regulate the budding and uncoating of the nascent vesicle from the plasma membrane following the release of neurotransmitters (**Figure 2**) (Saheki & De Camilli, 2012). Notably, both endophilin A1 and synaptojanin 1 were recently identified as LRRK2 phosphosubstrates (Ambroso et al., 2014; Islam et al., 2016; Matta et al., 2012; Pan et al., 2017), suggesting that LRRK2 kinase activity is heavily involved in this process. Previous studies showed that LRRK2-mediated phosphorylation of endophilin A1 or synaptojanin 1 altered their ability to interact with the lipid membrane and/or downstream SVE interactors, therefore negatively affecting their function in SVE (Ambroso et al., 2014; Pan et al., 2017). Furthermore, LRRK2 was linked to cyclin-G associated kinase (*GAK*)

which is a PD-risk gene and ~80% homologous to auxilin (Beilina et al., 2014; Lemmon, 2001), suggesting that LRRK2 might also interact with auxilin.

Here we confirm previous results indicating that LRRK2 is localized to the synapse (Biskup et al., 2006). Additionally, we identified a novel interaction between LRRK2 and the synaptic protein, auxilin (Nguyen & Krainc, 2018). We determine that LRRK2 phosphorylates auxilin at position Ser627, which is located in its clathrin-binding domain (Nguyen & Krainc, 2018). As auxilin is important for mediating the removal of the clathrin-coat by binding clathrin and recruiting hsc70, which is the ATPase that stimulates the removal of the clathrin-coat, we hypothesized that phosphoregulation of auxilin at position Ser627 would affect its clathrin-binding function. We show that LRRK2-mediated phosphorylation of auxilin leads to alterations in its association with clathrin but not its known binding partner, hsc70 (Nguyen & Krainc, 2018).

## Methods

Cell culture. HEK293 cells were cultured at 37°C and 5% CO<sub>2</sub> in Dulbecco's Modified Eagle Medium (DMEM) (Invitrogen, #11995-073) containing 10% heat-inactivated Fetal Bovine Serum (FBS) (Invitrogen, #16000-044) and 1X penicillin and streptomycin (Invitrogen, #15140-122). Cells were cultured and maintained up to 70% confluency before passaging. All culture passages were kept below P20. For experiments, cells were seeded at a density of 500K cells per well in a 6-well plate tissue culture-treated plate for transfections and immunoprecipitation experiments.

Plasmids and primers. The pDEST53-LRRK2-WT cDNA expression construct was obtained from Addgene (#25044) and the pLX304-DNAJC6-WT-V5 cDNA expression construct was obtained from Harvard PlasmID Database (#HsCD00414238). LRRK2 mutant constructs were generated using the Agilent site-directed mutagenesis kit (Fisher Scientific, #NC1220413), according to

manufacture protocols and further Sanger sequenced using the following Integrated DNA Technologies primers: LRRK2-WT-Flag For 5'-gatgatgataaagcccttatggctagtggc-3' and Rev 5'-atctttataatccatgaattcggagcctgctttttg-3', LRRK2 R1441C For 5'-cttggctcttcaatataaaggcttgcgcttctcttc-3' and Rev 5'-gaagaagaagcgaagcctttatattgaagagccaag-3', LRRK2 G2019S For 5'-caaagattgctgactacagcattgctcagtactgc-3' and Rev 5'-gcagtactgagcaatgctgtagtcagcaatctttg-3', LRRK2 K1906M For 5'-gaaggagaagaagtggctgtgatgattttaataaacatacatcac-3' and Rev 5'-gtgatgtatgtttataaaaatcatcacagccacttctctcttc-3', Auxilin S627A For 5'-cctccacctctgcggetccaaccctaaga-3' and Rev 5'-tcttagggttgagcccagaggtggagg-3', Auxilin S627D For 5'-cacctccacctctgcggatccaaccctaagagtg-3' and Rev 5'-cactcttagggttgatccgcagaggtggaggtg-3', Auxilin S49A For 5'-cagcggcgcgggctcccggccgac-3' and Rev 5'-gtcgggcgggagcccgcgcccgtg-3', Auxilin S49D For 5'-gcagcggcgcgggatcccggccgaca-3' and Rev 5'-tgtcgggcgggatcccgcgcccgtgc-3', Auxilin S59A For 5'-ccggaccgcgccaccatggacagc-3' and Rev 5'-gctgtccatggtggcggcgggtccgg-3', and Auxilin S59D For 5'-tccggaccgcgccacccatggacagct-3' and Rev 5'-agctgtccatggtgtcggcgcgggtccgga-3'. Sequencing primers for LRRK2 mRNA R1 5'-cgtgaacaccagcagatcctcc-3', F1 5'-atggctagtggcagctgtca-3', F2 5'-tgagagagtctcagaggagc-3', F3 5'-ccgcatgctgggcactaaat-3', F4 5'-ctggctctagcagctttgaa-3', F5 5'-gggagcagatgccaatcaagc-3', F6 5'-ccgagatgccgtattacagcg-3', F7 5'-cctgagaacctcactgatgtgg-3', F8 5'-ccctcctgagattggctgtc-3', F9 5'-gacgcagcagcattgtacc-3', F10 5'-cccagcactgcagttaagt-3', F11 5'-gggccaagtgtggaccaca-3', F12 5'-caggacaaagccagcctcac-3', F13 5'-atctggctgggctgtgggca-3', F14 5'-ggtggtagactgctctct-3'. Sequencing primers for DNAJC6 mRNA R1 5'-catgtcaaagagacctcccc-3', F1 5'-atgagcctctcgggagcta-3', F2 5'-attaggcaggctcccagctct-3', F3 5'-ttgaggtcaaccattgggag-3', F4 5'-ggctcctcccaccaattctg-3', F5 5'-agcaaacccaccacaccaac-3', F6 5'-actgggcaaccctatgaaca-3'.

Antibodies. For immunofluorescence: DNAJC6 (auxilin) 1:1000 (Sigma, #HPA031182), LRRK2 1:100 (Novus Biologicals, #NB300-268), synaptophysin 1:500 (EMD Millipore, #MAB5258). For Western Blot: DNAJC6 (auxilin) 1:1000 (ThermoFisher, #PA5-26981), clathrin heavy chain (2410) 1:1000 (Cell Signaling, #P1663),  $\beta$ -actin (AC-15) 1:5000 (Abcam, #ab6276), LRRK2 (MJFF 68-7) 1:1000 (Abcam, #ab181386), hsc70 (B-6) 1:2000 (Santa Cruz, #sc-7298), GAPDH (6C5) 1:5000 (EMD Millipore, #MAB374), pan-phosphoserine (16B4) 1:1000 (Santa Cruz, #sc-81514), and pan-phosphoserine 1:1000 (EMD Millipore, #AB1603).

Generation of protein lysates and SDS-PAGE/Western blotting. Cells were briefly washed with ice-cold 1X PBS and lysed using 1% Triton X-100 lysis buffer [1% Triton X-100, 10% glycerol, 1 mM EDTA, 150 mM NaCl, 50 mM HEPES, pH 7.4] + 1X cOmplete™ protease inhibitor cocktail (Sigma, #11836170001 Roche). Samples were incubated on ice for 30 minutes and vortexed briefly every 10 minutes to ensure full lysis of samples. Samples were then centrifuged at max RPM (~20,000 x g) for 20 minutes and the subsequent supernatant was used for immunoprecipitation experiments (see below) and then Western blot analysis, respectively. Boiled protein samples were separated on precasted 4-12% Tris-glycine, 4-20% Tris-glycine or 3-8% Tris-acetate gels (Invitrogen, #XP04120, #XP04205, #EA03752-5). Proteins were transferred to PVDF or nitrocellulose membranes using the semi-dry method with the Trans-blot® Turbo™ transfer system (Biorad). Following transfer, membranes were blocked with 5% milk in 1X Tris-buffered saline [50 mM Tris, pH 7.4, 150 mM NaCl] with 0.1% Tween (TBST) for 1 hour at room temperature. Membranes were subsequently washed 3X with 1X TBST for 5 minutes each and then immunoblotted overnight in primary antibody at 4°C, shaking. The following day, membranes were washed four times with 1X TBST for 5 minutes and incubated in secondary HRP

antibody (Jackson Laboratories) for 1 to 1.5 hours shaking at room temperature. Membranes were washed three times with 1X TBST for 10 minutes each with one additional wash step in water for 10 minutes. Membranes were then imaged using Clarity and femto chemiluminescence substrate (Biorad, #170-5061 and Thermo Fisher Scientific, #34095, respectively) on the ChemiDoc XRS+ imaging station (Biorad). Analysis and quantification of protein bands was done using Image Lab 5.0.

Immunofluorescence. Cells seeded on nitric acid treated, poly-D-lysine (Sigma, #P1149), and laminin coated (Invitrogen, #23017-015) coverslips were fixed using 3% paraformaldehyde in 1X PBS for 15 to 20 minutes at room temperature. Cells were then permeabilized using permeabilization buffer [10% FBS in 1X PBS + 0.1% fresh saponin] for 30 minutes at room temperature. Samples were then incubated in primary antibody diluted in permeabilization buffer either for 30 minutes at room temperature or overnight at 4°C. Coverslips were then washed three times with 1X PBS for 5 minutes each wash. Secondary antibodies corresponding to the primary antibodies were diluted in permeabilization buffer and added to the samples for 45 minutes to 2 hours at room temperature. Samples were washed three times with 1X PBS for 5 minutes each wash and then mounted onto Superfrost® Plus microscope slides (Fisherbrand, #12-550-15) using DAPI Fluoromount-G® (Southern Biotech, #0100-20). Samples were left at 4°C for at least 24 hours before imaging. Images were obtained on a Leica DMI4000B confocal microscope.

Immunoprecipitation. HEK293 cells (please refer to above for plating density) were transfected using Lipofectamine™ 2000 (Invitrogen, #11668-019), according to manufacture protocols at a lipid to DNA ratio of 1:3. 48 hours following transfection, cells were briefly washed with ice-cold

1X PBS, scraped and lysed using 1 ml of 1% Triton X-100 lysis buffer [1% Triton X-100, 10% glycerol, 1 mM EDTA, 150 mM NaCl, 50 mM HEPES, pH 7.4] + 1X cOmplete™ protease inhibitor cocktail (Sigma, #11836170001 Roche). Samples were incubated on ice for 30 minutes and vortexed briefly every 10 minutes to ensure full lysis of samples. Samples were then centrifuged at max RPM (~20,000 x g) for 20 minutes. The supernatant was added to prewashed anti-V5 agarose beads or anti-FLAG® M2 agarose beads (Sigma, #A7345 and #A4596, respectively). Protein lysate and beads were left to rotate overnight at 4°C. V5 or Flag-tagged agarose beads were briefly pelleted and washed with 1 mL of 1% Triton X-100 lysis buffer for 5 minutes rotating for a total of three times. Immunoprecipitated proteins were eluted from beads by adding equal volumes of 2X SDS sample buffer [125 mM Tris, pH 6.8, 15% glycerol, 4% SDS, 0.5 mM dithiothreitol, bromophenol blue] then subsequently boiled for 10 minutes at 95°C in preparation for SDS-PAGE and Western blotting analysis.

Preparation of samples for MS. HEK293 cells in 10 cm plates were cotransfected with Flag-tagged auxilin wild-type and corresponding LRRK2 wild-type or mutant R1441C or G2019S cDNA constructs using Lipofectamine for at least 48 hours, as stated previously according to the manufacturer's protocol. For the LRRK2 kinase inhibitor experiment, cells were transfected with Flag-tagged auxilin wild-type and either left untreated or were treated with DMSO or GSK2578215A at a final concentration of 2  $\mu$ M (Sigma, #SML0660). After 48 hours, cells were washed with 1X PBS and lysed in 1 mL of DOC lysis buffer [0.5% deoxycholic acid, 1% Triton X-100, 50 mM Tris, pH 7.4, 150 mM NaCl, 10 mM NaF, 1 mM EGTA, and 1 mM EDTA] + 1X cOmplete™ protease inhibitor cocktail. Auxilin was purified using prewashed Flag-tagged agarose beads, as described above. Proteins were eluted from the beads using dye-free sample buffer [62.5

$\mu\text{l}$  1M Tris-HCl, 200  $\mu\text{l}$  10% SDS, 687.5  $\mu\text{l}$  water, 50  $\mu\text{l}$   $\beta$ -mercapthoethanol] at 65°C for 10 minutes with short vortexing in-between. Proteins in suspension were diluted with 50 mM Tris, pH 6.8 and precipitated using 100% (w/v) trichloroacetic acid (TCA) overnight on ice at 4°C. Precipitated proteins were subsequently pelleted at 15,000 x RPM for 30 minutes. Ice-cold acetone was used to wash and fully dry the pellet for mass spectrometry processing.

Tandem mass spectrometry (MS). The precipitated protein pellets were initially solubilized in 100  $\mu\text{l}$  of 8 M urea for 30 minutes followed by the addition of 100  $\mu\text{l}$  of 0.2% ProteaseMAX (Promega) for 2 hours. All protein extracts were subsequently reduced and alkylated as previously described (E. I. Chen, McClatchy, Park, & Yates, 2008), followed with the addition of 300  $\mu\text{l}$  of 50 mM ammonium bicarbonate, 5  $\mu\text{l}$  1% ProteaseMAX and 0.5  $\mu\text{g}$  sequence-grade trypsin (Promega). Using a thermomixer at 37°C (Eppendorf), the samples were left to digest overnight. For Orbitrap Fusion Tribrid MS analysis, tryptic peptides were further purified using Pierce C18 spin columns (Thermo Scientific) and using a Thermo EASY nLC 1000 UPLC pump, 3  $\mu\text{g}$  of peptide was auto-sampler onto a vented Acclaim Pepmap 100, 75  $\mu\text{m}$   $\text{\AA}$ ~ 2 cm, nanoViper trap column coupled to a nanoViper analytical column (Thermo-164570, 3  $\mu\text{m}$ , 100  $\text{\AA}$ , C18, 0.075 mm, 500 mm) with a stainless steel emitter tip assembled on the Nanospray Flex Ion Source with a spray voltage of 2,000 V. For this protocol, Buffer A contained 94.785% H<sub>2</sub>O with 5% acetonitrile and 0.125% formic acid. Buffer B contained 99.875% acetonitrile with 0.125% formic acid. The chromatographic run was for a total of 4 hours under the following profile: 0–7% over 7 min, ramp to 10% over 6 min, ramp to 25% over 160 min, ramp to 33% over 40 min, ramp to 50% over 7 min, ramp to 95% for 5 min and stay at 95% for an additional 15 minutes. Some additional MS parameters include: ion transfer tube temperature to 300°C, Easy-IC internal mass calibration, default charge state set to 2, and cycle time set to 3 sec. The Detector type was set to Orbitrap with

60,000 resolution, with wide quad isolation, mass range set to normal, scan range set to 300–1,500 (m/z), max injection time set to 50 ms, AGC target set to 200,000, microscans set to 1, S-lens RF level set to 60, without source fragmentation, and data type set to positive and centroid. Monoisotopic precursor selection was set as on, including charge states equal to 2–6 (rejecting unassigned). Dynamic exclusion was enabled and set to 1 for 30 sec and 45 sec exclusion duration at 10 p.p.m. for high and low. Precursor selection decision was set to most intense, top 20, isolation window set to 1.6, scan range set to auto normal, first mass set to 110, collision energy set to 30%. The ion trap detector was used for CID, with ion trap resolution set to 30 K, ion trap scan rate set to rapid, maximum injection time set to 75 ms, AGC target set to 10,000, and Q set to 0.25. Finally, ions were injected for all available parallelizable time. Spectrum raw files were then extracted into ms1 and ms2 files using the in-house program RawXtractor or RawConverter (<http://fields.scripps.edu/downloads.php>) (He, Diedrich, Chu, & Yates, 2015) and the tandem mass spectra were searched against UniProt human database (downloaded on 03-25-2014) (The UniProt Consortium 2015) and matched to sequences using the ProLuCID database search program (ProLuCID ver. 3.1) (Eng, McCormack, & Yates, 1994; Xu et al., 2015). ProLuCID searches were done using an Intel Xeon cluster running on the Linux operating system. For search space, all fully and half-tryptic peptide candidates that fell within the no miscleavage, mass tolerance window constraint were included. Carbamidomethylation (+ 57.02146 Da) of cysteine was considered as a static modification and a differential modification of 79.9663 on serine, threonine, or tyrosine. Validity of peptide/spectrum matches (PSMs) were assessed in DTASelect2 (using two SEQUEST-defined parameters, the cross-correlation score (XCORR), and normalized difference in cross-correlation scores (DeltaCN) (Cociorva, D, & Yates, 2007; Eng et al., 1994; Tabb, McDonald, & Yates, 2002). The search results were grouped resulting in 12 distinct subgroups by charge state (+ 1, + 2, + 3, and greater than + 3) and tryptic status (fully tryptic, half-tryptic, and

nontryptic). In each of these subgroups, the distribution of Xcorr, DeltaCN, and DeltaMass values for (1) direct and (2) decoy database PSMs were first obtained and subsequently direct and decoy subsets were separated through discriminant analysis. Generally, full separation of the direct and decoy PSM subsets is not possible; therefore, peptide match probabilities were calculated on the basis of a nonparametric fit of the direct and decoy score distributions. A peptide confidence of 0.95 was used and set as the minimum threshold. The false discovery rate (FDR) was then calculated as the percentage of reverse decoy PSMs among all the PSMs that passed the confidence threshold. Each protein identified was required to have a minimum of one half-tryptic peptide. This peptide also had to be an excellent match with an FDR less than 0.001 which represents at least one excellent peptide match. Following this last filtering step, final protein FDRs were determined to be below 1% for each sample analysis based on decoy hits.

*In vitro* kinase assay. Flag-tagged LRRK2 wild-type, LRRK2 R1441C, and kinase-dead K1906M mutant cDNA constructs were overexpressed in HEK293 cells and purified using anti-FLAG® M2 agarose beads after 48 hours. In addition, V5-tagged auxilin wild-type and phosphodeficient auxilin S627A cDNA constructs were overexpressed in HEK293 cells and purified using anti-V5 agarose beads, as mentioned above. Equal amounts of beads were added at a 1:2 kinase to substrate ratio in kinase activity assay buffer [25 mM Tris, pH 7.4, 1 mM EDTA, 1mM, EGTA, 5 mM MgCl<sub>2</sub>] supplemented with or without 1 mM ATP up to a final reaction volume of 50 µl. Experimental samples were then incubated at 37°C for 90 minutes. The kinase reaction was terminated by adding an equal amount of 2X SDS sample buffer. Samples were then boiled and analyzed by SDS-PAGE and Western blotting analysis. Analysis was done comparing wild-type LRRK2 with wild-type auxilin or phosphodeficient auxilin S627A and LRRK2 R1441C or kinase-dead mutant LRRK2 K1906M with wild-type auxilin or phosphodeficient auxilin S627A with 1

mM ATP (phosphoserine signal without 1 mM ATP was initially subtracted). All results were normalized to the wild-type LRRK2 with wild-type auxilin experimental condition.

Statistical Analysis. One-way ANOVA with Tukey's post-hoc test was used for three or more dataset quantifications, unless indicated in figure legends. Two-tailed Student's t-test was utilized in two dataset analyses. Statistical calculations were performed with GraphPad Prism 7 Software (<http://www.graphpad.com>), p values  $\leq 0.05$  were considered significant, and all error bars in figures represent the standard error mean (SEM).

## Results

LRRK2 reportedly cofractionates with the presynaptic protein synapsin and phosphorylates several SVE proteins (Ambroso et al., 2014; Biskup et al., 2006; Islam et al., 2016; Matta et al., 2012; Pan et al., 2017; Stafa et al., 2014). Using primary, rat hippocampal neurons, we show that both auxilin and LRRK2 colocalize with synaptophysin, a protein marker of the presynaptic terminal (**Figure 3**). The synaptic LRRK2 substrates endophilin A1 and synaptojanin 1 are encoded by *SH3GL2* and *SYNJI*, respectively (Ambroso et al., 2014; Islam et al., 2016; Matta et al., 2012; Pan et al., 2017). Recently, *SH3GL2* was listed as a high PD-risk gene and several genetic mutations have been identified in *SYNJI* leading to early-onset parkinsonism (Chang et al., 2017; Kirola et al., 2016; Krebs et al., 2013; Olgiati et al., 2014; Quadri et al., 2013). From this we hypothesized that LRRK2 might have important kinase function at the synapse and that PD-linked mutations which alter kinase activity would affect synaptic integrity through proteins specifically involved in SVE regulation.

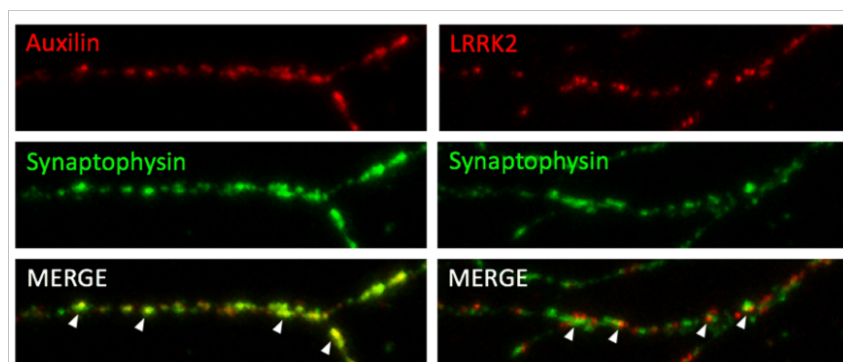


**Figure 3. LRRK2 and auxilin colocalize in the presynaptic compartment.** Rat hippocampal neurons were immunostained at div 7 days in culture. Neurons were immunostained using antibodies against auxilin and LRRK2. Synaptophysin was used as a marker of the presynaptic compartment. Merged images show abundant colocalization of auxilin and synaptophysin, as well as colocalization of LRRK2 and synaptophysin indicating that both proteins can localize at the synapse.

During SVE, both endophilin A1 and synaptojanin 1 interact to mediate the invagination and fission of a nascent clathrin-coated vesicle from the plasma membrane (**Figure 1**) (Saheki & De Camilli, 2012; Schuske et al., 2003). Auxilin, involved in the last step of SVE, is responsible for binding to the clathrin-coat and then recruiting hsc70, the ATPase that provides the energy to remove the clathrin-coat (Eisenberg & Greene, 2007; Morgan, Prasad, Jin, Augustine, & Lafer, 2001; Rapoport et al., 2008; Saheki & De Camilli, 2012). Mutations in *DNAJC6*, which encode auxilin, were recently discovered in juvenile or early-onset atypical parkinsonism patients (Edvardson et al., 2012; Koroglu et al., 2013; Olgiati et al., 2016). Interestingly, auxilin is highly homologous to cyclin G-associated kinase (*GAK*) (Lemmon, 2001), a PD-risk gene which was previously shown to interact in complex with LRRK2 (Beilina et al., 2014; Nagle et al., 2016; Nalls et al., 2014; Rhodes, Sinsheimer, Bordelon, Bronstein, & Ritz, 2011). To determine whether LRRK2 also specifically interacts with auxilin, we generated V5-tagged wild-type auxilin and overexpressed wild-type auxilin protein in HEK293 cells. We found that auxilin co-immunoprecipitated endogenous LRRK2, as well as hsc70, its known interaction partner, but not

GAPDH (**Figure 4B**). Together, these results suggest that a percentage of LRRK2 is localized to the synapse and that LRRK2 interacts with auxilin to potentially regulate synaptic function.

The LRRK2 G2019S mutation leads to an increase in kinase activity while the R1441C/H/G mutation has been shown to alter LRRK2 kinase activity by decreasing its GTPase function by disrupting GDP/GTP cycling which is essential for kinase activity (Greggio, 2012; Henry et al., 2015; Lewis et al., 2007; Webber et al., 2011; West et al., 2007). Additionally, compared to wild-type LRRK2, both mutations have been shown to modulate several SVE phosphosubstrates (endophilin A1 and synaptojanin 1) acting upstream of auxilin (Ambroso et al., 2014; Islam et al., 2016; Matta et al., 2012; Pan et al., 2017).

Auxilin is a highly phosphoregulated protein containing numerous serine and threonine residues in both its PTEN-like and clathrin-binding domains (**Figure 4A**). To examine whether auxilin might be a substrate of LRRK2 kinase activity, we coexpressed V5-tagged wild-type auxilin with either wild-type LRRK2, LRRK2 G2019S or LRRK2 R1441C constructs and immunoprecipitated auxilin from HEK293 cells. Using a pan-phosphoserine antibody, which recognizes all phosphorylated serine residues, we found that coexpression of wild-type auxilin with either LRRK2 G2019S or LRRK2 R1441C led to an increase in phosphoserine signal compared to coexpression with wild-type LRRK2 (**Figure 5**). Taken together, this suggests that the presence of mutant LRRK2 increases auxilin phosphorylation state compared to wild-type LRRK2. Importantly, wild-type auxilin coexpressed with an empty plasmid also showed basal levels of pan-phosphoserine signal, suggesting that auxilin may have additional kinases that may regulate its phosphorylation state (**Figure 5**).

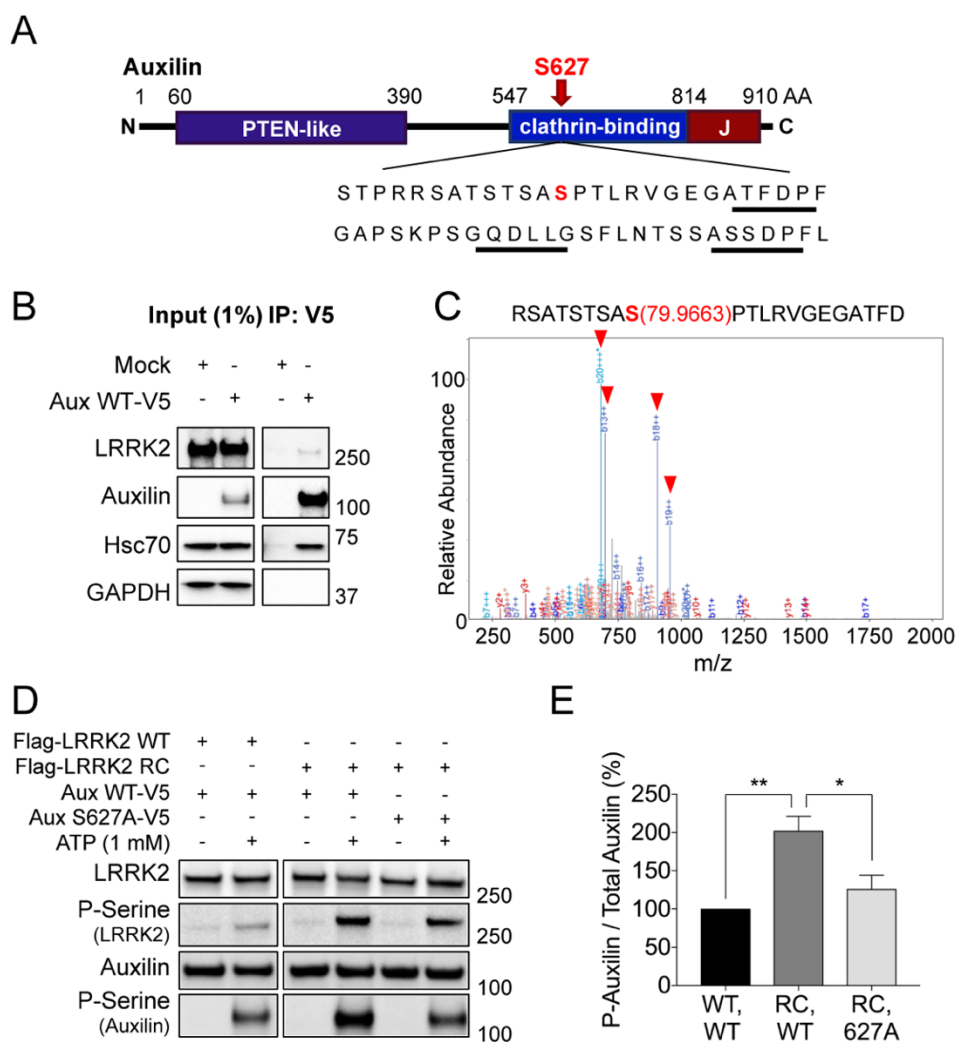


**Figure 4. LRRK2 phosphorylates auxilin in its clathrin-binding domain at Ser627.** (A) Schematic of auxilin protein mapping the Ser627 phosphosite to its clathrin-binding domain (clathrin-binding motifs are underlined). (B) Western blot analysis of co-immunoprecipitated proteins with V5-tagged wild-type (WT) auxilin from HEK 293 cells, probed for auxilin, LRRK2, hsc70 (positive control), and GAPDH (loading control). Left panels represent 1% input of whole cell lysate. (C) Representative tandem mass spectra identifying phosphorylated Ser627 site in auxilin. B-ions containing the phosphate group are indicated (red triangle) (overexpression, n=2; LRRK2 kinase inhibitor, GSK2578215A (2  $\mu$ M), n=1). (D) Western blot analysis of purified Flag-tagged LRRK2 WT or LRRK2 R1441C (RC) and V5-tagged auxilin WT or phosphodeficient auxilin S627A from HEK 293 cells following *in vitro* phosphorylation assays with or without 1 mM ATP probed for LRRK2, auxilin, and pan-phosphoserine (P-serine). All experimental conditions were run on the same Western blot. (E) Quantification of pan-phosphoserine auxilin signal in (D) normalized to total auxilin levels. All results were analyzed using one-way ANOVA statistical analysis (\* $p < 0.05$ , \*\* $p < 0.005$ , \*\*\*\* $p < 0.00005$ ), with all error bars representing SEM, n=3.

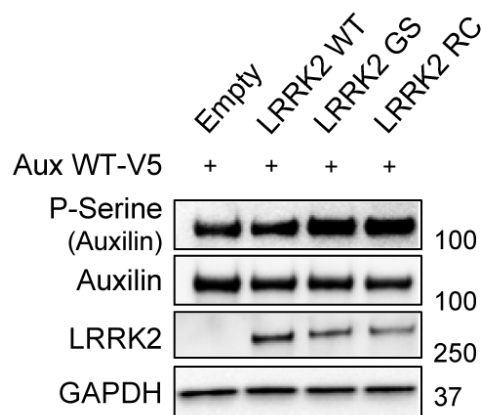


**Figure 5. Mutant LRRK2 overexpression increases auxilin phosphorylation state.** HEK 293 cells were cotransfected with V5-tagged auxilin wild-type (WT) and either LRRK2 WT, LRRK2 G2019S (GS) or LRRK2 R1441C (RC). Auxilin was purified using an antibody against V5. Western blot analysis of immunoprecipitated samples probed for pan-phosphoserine (P-Serine), auxilin, LRRK2, and GAPDH (loading control). Representative blots are n=3 experiments.

To identify potential LRRK2-mediated auxilin phosphorylation sites, we subjected purified Flag-tagged wild-type auxilin to tandem mass spectrometry. Flag-tagged wild-type auxilin was first coexpressed with either wild-type LRRK2-GFP, LRRK2 G2019S-GFP, LRRK2 R1441C-GFP tagged or eGFP, and auxilin was immunoprecipitated using a Flag antibody (**Figure 6A**). From this analysis, we identified auxilin with an amino acid sequence coverage generally > 90% and identified a novel auxilin phosphorylation site at Ser627 in each experimental condition (**Figure 4C, Table 1 and 2**). As HEK293 cells have high, endogenous expression of wild-type LRRK2, we additionally performed phosphoanalysis of Flag-tagged wild-type auxilin purified from cells which were untreated or pretreated with DMSO or the LRRK2 kinase inhibitor, GSK2578215A, which attenuated endogenous wild-type LRRK2 kinase activity (**Figure 6B-D**) (Reith et al., 2012). We again identified the same Ser627 phosphosite in untreated and DMSO conditions, but not when the LRRK2 kinase inhibitor, GSK2578215A, was used, suggesting that phosphorylation of auxilin Ser627 is lost when LRRK2 kinase activity is abolished in the cell (**Figure 6C, D and Table 2**). Importantly, we identified that this phosphosite is localized in

auxilin's clathrin-binding domain near a previously identified clathrin-binding motif (**Figure 4A**) (Scheele et al., 2003), suggesting that Ser627 phosphorylation may have important consequences for auxilin's previously reported functions during clathrin-mediated SVE. From the first phosphoanalysis, we also identified two additional novel auxilin phosphosites at positions Ser49 and Ser59 in close proximity to the start of the PTEN-like domain when wild-type auxilin was coexpressed with wild-type LRRK2 and LRRK2 R1441C, but not LRRK2 G2019S (**Figure 8A**).

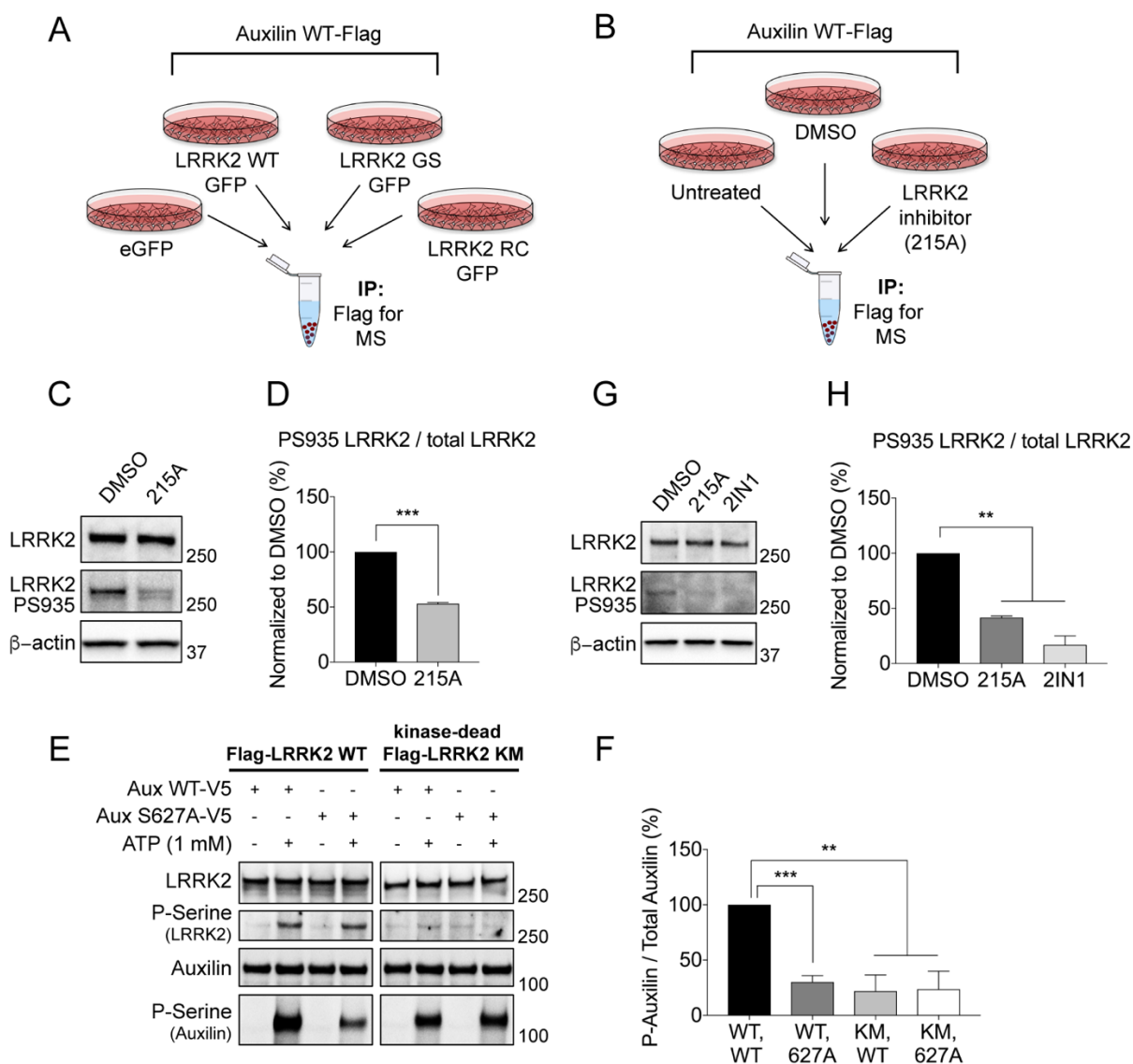


**Figure 6. LRRK2 mediates phosphorylation of auxilin at Ser627.** (A) Schematic for Flag-tagged wild-type auxilin coexpression with eGFP (negative control), GFP-tagged wild-type (WT) LRRK2, GFP-tagged mutant LRRK2 G2019S (GS) or GFP-tagged mutant LRRK2 R1441C (RC) cDNA constructs. Auxilin was

purified using anti-Flag agarose beads and TCA precipitated in preparation for mass spectrometry (MS) phosphoanalysis. **(B)** Schematic for mass spectrometry phosphoproteomics of Flag-tagged wild-type auxilin purified from HEK 293 cells left untreated or pretreated with DMSO or the LRRK2 kinase inhibitor, GSK2578215A (215A, 2  $\mu$ M). Auxilin was purified using anti-Flag agarose beads and TCA precipitated in preparation for MS phosphoanalysis. **(C)** Western blot analysis of pS935 LRRK2, LRRK2, and  $\beta$ -actin levels following 18 hour treatment with LRRK2 kinase inhibitor, GSK2578215A (2  $\mu$ M) in conjunction with mass spectrometry phosphoanalysis in **Figure 4C**. Loss of pS935 signal is indicative of LRRK2 kinase activity inhibition. **(D)** Quantification of ratio between pS935 LRRK2 and total LRRK2 protein levels first normalized to  $\beta$ -actin in **(C)**. **(E)** Western blot analysis of purified Flag-tagged LRRK2 WT or kinase-dead LRRK2 K1906M (KM) and V5-tagged auxilin WT or phosphodeficient auxilin S627A from HEK 293 cells following *in vitro* phosphorylation assays with or without 1 mM ATP probed for LRRK2, auxilin, and pan-phosphoserine (P-serine). All experimental conditions were run on the same Western blot. **(F)** Quantification of pan-phosphoserine auxilin signal in **(E)** normalized to total auxilin levels. **(G)** Western blot analysis of pS935 LRRK2, LRRK2, and  $\beta$ -actin levels following 18 hour treatment with LRRK2 kinase inhibitors, GSK2578215A (215A, 2  $\mu$ M) or LRRK2-IN-1 (2IN1, 2  $\mu$ M) done in conjunction for experiments in **Figure 7 D-F**. Loss of pS935 signal is indicative of LRRK2 kinase activity inhibition. **(H)** Quantification of ratio between pS935 LRRK2 and total LRRK2 protein levels first normalized to  $\beta$ -actin in **(H)**. The results were analyzed using unpaired t test or one-way ANOVA statistical analysis (\*\*p < 0.005, \*\*\*p < 0.0005), with all error bars representing SEM, n=3.

Previous studies have shown that truncated auxilin containing only the clathrin-binding and J-domains is sufficient for retaining auxilin function (Greener et al., 2001; Ma et al., 2002; J. Xiao, Kim, & Graham, 2006). Thus, to determine whether LRRK2-mediated phosphorylation might modulate auxilin's clathrin-binding activity, we further examined the Ser627 phosphorylation site. To first confirm Ser627 as a LRRK2-mediated phosphosite, we generated phosphodeficient auxilin S627A by mutating the serine residue to an alanine, rendering the site unable to be phosphorylated. We additionally, generated a Flag-tagged kinase-dead mutant LRRK2 K1906M, as previously reported (Webber et al., 2011). We overexpressed these cDNA constructs in HEK293 cells individually and immunoprecipitated V5-tagged wild-type auxilin or auxilin S627A and Flag-tagged wild-type LRRK2 or kinase-dead LRRK2 K1906M from HEK293 cells and subjected the purified proteins to *in vitro* phosphorylation assays. We confirm that addition of wild-type LRRK2 to wild-type auxilin led to an increase in auxilin's pan-phosphoserine signal in the presence of ATP (**Figure 6E, F**). Furthermore, mutation of the Ser627 phosphosite attenuated the increase in auxilin's pan-phosphoserine signal in the presence of wild-type LRRK2

and ATP (**Figure 6E, F**). Importantly, kinase-dead LRRK2 K1906M did not result in any significant changes in auxilin's pan-phosphoserine signal between either wild-type auxilin or phosphodeficient auxilin S627A (**Figure 6E, F**). As an additional control, we confirmed that wild-type LRRK2 but not kinase-dead LRRK2 K1906M had increased pan-phosphoserine signal with the addition of ATP (**Figure 6E, F**). This is consistent with previous reports, that active LRRK2 is able to autophosphorylate itself at several serine residues (Sheng et al., 2012; Webber et al., 2011). We repeated similar *in vitro* phosphorylation assays using mutant LRRK2 R1441C. We found that the presence of mutant LRRK2 R1441C, which leads to an increase in kinase activity (Steger et al., 2016), led to a greater fold change in auxilin pan-phosphoserine signal compared to wild-type LRRK2 (**Figure 4D, E**). When LRRK2 R1441C was incubated with phosphodeficient auxilin S627A, no increase in pan-phosphoserine signal was observed (**Figure 4D, E**). Therefore, we show that expression of phosphodeficient auxilin S627A decreased auxilin phosphorylation state in both LRRK2 wild-type and mutant LRRK2 R1441C conditions (**Figure 4D, E and Figure 6E, F**). Together, these data suggest that auxilin Ser627 is specifically targeted by LRRK2 kinase activity.

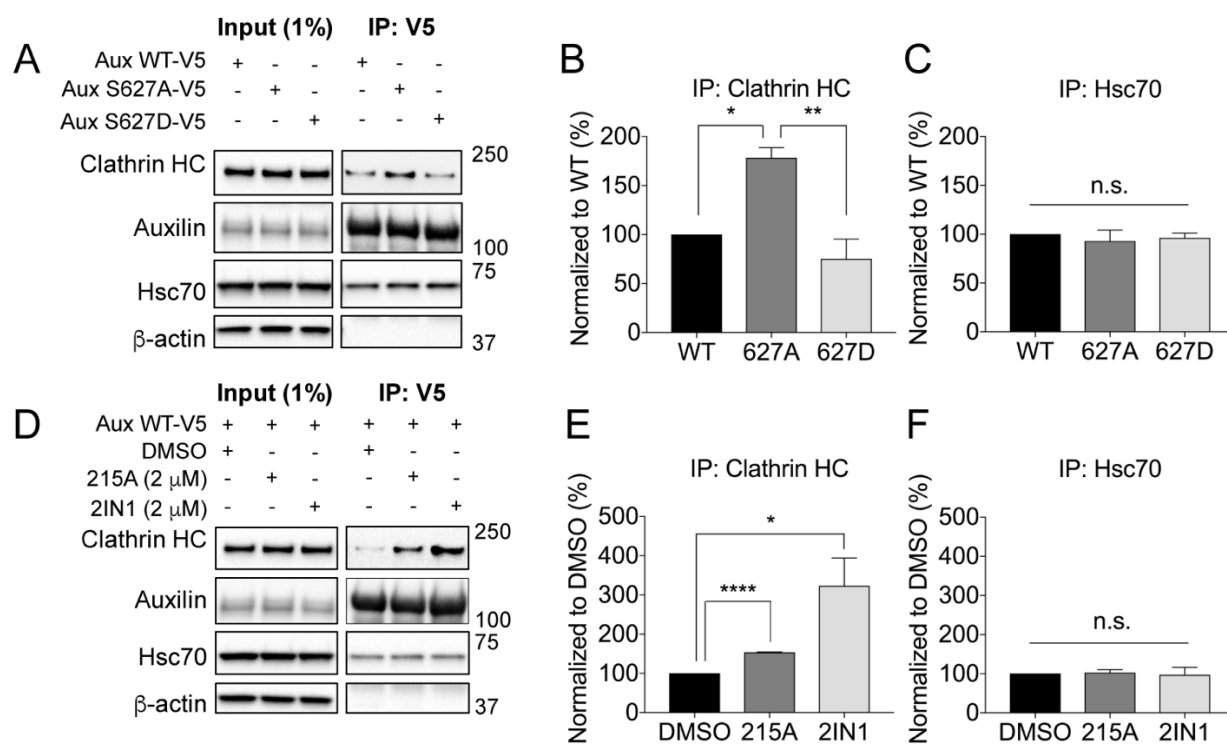
To determine whether phosphorylation of auxilin at position Ser627 regulated its binding to clathrin, we generated a phosphomimetic auxilin S627D by mutating the serine to an aspartate residue which is chemically similar to phosphoserine. We then examined the ability of phosphodeficient auxilin S627A and phosphomimetic auxilin S627D to bind clathrin and hsc70, both of which are known interaction partners of auxilin, in co-immunoprecipitation experiments carried out in HEK293 cells. We found that phosphodeficient auxilin S627A co-immunoprecipitated significantly more endogenous clathrin compared to either wild-type auxilin or phosphomimetic auxilin S627D (**Figure 7A, B**).

Table 1. Additional mass spectrometry information on peptide coverage and spectral counts.

N = X	Experimental condition	Accession	Sequence Coverage	Peptide Count	Spectra Count	Description
1	Flag-Auxilin WT, eGFP	O75061-2	56.50%	66	86	Isoform 2 of Putative tyrosine-protein phosphatase auxilin OS=Homo sapiens GN=DNAJC6
1	Flag-Auxilin WT, LRRK2 WT	O75061-2	87.00%	313	521	Isoform 2 of Putative tyrosine-protein phosphatase auxilin OS=Homo sapiens GN=DNAJC6
1	Flag-Auxilin WT, LRRK2 G2019S	O75061-2	90.60%	327	543	Isoform 2 of Putative tyrosine-protein phosphatase auxilin OS=Homo sapiens GN=DNAJC6
1	Flag-Auxilin WT, LRRK2 R1441C	O75061-2	88.80%	351	629	Isoform 2 of Putative tyrosine-protein phosphatase auxilin OS=Homo sapiens GN=DNAJC6
2	Flag-Auxilin WT, eGFP	O75061-2	26.00%	30	45	Isoform 2 of Putative tyrosine-protein phosphatase auxilin OS=Homo sapiens GN=DNAJC6
2	Flag-Auxilin WT, LRRK2 WT	O75061-2	34.00%	46	109	Isoform 2 of Putative tyrosine-protein phosphatase auxilin OS=Homo sapiens GN=DNAJC6
2	Flag-Auxilin WT, LRRK2 G2019S	O75061-2	34.90%	51	132	Isoform 2 of Putative tyrosine-protein phosphatase auxilin OS=Homo sapiens GN=DNAJC6
2	Flag-Auxilin WT, LRRK2 R1441C	O75061-2	34.10%	62	142	Isoform 2 of Putative tyrosine-protein phosphatase auxilin OS=Homo sapiens GN=DNAJC6
N = X	Experimental condition	Accession	Sequence Coverage	Peptide Count	Spectra Count	Description
1	Flag-Auxilin WT, untreated	O75061-2	94.90%	296	510	Isoform 2 of Putative tyrosine-protein phosphatase auxilin OS=Homo sapiens GN=DNAJC6
1	Flag-Auxilin WT, DMSO	O75061-2	83.30%	215	374	Isoform 2 of Putative tyrosine-protein phosphatase auxilin OS=Homo sapiens GN=DNAJC6
1	Flag-Auxilin WT, GSK2578215A	O75061-2	87.10%	212	399	Isoform 2 of Putative tyrosine-protein phosphatase auxilin OS=Homo sapiens GN=DNAJC6
2	Flag-Auxilin WT, untreated	O75061-2	95.80%	308	631	Isoform 2 of Putative tyrosine-protein phosphatase auxilin OS=Homo sapiens GN=DNAJC6
2	Flag-Auxilin WT, DMSO	O75061-2	96.90%	338	723	Isoform 2 of Putative tyrosine-protein phosphatase auxilin OS=Homo sapiens GN=DNAJC6
2	Flag-Auxilin WT, GSK2578215A	O75061-2	92.30%	238	427	Isoform 2 of Putative tyrosine-protein phosphatase auxilin OS=Homo sapiens GN=DNAJC6

Table 2. Additional mass spectrometry information on spectra count for auxilin Ser627 phosphosite.

N = X	Experimental Condition	Phosphosite	Sequence	Spectra Count	Confidence (%)	Scan	Charge	Primary Score	Delta CN	M+H+ (calculated)	M+H+ (measured)	ppm
1	Flag-Auxilin WT, LRRK2 WT	Ser627	R.SAITSAS(79.9663)PTLRVGEGETFD.P	1	100	21060	2	4.2219	0.5056	2034.9015	2034.895	-3.2
1	Flag-Auxilin WT, LRRK2 G2019S	Ser627	R.SAITSAS(79.9663)PTLRVGEGETFD.P	1	100	12947	3	3.3672	0.4982	2191.0027	2191.0059	1.4
1	Flag-Auxilin WT, LRRK2 R1441C	Ser627	R.SAITSAS(79.9663)PTLRVGEGETFD.P	1	100	21797	2	3.9991	0.4646	2034.9015	2034.9088	3.6
1	Flag-Auxilin WT, LRRK2 R1441C	Ser627	R.SAITSAS(79.9663)PTLRVGEGETFD.P	1	100	50605	4	3.3664	0.3787	5422.575	5422.5527	-4.1
2	Flag-Auxilin WT, eGFP	Ser627	R.SAITSAS(79.9663)PTLR.V	1	100	22171	2	2.4185	0.3124	1258.5675	1258.5737	4.9
2	Flag-Auxilin WT, LRRK2 WT	Ser627	R.SAITSAS(79.9663)PTLR.V	1	100	16814	2	2.9763	0.3682	1258.5675	1258.5679	0.3
2	Flag-Auxilin WT, LRRK2 WT	Ser627	R.SAITSAS(79.9663)PTLRVGEGETFD.P	1	100	56563	4	4.311	0.3847	5422.575	5423.596	3.3
2	Flag-Auxilin WT, LRRK2 G2019S	Ser627	R.SAITSAS(79.9663)PTLRVGEGETFD.P	1	100	57744	5	4.5597	0.3772	5422.575	5424.588	1.1
2	Flag-Auxilin WT, LRRK2 R1441C	Ser627	R.SAITSAS(79.9663)PTLR.V	1	100	14444	2	3.1986	0.457	1258.5675	1258.5682	0.6
2	Flag-Auxilin WT, LRRK2 R1441C	Ser627	R.SAITSAS(79.9663)PTLRVGEGETFD.P	1	100	60704	5	3.2672	0.4027	5422.575	5424.5977	2.9
N = X	Experimental Condition	Phosphosite	Sequence <th>Spectra Count</th> <th>Confidence (%)</th> <th>Scan</th> <th>Charge</th> <th>Primary Score</th> <th>Delta CN</th> <th>M+H+ (calculated)</th> <th>M+H+ (measured)</th> <th>ppm</th>	Spectra Count	Confidence (%)	Scan	Charge	Primary Score	Delta CN	M+H+ (calculated)	M+H+ (measured)	ppm
1	Flag-Auxilin WT, untreated	Ser627	R.SAITSAS(79.9663)PTLRVGEGETFD.P	1	100	###	4	4.7581	0.545	5422.575	5424.5933	2.1
1	Flag-Auxilin WT, DMSO	Ser627	R.SAITSAS(79.9663)PTLRVGEGETFD.P	1	100	###	5	5.4263	0.479	5422.575	5422.5347	-8
1	Flag-Auxilin WT, DMSO	Ser627	R.SAITSAS(79.9663)PTLRVGEGETFD.P	1	100	###	5	4.733	0.323	5422.575	5423.587	1.5
1	Flag-Auxilin WT, DMSO	Ser627	R.SAITSAS(79.9663)PTLRVGEGETFD.P	1	100	###	4	4.7486	0.499	5422.575	5423.575	-1
1	Flag-Auxilin WT, DMSO	Ser627	R.SAITSAS(79.9663)PTLRVGEGETFD.P	1	100	###	4	4.4632	0.561	5422.575	5424.5815	-0
1	Flag-Auxilin WT, DMSO	Ser627	R.SAITSAS(79.9663)PTLRVGEGETFD.P	1	100	###	5	5.5051	0.376	5422.575	5424.584	0.4



**Figure 7. LRRK2 mediated regulation of auxilin alters its association with clathrin.** (A) Western blot analysis of co-immunoprecipitated proteins with V5-tagged auxilin WT, auxilin S627A and S627D from HEK 293 cells probed for clathrin heavy chain (HC), auxilin, hsc70, and  $\beta$ -actin (loading control). Left panels represent 1% input of whole cell lysate. (B, C) Quantification of co-immunoprecipitated clathrin and hsc70 normalized to immunoprecipitated auxilin in (A). (D) Western blot analysis of co-immunoprecipitated proteins with V5-tagged auxilin WT upon LRRK2 kinase inhibitor, GSK2578215A (215A, 2  $\mu$ M) or LRRK2-IN-1 (2IN1, 2  $\mu$ M), treatment in HEK 293 cells probed for clathrin HC, auxilin, hsc70, and  $\beta$ -actin. Left panels represent 1% input of whole cell lysate. (E, F) Quantification of co-immunoprecipitated clathrin and hsc70 normalized to immunoprecipitated auxilin in (D). All results were analyzed using one-way ANOVA statistical analysis (\* $p < 0.05$ , \*\* $p < 0.005$ , \*\*\*\* $p < 0.00005$ ), with all error bars representing SEM,  $n=3$ .

As expected, both phosphomutants did not differentially bind hsc70, as the phosphosite Ser627 is not located in the auxilin J-domain which binds directly to hsc70 (Figure 7A, C). To further examine whether *de novo* LRRK2-mediated phosphorylation of auxilin could affect its downstream function, we overexpressed V5-tagged wild-type auxilin in HEK293 cells and treated cells with either DMSO or two independent LRRK2 kinase inhibitors, GSK2578215A or LRRK2-IN-1. We confirmed efficient inhibition of LRRK2 kinase activity by measuring the levels of

phosphorylated LRRK2 Ser935, which is autophosphorylated when LRRK2 is active (**Figure 6G, H**) (Webber et al., 2011). Upon inhibition of LRRK2 kinase activity, auxilin binding to clathrin was significantly increased (**Figure 7D, E**). This is consistent with our previous results that phosphodeficient auxilin S627A binds significantly more endogenous clathrin compared to both wild-type auxilin and phosphomimetic auxilin S627D (**Figure 7A, B**). Again, auxilin binding to endogenous hsc70 was not altered as a result of LRRK2 kinase inhibition, as expected (**Figure 7D, F**).

Although not necessary for proper auxilin function, previous studies have shown that the PTEN-like domain of auxilin is involved in sensing clathrin-coated vesicles (**Figure 8A**) (Guan et al., 2010). To determine whether the additional auxilin phosphosites (Ser49 and Ser59) identified through mass spectrometry analysis also regulated auxilin's clathrin-binding function (**Figure 8A**), we generated the corresponding phosphomutant constructs as mentioned in previous studies and overexpressed phosphodeficient auxilin S49A and S59A and phosphomimetic auxilin S49D and S59D individually in HEK293 cells. We then co-immunoprecipitated endogenous clathrin and hsc70 by purifying V5-tagged wild-type auxilin and phosphomutants from HEK293 cells. Both phosphodeficient auxilin S49A and S59A did not bind more clathrin or hsc70 compared to wild-type auxilin (**Figure 8B-G**). Conversely, phosphomimetic auxilin S59D led to significantly less binding with both endogenous clathrin and hsc70 (**Figure 8E-G**). The Ser59 phosphosite is located at the start of the PTEN-like domain and not in the domains responsible for binding clathrin and hsc70. Therefore, the decrease in binding to clathrin and hsc70 that was observed could potentially be due to altered protein folding induced by the S59D mutation. Taken together, these data suggest that LRRK2-mediated phosphorylation of auxilin in the clathrin-binding domain at Ser627 preferentially alters its ability to bind clathrin during SVE.

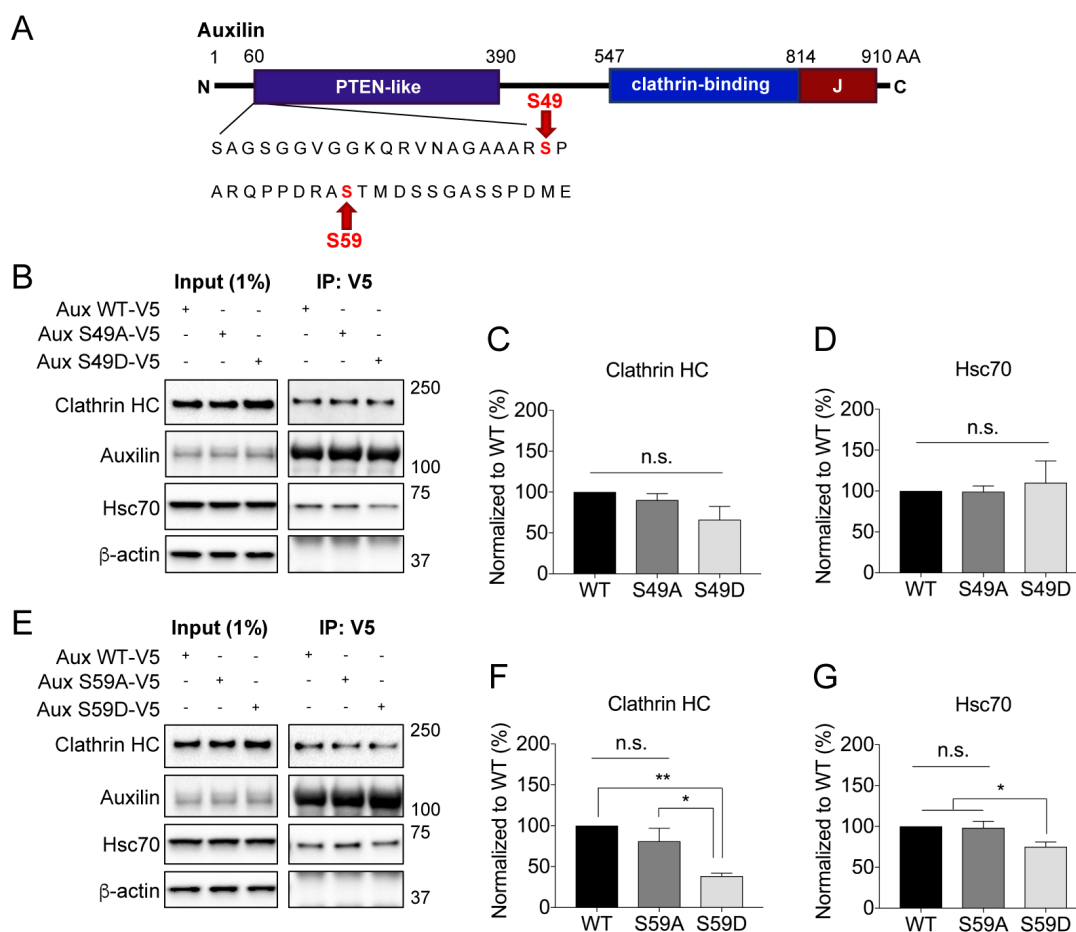


**Figure 8. Functional analyses of additional LRRK2-mediated phosphosites.** (A) Schematic of auxilin protein mapping additional LRRK2-mediated phosphorylation sites near its PTEN-like domain. (B) Western blot analysis of co-immunoprecipitated proteins with V5-tagged wild-type auxilin, auxilin S49A and S49D following 48 hr overexpression in HEK 293 cells. The Western blot was probed with clathrin heavy chain (HC), auxilin, hsc70, and  $\beta$ -actin (loading control) antibodies. Left panels represent 1% input of whole cell lysate prior to immunoprecipitation. (C) Quantification of co-immunoprecipitated clathrin normalized to immunoprecipitated auxilin in (B). (D) Quantification of co-immunoprecipitated hsc70 normalized to immunoprecipitated auxilin in (B). (E) Western blot analysis of co-immunoprecipitated proteins with V5-tagged wild-type auxilin, auxilin S59A and S59D following 48 hr overexpression in HEK 293 cells. The Western blot was probed with clathrin heavy chain (HC), auxilin, hsc70, and  $\beta$ -actin (loading control) antibodies. Left panels represent 1% input of whole cell lysate prior to immunoprecipitation. (F) Quantification of co-immunoprecipitated clathrin normalized to immunoprecipitated auxilin in (E). (G) Quantification of co-immunoprecipitated hsc70 normalized to immunoprecipitated auxilin in (E). The results were analyzed using one-way ANOVA statistical analysis (\* $p < 0.05$ , \*\* $p < 0.005$ ), with all error bars representing SEM,  $n=3$ .

## Conclusions

We showed that auxilin and LRRK2 interact and that auxilin phosphorylation state is mediated by LRRK2 kinase activity. LRRK2-mediated phosphorylation of auxilin at Ser627, located within its clathrin-binding domain, leads to differential association of auxilin with clathrin. Moving forward, we hypothesized that mutant LRRK2 regulation of auxilin ultimately leads to loss of its function in SVE.

LRRK2 has been shown to interact with and phospho-regulate several SVE proteins including endophilin A1 and synaptojanin 1, both of which have distinct roles upstream of auxilin (Saheki & De Camilli, 2012). Moreover, LRRK2 G2019S-mediated phosphorylation of endophilin A1 alters its ability to associate with membranes while LRRK2 R1441C knock-in *Drosophila* models displayed an altered presynaptic proteome and LRRK2-mediated phosphorylation of synaptojanin 1 (Ambroso et al., 2014; Islam et al., 2016; Matta et al., 2012; Pan et al., 2017), suggesting that LRRK2 has an important regulatory kinase role for multiple proteins at the presynaptic terminal.

Interestingly, LRRK2 has also been shown to interact in complex with GAK (Beilina et al., 2014), a ubiquitously expressed clathrin-uncoating protein localized at the trans-Golgi network (Beilina et al., 2014; Greener, Zhao, Nojima, Eisenberg, & Greene, 2000). GAK is highly homologous to auxilin and is also a PD risk factor (Beilina et al., 2014; Lemmon, 2001; Nagle et al., 2016; Nalls et al., 2014; Rhodes et al., 2011). Here, we show that LRRK2 and auxilin also interact and that the presence of mutant LRRK2 increases auxilin phosphorylation state. Through tandem mass spectrometry, we determined that wild-type LRRK2 and PD-linked LRRK2 mutants R1441C and G2019S phosphorylate auxilin at Ser627 and that this phosphorylation was abolished by the LRRK2 kinase inhibitor, GSK2578215A. Generation of a phosphodeficient auxilin S627A resulted in a significantly reduced auxilin phosphorylation state in the presence of wild-type

LRRK2, LRRK2 R1441C or kinase-dead LRRK2 K1906M. As the Ser627 phosphosite is located within auxilin's clathrin-binding domain, which is important for recognizing and binding to clathrin-coated vesicles (Rapoport et al., 2008; Scheele et al., 2003), we further found that inhibition of endogenous LRRK2 kinase activity or expression of phosphodeficient auxilin S627A, but not phosphomimetic auxilin S627D, resulted in increased auxilin association with clathrin. These data thus further validate auxilin Ser627 as a LRRK2-kinase activity dependent phosphosite that is important in modulating auxilin binding to clathrin.

## CHAPTER 3.

### SYNAPTIC DYSFUNCTION IN LRRK2 PATIENT-DERIVED NEURONS

#### Summary

We previously showed that LRRK2 is able to interact with and regulate auxilin function through phosphorylation (**Figure 4B, C**). However, it is not known how dysregulation of auxilin function affects dopaminergic neurons in PD pathogenesis. Previous studies have shown that LRRK2-mediated regulation of other synaptic proteins involved in SVE, such as endophilin A1 and synaptojanin 1, led to delayed endocytosis (Matta et al., 2012; Pan et al., 2017). This data is consistent with endophilin A1 or mutant synaptojanin 1 knockin/knockout mice, which also showed delayed endocytosis upon loss of functional protein (Cao et al., 2014; Cao et al., 2017; Kim et al., 2002; Milosevic et al., 2011). Altogether, these data suggest that mutant LRRK2 regulation of wild-type SVE proteins can also lead to dysfunctions at the synapse. In our studies, we generated and analyzed the role of synaptic dysfunction in human-derived dopaminergic neurons from induced pluripotent stem cells (iPSCs) harboring the LRRK2 R1441C/G or G2019S mutations.

We found that LRRK2 mutant dopaminergic neurons displayed decreased SVE proteins including auxilin, adaptor protein 2 (AP-2), dynamin 1, and endophilin A1 as compared to controls (**Figure 11A-F**). Additionally, using a well-established endocytic assay through FM 1-43 styryl dye uptake, we show that endocytic rates are delayed in LRRK2 mutant dopaminergic neurons (**Figure 11G, H**). A previous study found that auxilin knockout mice displayed endocytic defects including decreased synaptic vesicle density and the appearance of membraneless clathrin cages at the presynaptic terminal (Hirst et al., 2008; Yim et al., 2010). We submitted LRRK2 R1441C

and control dopaminergic neurons for electron microscopy analysis to assess the synaptic architecture. Similar to auxilin knockout mice, we observed decreased synaptic vesicle density, as well as enlarged vesicles and the appearance of membraneless clathrin cages (**Figure 12A, C**). This suggests that mutant LRRK2-mediated regulation of auxilin leads to loss of normal auxilin function.

Newly synthesized and recycled dopamine (DA) is rapidly packaged into an incoming population of nascent vesicles to prevent its oxidation (Lotharius & Brundin, 2002). Therefore, we hypothesized that disruptions in the SVE pathway would lead to deficiencies in DA packaging and increased cytosolic DA in human-derived dopaminergic neurons. Using a sensitive near infrared fluorescence (nIRF) assay (Mazzulli, Burbulla, Krainc, & Ischiropoulos, 2016), we measured the levels of oxidized DA in LRRK2 mutant and control neurons. We found that LRRK2 mutant neurons displayed higher levels of oxidized DA in a time dependent manner (**Figure 13A-C and Figure 15A, B**). In addition, downstream pathological phenotypes were also observed in LRRK2 mutant dopaminergic neurons including increased  $\alpha$ Syn accumulation and decreased GCase activity (**Figure 13D-F and Figure 15C-E**). Importantly, these phenotypes were attenuated when wild-type auxilin and not phosphomimetic S627D or phosphodeficient S627A auxilin was overexpressed in dopaminergic neurons (**Figure 16 and Figure 17**). To further confirm that SVE dysfunction leads to the generation of oxidized DA in dopaminergic neurons, we infected neurons with independent lentiviral auxilin shRNAs and found increased oxidized DA accumulation through loss of auxilin function (**Figure 19**). This indicates that disruptions in SVE in part lead to the accumulation of toxic oxidized DA species in human neurons.

## Methods

iPSC culture and midbrain-dopaminergic neuron differentiation. LRRK2 patient fibroblasts were obtained from the NINDS Human Cell and Data Repository (formerly Coriell). Patient fibroblasts were reprogrammed using retroviruses at the Human Embryonic and Induced Pluripotent Stem Cell Facility at Northwestern University. iPSCs were routinely characterized through g-band karyotype analysis by Cell Line Genetics (<https://www.clgenetics.com/>) and Sanger sequenced by the Comprehensive Cancer Center DNA Sequencing and Genotyping facility at the University of Chicago (<http://cancer-seqbase.uchicago.edu/>) to ensure proper maintenance of LRRK2 mutations (**Figure 10**). LRRK2 mutant cell lines used in this study include: Coriell lines ND32975 clone 2 and ND32976 clone 1 and 2 – LRRK2 c.4321C>G (p.R1441G), L295-4 – LRRK2 c.4321C>T (p.R1441C), ND29423-3 – LRRK2 c.6055G>A (p.G2019S), and control lines PPS31F clone 1 (control 1), KT clone 6 (control 2), 2131 (control 3), and 2132 (control 4). Controls 3 and 4 are previously published cells lines (Burbulla et al., 2017). LRRK2 iPSCs were differentiated along with healthy control lines into dopaminergic neurons according to previously published protocols (Burbulla et al., 2017; Kriks et al., 2011). Prior to the start of differentiation, iPSCs were accutased and seeded onto 6-well plates at a density of 1 million cells per well. iPSCs were fed daily until cells had reached 80% confluency in order to initiate the differentiation protocol (day 0). Cells were fed a combination of LDN193189, SB431542, sonic hedgehog (SHH), purmorphamine, FGF8, CHIR99021 factors. On day 13, cells were transferred to poly-D-lysine/laminin coated 10 cm plates. Cells were fed every 3<sup>rd</sup> day by half volume feeding with Neurobasal + SM1 supplement and bDNF, ascorbic acid, gDNF, TGF- $\beta$ 3, cAMP, DAPT factors. On day 25, cells were finally passaged onto poly-D-lysine/laminin coated tissue culture plates. Dopaminergic neurons were maintained in culture at 37°C with 5% CO<sub>2</sub> and continuously fed by half volume feeding every 3<sup>rd</sup>

or 4<sup>th</sup> day with Neurobasal + SM1 supplement and bDNF, ascorbic acid, gDNF, TGF- $\beta$ 3, cAMP, DAPT factors until day 40, then the media was switched over to Neurobasal + SM1 supplement until cells were ready to be assayed (day 40+).

Plasmids and primers. Sequencing primers were obtained from Integrated DNA Technologies: Sequencing primers for LRRK2 gDNA exon 31 For 5'-tcttttcttcttgaagtctgct-3' and Rev 5'-ttctctaccagcctaccatgt-3', LRRK2 gDNA exon 41 For 5'-aagatttctgtgcattttctggc-3' and Rev 5'-tcacatctgaggtcagtggttacc-3'. Sequencing primers for DNAJC6 mRNA R1 5'-catgtcaaagagacctcccc-3', F1 5'-atgagcctctcgggagcta-3', F2 5'-attagcaggctcccagtct-3', F3 5'-ttgaggtcaaccattgggag-3', F4 5'-ggctctcccaccaattctg-3', F5 5'-agcaaaccaccacaccaac-3', F6 5'-actgggcaaccctatgaaca-3'.

Antibodies. For immunofluorescence: DNAJC6 (auxilin) 1:1000 (Sigma, #HPA031182), LRRK2 1:100 (Novus Biologicals, #NB300-268), synaptophysin 1:500 (EMD Millipore, #MAB5258), tomm20 1:200 (Abcam, #ab78547), Oct4 1:100 (Abcam, #ab19857), SSEA1 1:100 (EMD Millipore, #MAB4304), Nanog 1:50 (R&D Systems, #AF1997), tra-1-81 1:100 (EMD Millipore, #MAB4381). For Western Blot: DNAJC6 (auxilin) 1:1000 (Sigma, #HPA031182), DNAJC6 (auxilin) 1:1000 (ThermoFisher, #PA5-26981), AP-2 1:2000 (BD Transduction, #610501), clathrin heavy chain (2410) 1:1000 (Cell Signaling, #P1663), dynamin 1 1:1000 (ThermoFisher, #PA1-660), endophilin A1 (E1E6Q) 1:1000 (Cell Signaling, #65169), synaptophysin 1:2000 (EMD Millipore, #MAB5258),  $\beta$ -actin (AC-15) 1:5000 (Abcam, #ab6276), hsc70 (B-6) 1:2000 (Santa Cruz, #sc-7298), GAPDH (6C5) 1:5000 (EMD Millipore, #MAB374),  $\alpha$ Synuclein (LB509)

1:1000 (Invitrogen, #180215),  $\alpha$ Synuclein (C-20) 1:1000 (Santa Cruz, #sc-7011-R), and tyrosine hydroxylase 1:2000 (Calbiochem, #657012).

Immunofluorescence. Cells seeded on nitric acid treated, poly-D-lysine (Sigma, #P1149), and laminin coated (Invitrogen, #23017-015) coverslips were fixed using 3% paraformaldehyde in 1X PBX for 15 to 20 minutes at room temperature. Cells were then permeabilized using permeabilization buffer [10% FBS in 1X PBS + 0.1% fresh saponin] for 30 minutes at room temperature. Samples were then incubated in primary antibody diluted in permeabilization buffer either for 30 minutes at room temperature or overnight at 4°C. Coverslips were then washed three times with 1X PBS for 5 minutes each wash. Secondary antibodies corresponding to the primary antibodies were diluted in permeabilization buffer and added to the samples for 45 minutes to 2 hours at room temperature. Samples were washed three times with 1X PBS for 5 minutes each wash and then mounted onto Superfrost® Plus microscope slides (Fisherbrand, #12-550-15) using DAPI Fluoromount-G® (Southern Biotech, #0100-20). Samples were left at 4°C for at least 24 hours before imaging. Images were obtained on a Leica DMI4000B confocal microscope.

FM<sup>TM</sup>1-43 styryl dye uptake assay. Cells were briefly washed twice with HBSS media containing Ca<sup>2+</sup> and then incubated in the same assay medium for 10 minutes at 37°C. The assay medium was aspirated and then cells were incubated in HBSS with Ca<sup>2+</sup> containing 60 mM KCl along with 5  $\mu$ g/mL of FM<sup>TM</sup> 1-43X styryl dye (ThermoFisher, #F35355) solubilized in water for 1 minute at 37°C. Cells were then incubated in HBSS with Ca<sup>2+</sup> containing 5  $\mu$ g/mL of FM<sup>TM</sup>1-43X styryl dye for an additional 15 minutes at 37°C. Following this incubation step, the cells were quickly washed, 2 times, using HBSS without Ca<sup>2+</sup> and subsequently incubated in this media overnight at

4°C to wash out any nonspecific dye binding. The next day, cells were fixed using 3% paraformaldehyde for 20 minutes and mounted onto Superfrost® Plus microscope slides (Fisherbrand, #12-550-15) using DAPI Fluoromount-G® (Southern Biotech, #0100-20). Images were obtained on a Leica DMI4000B confocal microscope. The intensity values reported were normalized to the length of each neurite determined in the analysis per condition.

Transmission electron microscopy (TEM). DA neurons on treated coverslips were fixed with 2% paraformaldehyde, 2% glutaraldehyde in 100 mM phosphate buffer, pH 7 initially for 1 hour at room temperature and then overnight at 4°C. TEM preparation of DA neurons was done at the Center for Advanced Microscopy supported by the NCI CCSG P30 CA060553 grant awarded to the Robert H. Lurie Comprehensive Cancer Center at Northwestern University. TEM imaging was done on the CAM/FEI Spirit G2 TEM microscope and analyzed using Image J software.

Oxidized dopamine (DA) measurement. Oxidized DA was quantitated using the near-infrared fluorescent (nIRF) assay as previously described (Mazzulli et al., 2016). DA neurons were washed and collected with ice-cold 1X PBS and then centrifuged at 300 x g for 5 minutes to sediment cells into a pellet. The sample pellets were lysed using 1% Triton X-100 lysis buffer containing 1X cOmplete™ protease inhibitor cocktail (Sigma, #11836170001 Roche) and further homogenized using a dounce glass-tissue homogenizer. Homogenized samples were centrifuged at 100,000 x g for 30 minutes at 4°C in a Beckman Coulter® Optima™ Max-XP ultracentrifuge. A BCA assay was performed on the supernatant collected from each sample to determine the total amount of protein. The insoluble fraction was extracted from the pellet using 2% SDS in 50 mM Tris, pH 7.4 in proportion to the amount of total protein. The resuspended samples were then boiled at 100°C

for 10 minutes, briefly sonicated, and boiled again for an additional 10 minutes before being centrifuged at 150,000 x g for 30 minutes at 4°C in the Beckman Coulter® Optima™ Max-XP ultracentrifuge. The pellets were further treated with 1N NaOH overnight at 55°C in an amount proportional to the total amount of protein. The next day, samples were lyophilized, followed by a wash with water, and lyophilized again before being resuspended in water and blotted onto Biodyne® B nylon membrane (Pall Life Sciences, #60208) for nIRF imaging and analysis on the Odyssey® CLx (LI-COR Biosciences) and Image Studio Lite software, respectively. The standard curve used to determine the total levels of oxidized DA species was generated through serial dilutions of a known concentration of oxidized DOPAC, and finally fitted to a polynomial function. Oxidized DOPAC was generated by adding equimolar amounts of sodium periodate, followed with an incubation step at room temperature for 30 minutes.

Glucocerebrosidase (GCase) activity assay. DA neuronal pellets were resuspended in 50 µl of radioimmunoprecipitation (RIPA) assay buffer [50 mM Tris, pH 8.0, 150 mM NaCl, 1% Triton X-100, 0.1% SDS, 0.5% sodium deoxycholate] + 1X cOmplete™ protease inhibitor cocktail. Samples were left on ice for 30 minutes with brief vortexing every 10 minutes to ensure full lysis of proteins. The samples were centrifuged at 3000 x RPM for 10 minutes to sediment nuclear components and dead cells and the remaining supernatant was collected for subsequent BCA and activity assays. 10 µg of protein lysate was incubated with 10 µl of 10% bovine serum albumin (BSA), and 20 µl of 5 mM of artificial enzyme substrate 4-methylumbelliferyl β-glucopyranoside (4-MU) (Sigma, #M36333) diluted in activity assay buffer [0.25% taurocholate, 0.25% Triton X-100, 1 mM EDTA, citrate/phosphate buffer, pH 5.4]. Each experimental condition was made up to 90 µl with activity assay buffer and either 10 µl of water or the specific GCase inhibitor,

conduritol B epoxide (CBE) (final concentration 100  $\mu$ M) was added for a final volume of 100  $\mu$ l. The components were mixed and incubated in a white 96-well, black bottomed plate (Thermo Fisher Scientific, #437796) for 30 minutes at 37°C. The reaction was stopped by adding 100  $\mu$ l of 1M glycine, pH 12.5 to each well. The resulting fluorescence was read on the SpectraMax™ i3 at wavelengths  $\text{ex} = 355$  nm and  $\text{em} = 460$  nm for 0.1 sec. The values from CBE treated samples was subtracted from water treated samples to obtain the specific GCase activity of each sample.

Generation of lentiviral constructs. Wild-type auxilin cDNA (Harvard PlasmID Database, #HsCD00414238) was subcloned into the pER4 lentiviral expression vector using standard subcloning procedures as outlined by Addgene (<https://www.addgene.org/protocols/subcloning/>). The subcloning primers used include EcoRI-Start 5'- ccggaattcatgagcctcctcgggagcta-3' and End-NotI 5'- ccggcgccgcgcatataagggtttggccttgg-3'. Phosphomutant auxilin lentiviral expression vectors were generated through site-directed mutagenesis (Fisher Scientific, #NC1220413), accordingly to manufacture's protocol. DNAJC6 shRNA and scramble lentiviral expression vectors were obtained from ThermoScientific (#RMM4534-EG72685). Lentiviral vectors were packaged and transfected into HEK 293FT cells using X-treme Gene HP DNA transfection (Roche, #06366236001) along with helper plasmids psPAX2 (Addgene, #12260) and pLP3 (Invitrogen). Quantitation of retroviral antigens was determined using ZeptoMetrix Corporation RETROtek HIV-1 p24 Antigen ELISA kits (Fisher Scientific, #22-156-700). Concentrated viruses were aliquoted and kept at -80°C for future use. Neuronal cultures were transduced in 12-well tissue culture plates containing 500K cells at a MOI of 2 at day 70 or day 150 post-differentiation and analyzed at day 100 or day 180 post-differentiation.

Statistical Analysis. One-way ANOVA with Tukey's post-hoc test was used for three or more dataset quantifications, unless indicated in figure legends. Two-tailed Student's t-test was utilized in two dataset analyses. Statistical calculations were performed with GraphPad Prism 7 Software (<http://www.graphpad.com>), p values  $\leq 0.05$  were considered significant, and all error bars in figures represent the standard error mean (SEM).

## Results

We generated induced pluripotent stem cell (iPSC)-derived midbrain dopaminergic neurons (**Figure 9**), from reprogrammed PD patient fibroblasts harboring the R1441C/G or G2019S mutations along with healthy control cell lines, using previously published protocols (**Figure 10**) (Kriks et al., 2011; Takahashi & Yamanaka, 2006).

Following differentiation at day 70 in culture, synaptic proteins primarily involved in SVE, such as auxilin, dynamin 1, AP-2, and endophilin A1 were significantly decreased in LRRK2 R1441G dopaminergic neurons compared to healthy controls (**Figure 11A-F**). Importantly, the levels of synaptophysin, a presynaptic marker, and  $\beta$ -actin levels remained unaltered (**Figure 11A**).

To determine whether the loss of key synaptic proteins involved in SVE would affect the endocytic function of the mutant LRRK2 neurons, we utilized a well-established FM 1-43 styryl dye based endocytic capacity assay and found that activity-dependent endocytosis was significantly decreased in LRRK2 R1441C/G dopaminergic neurons as compared to controls (**Figure 11G, H**). Of the proteins decreased in mutant LRRK2 neurons, auxilin has been linked to juvenile or early-onset PD via recently identified mutations (Edvardson et al., 2012; Koroglu et al., 2013; Olgiati et al., 2016).

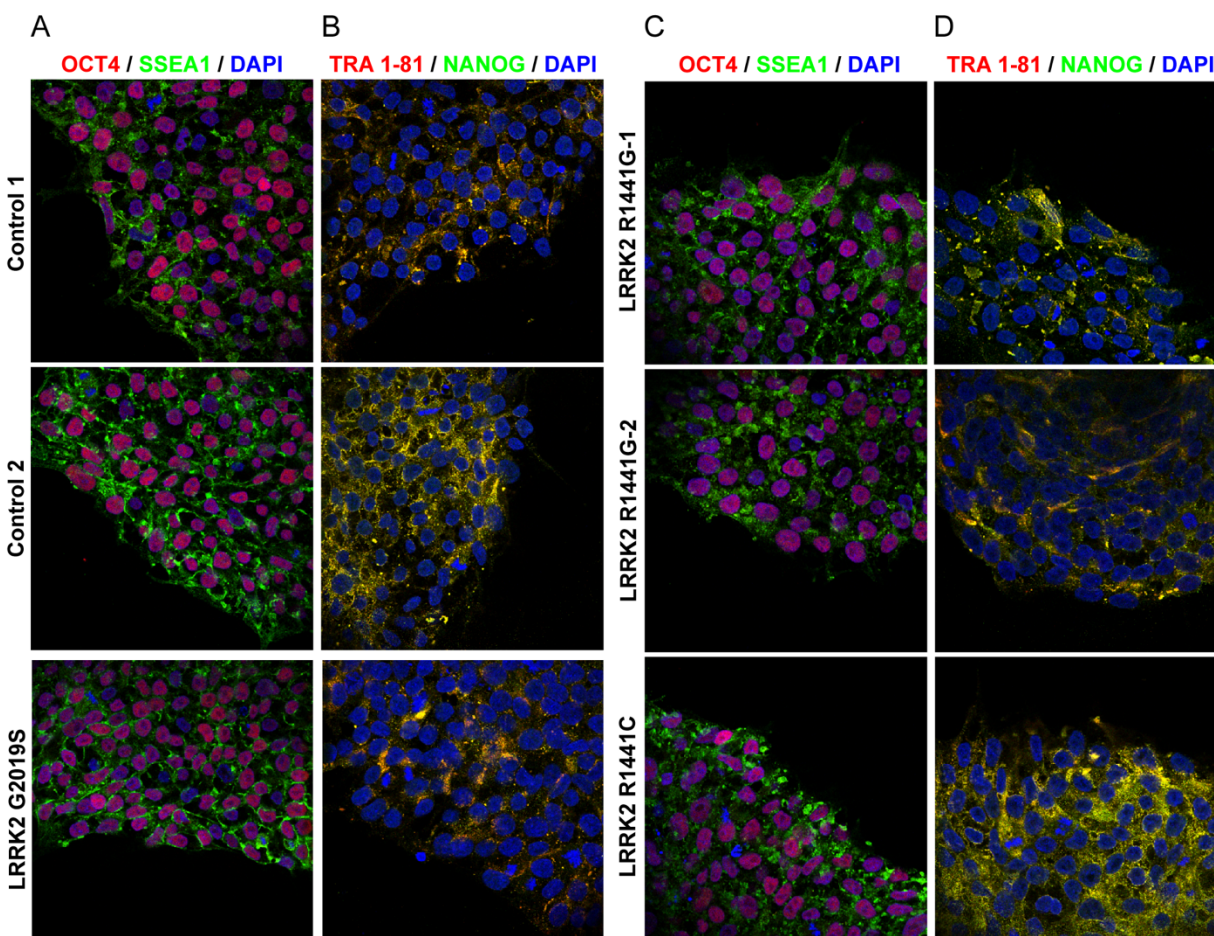


**Figure 9. Pluripotency marker expression in healthy controls and mutant LRRK2 induced pluripotent stem cells.** (A) Immunostain of iPSCs from two healthy controls and one LRRK2 PD patient harboring the G2019S mutation. Cells were stained with Oct4 (red), SSEA1 (green), and DAPI nuclear stain (blue). Merged images are represented above. (B) Immunostain of iPSCs from two healthy controls and one LRRK2 PD patient harboring the G2019S mutation. Cells were stained with Tra 1-81 (red), Nanog (green), and DAPI nuclear stain (blue). Merged images are represented above. (C) Immunostain of iPSCs from three LRRK2 PD patients harboring either R1441C or G mutations. Cells were stained with Oct4 (red), SSEA1 (green), and DAPI nuclear stain (blue). Merged images are represented above. (D) Immunostain of iPSCs from three LRRK2 PD patients harboring either R1441C or G mutations. Cells were stained with Tra 1-81 (red), Nanog (green), and DAPI nuclear stain (blue). Merged images are represented above.

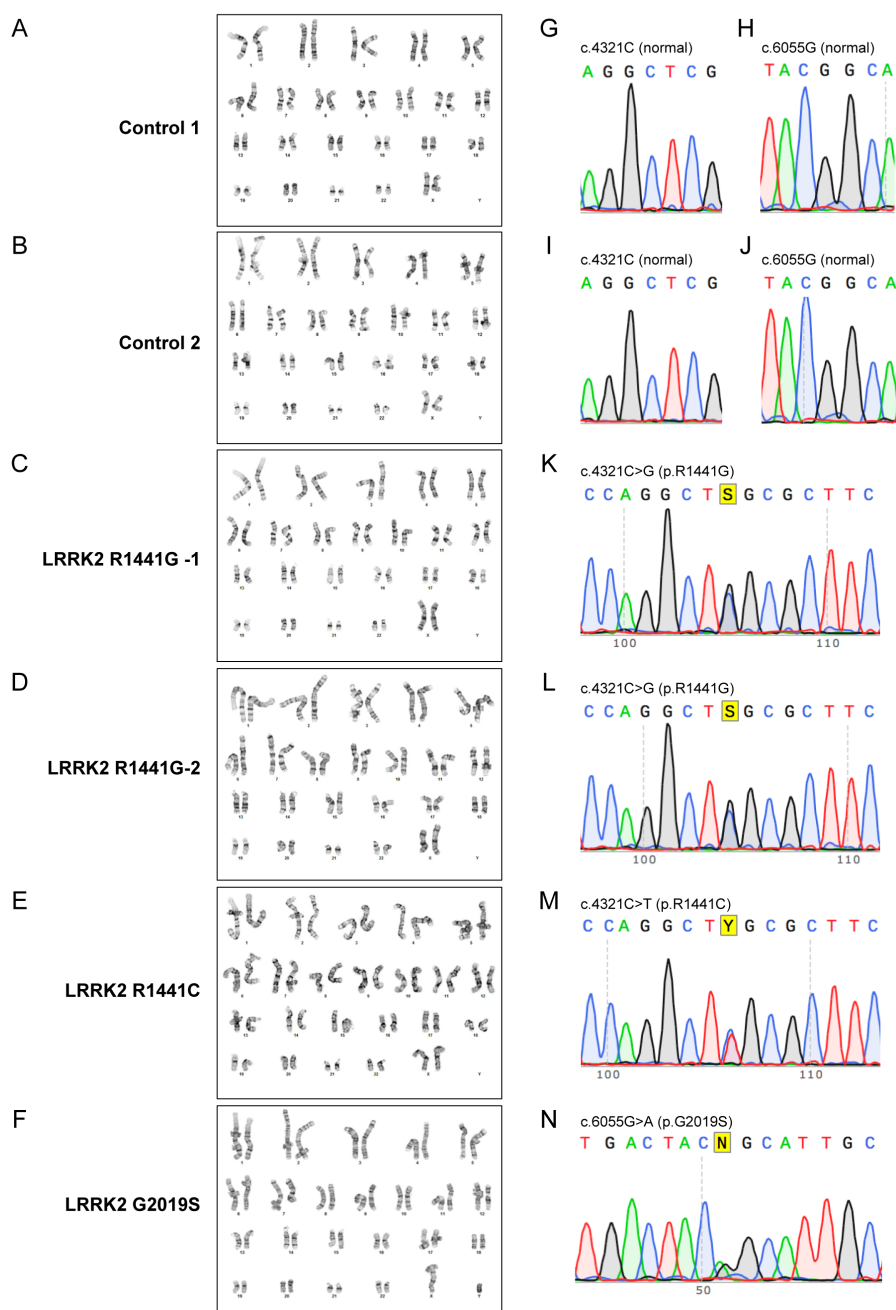


**Figure 10. G-band karyotyping analysis and Sanger sequencing results for reprogrammed cell lines.** (A, B) Standard G-band karyotype for control iPSCs 1 and 2. (C-F) Standard G-band karyotype for mutant LRRK2 R1441C/G and G2019S iPSCs. (G-J) Sanger sequencing results for control iPSCs 1 and 2. Results revealed normal genomic DNA sequences for LRRK2 exons 31 and 41 (exons that contain the R1441C/G/H and G2019S mutations, respectively). (K, L) Sanger sequencing results for mutant LRRK2 R1441G iPSCs. Results reveal heterozygous C to G mutation (“S”) in mutant LRRK2 R1441G iPSCs. (M) Sanger sequencing results for mutant LRRK2 R1441C iPSC. Results reveal heterozygous C to T mutation (“Y”) in mutant LRRK2 R1441C iPSC. (N) Sanger sequencing results for mutant LRRK2 G2019S iPSC. Results reveal heterozygous G to A mutation (“N”) in mutant LRRK2 G2019S iPSC.

To further determine whether an altered synaptic proteome and endocytic capacity might disrupt synaptic vesicle density and morphology in LRRK2 PD patient neurons, we analyzed iPSC-derived dopaminergic neurons by transmission electron microscopy (TEM). LRRK2 R1441C dopaminergic neurons showed significantly reduced synaptic vesicle densities by ~40% compared to healthy control neurons (**Figure 12A, C**), and contained dense structures lacking distinct surrounding membranes, consistent with the membraneless clathrin cages that were observed in auxilin knockout mice (Hirst et al., 2008; Yim et al., 2010). This previous study found that the appearance of membraneless clathrin cages was the result of defective clathrin uncoating due to loss of auxilin function (Hirst et al., 2008; Yim et al., 2010). Additionally, the membraneless clathrin cages observed in mutant LRRK2 neurons was not the result of improper fixation, as synaptic plasma membranes were still clearly observed in these neurons. An increase in enlarged endosomal-like vacuoles were also observed in the presynaptic terminal of LRRK2 R1441C neurons, a further indication of defective SVE (**Figure 12B, D**) (Jakobsson et al., 2008; Zhang et al., 1998).

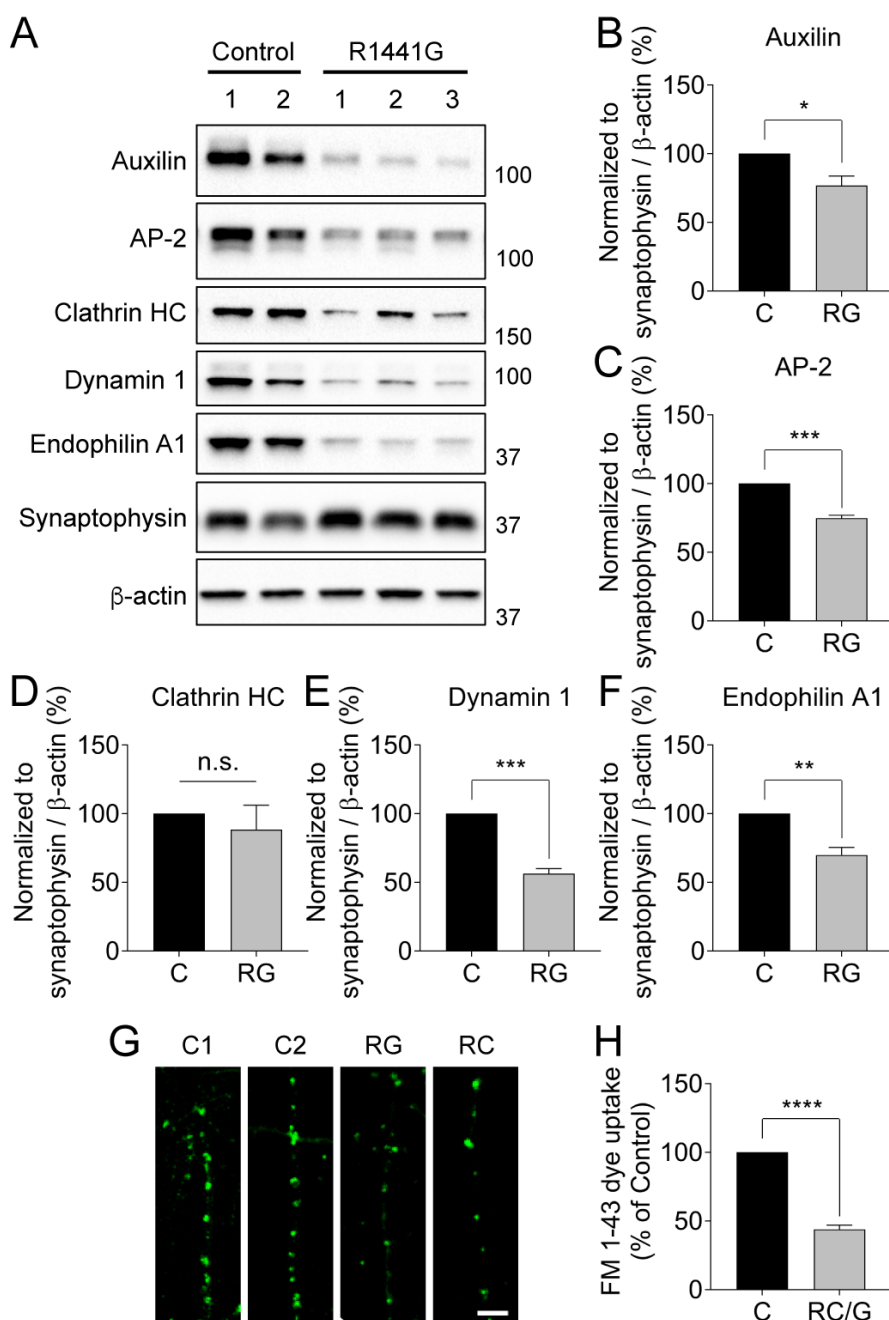


**Figure 11. Dopaminergic neurons from patients with LRRK2-linked PD exhibit decreased levels of SVE proteins.** (A) Western blot analysis of day 70 dopaminergic neurons probed with auxilin, adaptor protein 2 (AP-2), clathrin heavy chain (clathrin HC), dynamin 1, and endophilin A1. Synaptophysin and  $\beta$ -Actin were used as loading controls. (B-F) Quantification of Western blots in (A), normalized to both synaptophysin and  $\beta$ -Actin protein signals. (G) Representative images of FM 1-43 labeling in human dopaminergic neurons at day 120. Scale bar (white) = 5  $\mu$ m. (H) Quantification of FM 1-43 intensity per length of neurite. All data from control lines (C) and similar LRRK2 R1441G (RG) or R1441C (RC) clones were grouped preceding statistical analysis. The results were analyzed using unpaired t test (\* $p < 0.05$ , \*\* $p > 0.005$ , \*\*\* $p < 0.0005$ , \*\*\*\* $p < 0.00005$ ), with all error bars representing SEM,  $n=3$ .

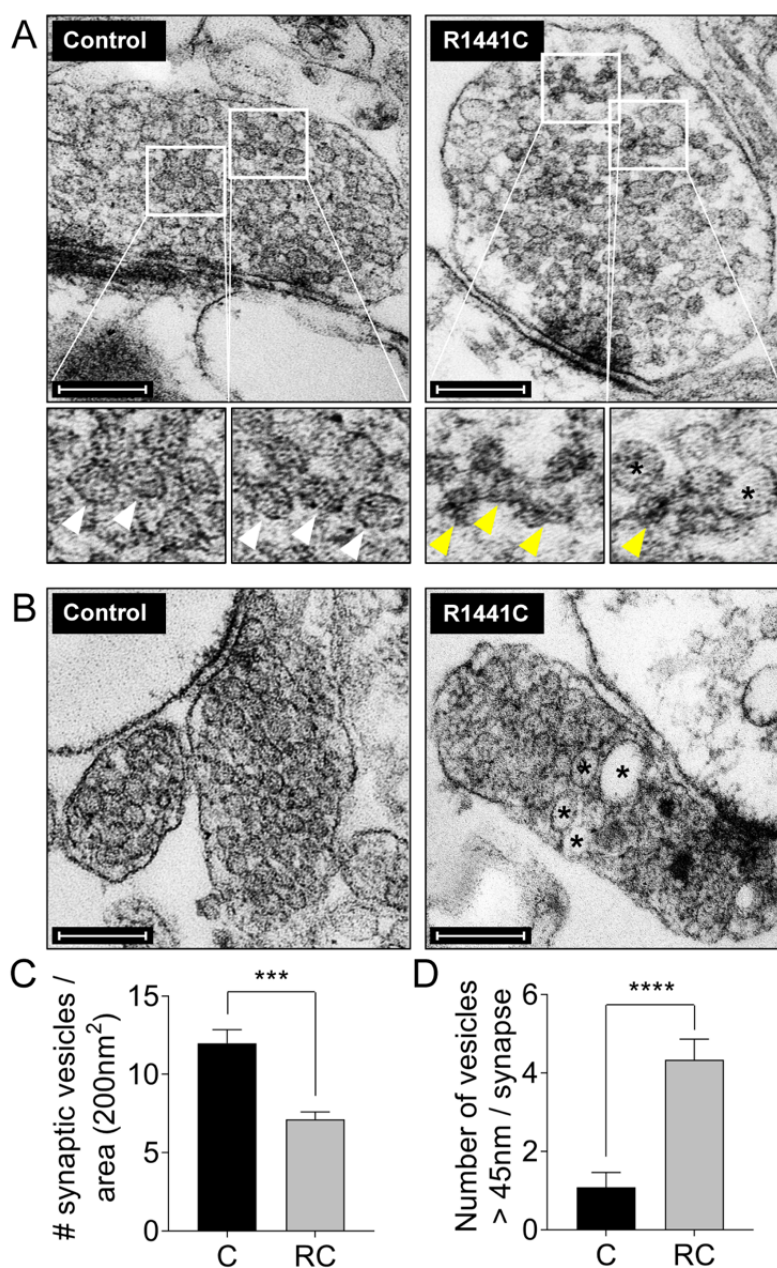


**Figure 12. Synaptic abnormalities in mutant LRRK2 dopaminergic neurons.** (A) Transmission electron microscopy (TEM) analysis of human dopaminergic neurons at day 100, scale bar 200 nm. Bottom two panels display higher magnification of insets in upper panel to show the presence of membraneless clathrin cages and enlarged endosomal-like (black asterisks) vacuoles in mutant neurons. Insets: synaptic vesicles are identified with white (control) and membraneless clathrin cages are indicated with yellow (mutant) arrowheads. (B) TEM analysis of enlarged endosomal-like vacuoles (black asterisks) in dopaminergic neurons. (C) Quantification of synaptic vesicle density in (A). (D) Quantification of the number of enlarged synaptic compartments per synapse in (B). All comparisons were made between control (C) and LRRK2 R1441C (RC) dopaminergic neurons and results were analyzed using an unpaired t test (\*\*\*) $p < 0.0005$ , (\*\*\*\*) $p > 0.00005$ , with error bars representing SEM,  $n=10$  and  $12$  images, respectively.

The efficient packaging of dopamine (DA) into synaptic vesicles is dependent on properly regenerated synaptic vesicles at the presynaptic terminal (**Figure 20**) (Lotharius & Brundin, 2002). As we observed decreased synaptic vesicles in mutant LRRK2 neurons, we hypothesized that defective SVE might lead to elevated cytosolic DA levels, which can be further oxidized to generate toxic DA-quinones and aminochromes in the cell (Graham, 1978; Hastings, Lewis, & Zigmond, 1996). We found that oxidized DA levels were significantly increased in LRRK2 R1441C/G and G2019S dopaminergic neurons compared to healthy control neurons in a time-dependent manner (**Figure 13A-C and Figure 15A, B**). Importantly, tyrosine hydroxylase (TH) levels were unaltered, demonstrating that increased oxidized DA was not due to increased DA synthesis in LRRK2 mutant dopaminergic neurons (**Figure 14A, B**). Our previous work showed that increased oxidized DA modifies the lysosomal hydrolase, glucocerebrosidase (GCase), leading to decreased activity (Burbulla et al., 2017), and that increased  $\alpha$ Synuclein ( $\alpha$ Syn) levels are correlated with decreased GCase activity (Mazzulli et al., 2011). Both LRRK2 R1441C/G and G2019S dopaminergic neurons, which had increased levels of oxidized DA, additionally displayed decreased GCase activity and increased  $\alpha$ Syn levels compared to healthy control neurons (**Figure 13D-F and Figure 15C-E**).

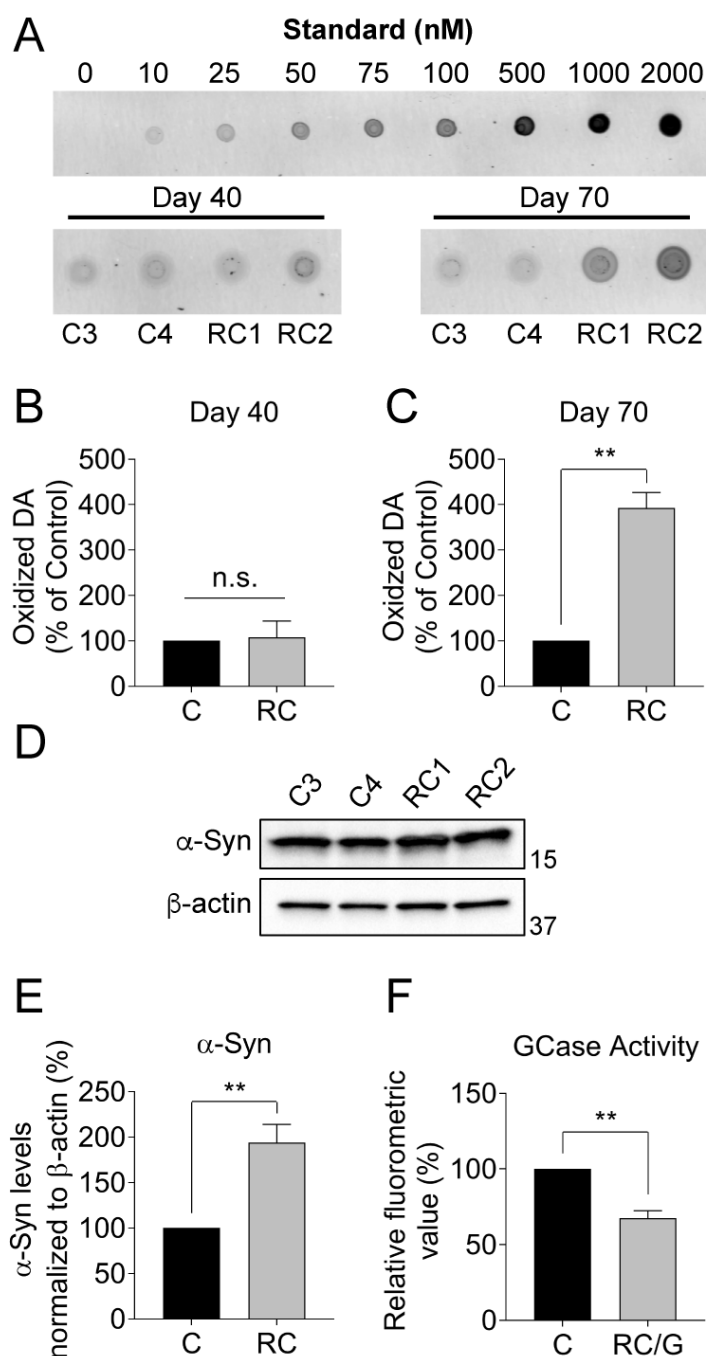


**Figure 13. LRRK2 R1441C/G dopaminergic neurons display increased levels of oxidized DA,  $\alpha$ Syn accumulation, and decreased GCCase activity.** (A) nIRF analysis of human dopaminergic neurons at day 40 and 70. (B-C) Quantification of oxidized DA levels in dopaminergic neurons at day 40 and 70, respectively. (D) Western blot analysis of human dopaminergic neurons at day 100. The blot was probed with  $\alpha$ Syn and  $\beta$ -actin antibodies. (E) Quantification of (D). (F) GCCase activity in whole cell lysate of human dopaminergic neurons at day 100. All data from control (C) lines and similar LRRK2 R1441C (RC) or R1441G (RG) mutations were grouped preceding statistical analysis. The results were analyzed using unpaired t test or one-way ANOVA (\*\* $p < 0.005$ ), with all error bars representing SEM,  $n=3$ .

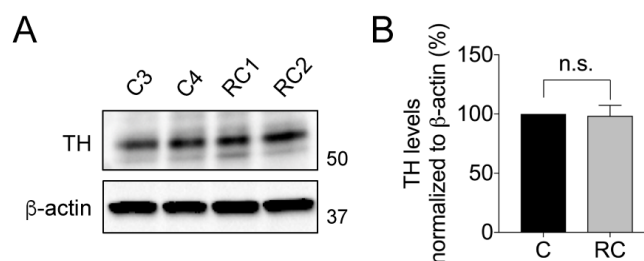


**Figure 14. Tyrosine hydroxylase levels from iPSC-derived dopaminergic neurons.** (A) Western blot analysis of corresponding human dopaminergic neurons at day 70 post-differentiation (Figure 12A, C). The Western blot was probed with tyrosine hydroxylase (TH), the enzyme that mediates dopamine synthesis, and  $\beta$ -actin (loading control). (B) Quantification of TH levels normalized to  $\beta$ -actin loading control. All data from control lines and similar mutation carrying LRRK2 R1441C (RC) clones were grouped preceding statistical analysis. The results were analyzed using unpaired t test, with all error bars representing SEM, n=3.

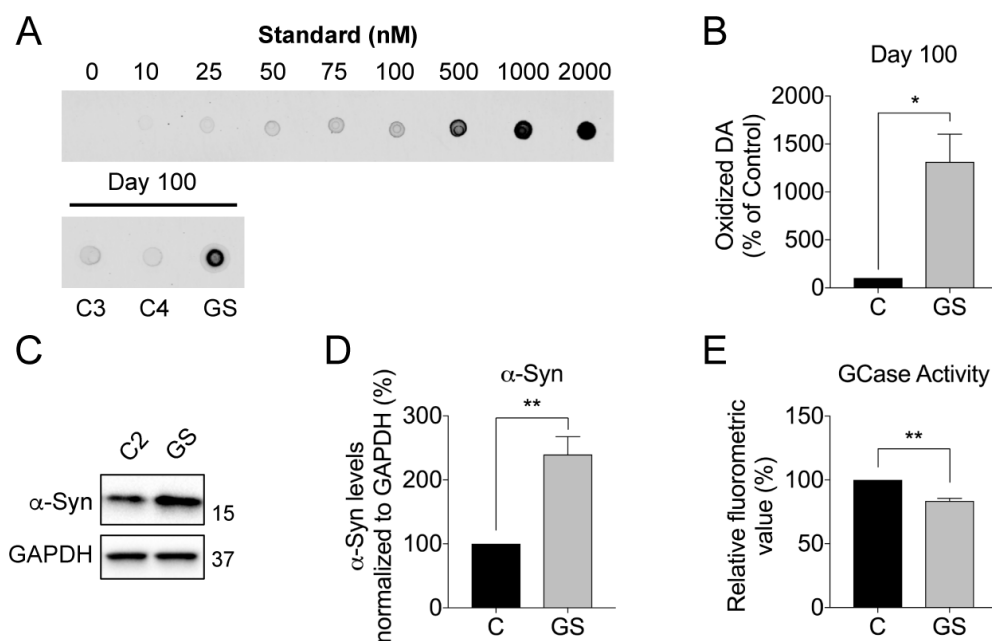


**Figure 15. LRRK2 G2019S dopaminergic neurons display increased levels of oxidized DA,  $\alpha$ Syn accumulation, and decreased GCase activity.** (A) nIRF analysis of control and mutant LRRK2 G2019S dopaminergic neurons at day 100 post-differentiation. (B) Quantification of oxidized DA levels in mutant LRRK2 G2019S dopaminergic neurons compared to controls at day 100. (C) Western blot analysis of control and mutant LRRK2 G2019S dopaminergic neurons at day 100 post-differentiation. The blot was probed with  $\alpha$ Syn (C-20) and GAPDH (loading control) antibodies. (D) Quantification of  $\alpha$ Syn levels normalized to GAPDH for control and mutant LRRK2 G2019S dopaminergic neurons. (E) GCase activity in whole cell lysate of iPSC-derived dopaminergic neurons from two controls and a mutant LRRK2 G2019S patient at day 100 post-differentiation. All data from control lines were grouped preceding statistical analysis. The results were analyzed using unpaired t test (\* $p < 0.05$ , \*\* $p < 0.005$ ), with all error bars representing SEM, n=3.

To examine whether increased oxidized DA observed in mutant LRRK2 dopaminergic neurons was mediated by mutant LRRK2 hyperphosphorylation of auxilin at Ser627, we generated phosphomutant auxilin S627A and S627D lentiviral constructs and transduced LRRK2 R1441C neurons at day 70 in culture (**Figure 16E-H**). We found that overexpression of phosphodeficient auxilin S627A was not sufficient to reduce the levels of accumulated oxidized DA while overexpression of phosphomimetic auxilin S627D further exacerbated the increase in oxidized DA levels in LRRK2 R1441C neurons (**Figure 16A-D**). Together, these data suggest that increased levels of phosphorylated auxilin at Ser627 contribute to the accumulation of oxidized DA similar to that observed in LRRK2 mutant neurons. Importantly, we overexpressed wild-type auxilin in healthy control and LRRK2 R1441G dopaminergic neurons and found that increased expression of wild-type auxilin led to significantly decreased oxidized DA (**Figure 17A, B and Figure 18A, B**). We further assessed the downstream phenotypes mediated by toxic oxidized DA accumulation and found that overexpression of wild-type auxilin further reduced  $\alpha$ Syn levels and significantly increased GCase activity in mutant LRRK2 R1441G neurons (**Figure 17C-E**). Moreover, SVE synaptic protein levels in mutant LRRK2 neurons, such as AP-2, clathrin, dynamin 1, and endophilin A1 remained reduced, suggesting that wild-type auxilin expression was responsible for attenuating the previously observed pathogenic phenotypes (**Figure 18A-F**). Concomitantly, knockdown of endogenous auxilin via shRNA lentiviral expression in healthy control dopaminergic neurons led to the accumulation of oxidized DA compared to neurons transduced with a scramble control (**Figure 19A-D**). This supports our previous findings that deficiencies in SVE mediated through loss of auxilin function in part contributes to the accumulation of toxic oxidized DA species. Altogether, our results suggest that synaptic dysfunction mediated by mutant LRRK2 hyperphosphorylation of auxilin contributes to the accumulation of oxidized DA in mutant LRRK2 neurons which is attenuated by directly restoring auxilin function in SVE.

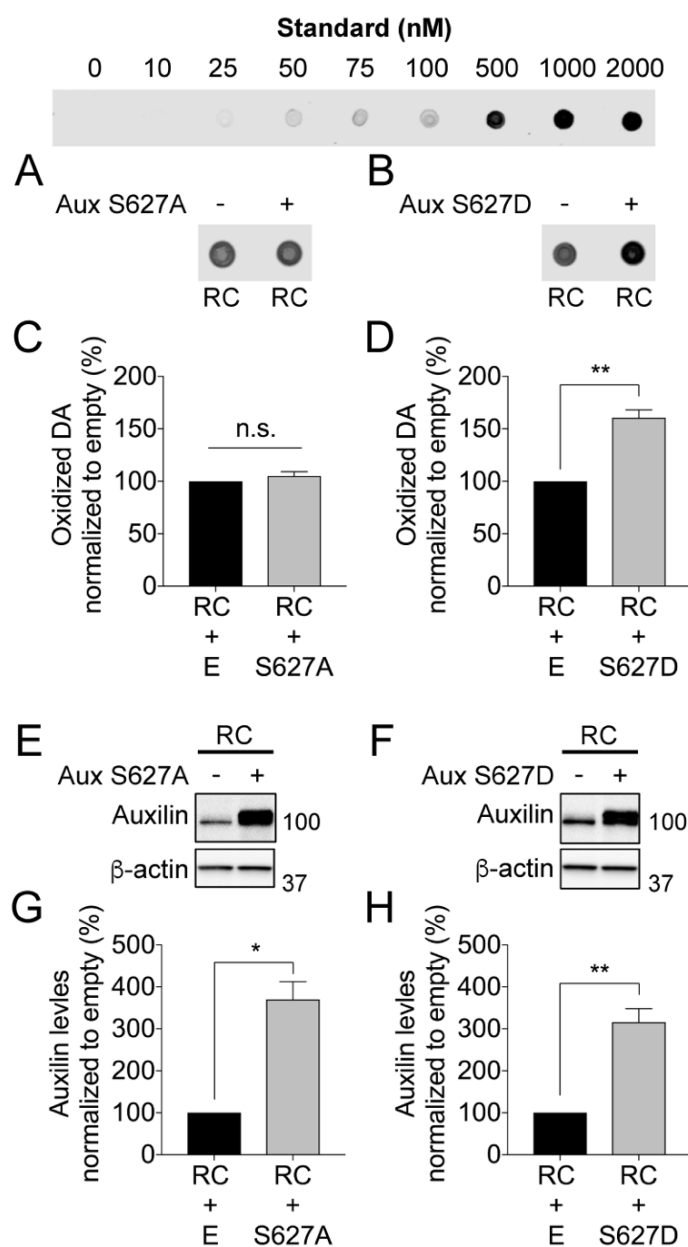


**Figure 16. Overexpression of phosphomutant auxilin does not attenuate increased oxidized DA levels in mutant LRRK2 neurons.** (A, B) nIRF analysis of mutant LRRK2 dopaminergic neurons at day 120 following transduction of either phosphodeficient or phosphomimetic auxilin for 30 days, starting at day 90 post-differentiation. (C, D) Quantification of oxidized DA levels in (A, B). (E, F) Western blot analysis of dopaminergic neurons following transduction with phosphodeficient or phosphomimetic auxilin at day 120. The blot was probed with auxilin and  $\beta$ -actin antibodies. (G, H) Quantification of (E, F). The results were analyzed using unpaired t test (\* $p < 0.05$ , \*\* $p < 0.005$ ), with all error bars representing SEM,  $n=3$ .

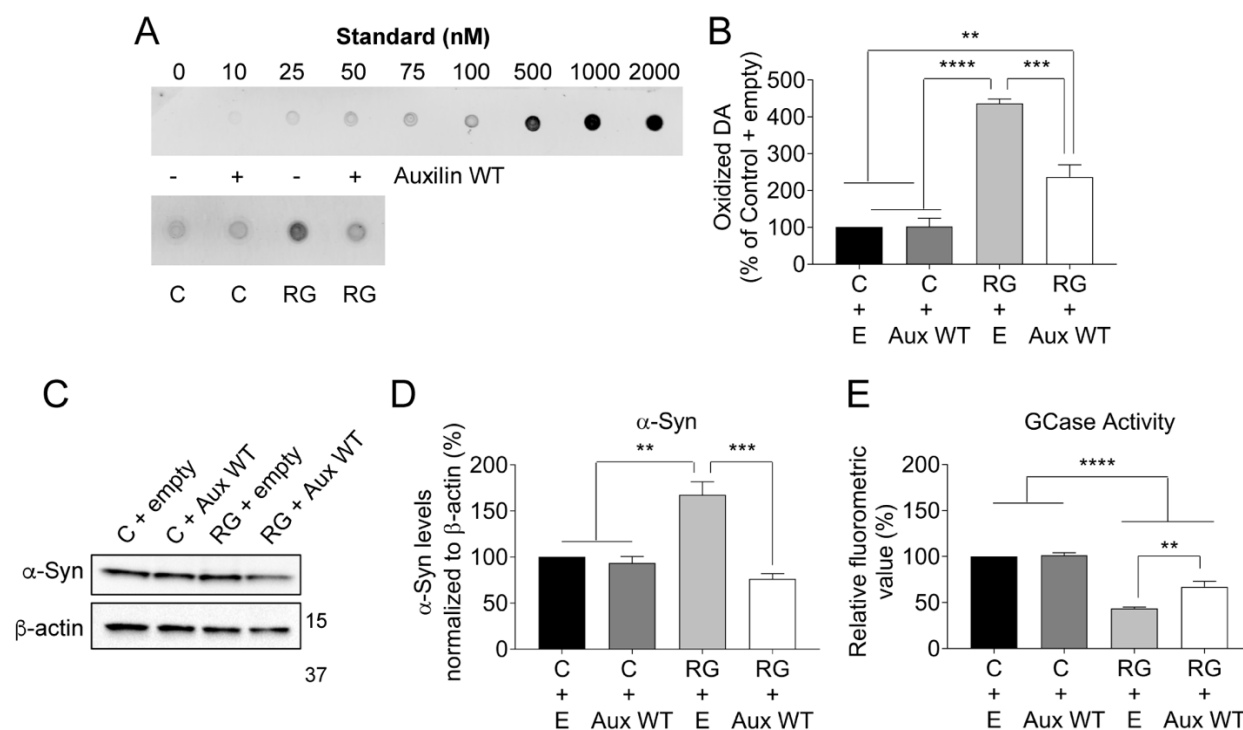


**Figure 17. Overexpression of wild-type auxilin reduces oxidized DA and attenuates downstream phenotypes in mutant LRRK2 neurons.** (A) nIRF analysis of human dopaminergic neurons at day 100 following transduction of either empty (E) vector or wild-type (WT) auxilin for 30 days, starting at day 70 post-differentiation. (B) Quantification of oxidized DA levels in (A). (C) Western blot analysis of dopaminergic neurons following transduction with auxilin WT at day 100. The blot was probed with  $\alpha$ Syn and  $\beta$ -actin antibodies. (D) Quantification of (C). (E) GCCase activity in whole cell lysate of transduced auxilin WT dopaminergic neurons at day 100. All data from control (C) lines and similar LRRK2 R1441C (RC) or R1441G (RG) mutations were grouped preceding statistical analysis. The results were analyzed using unpaired t test or one-way ANOVA (\*\* $p < 0.005$ , \*\*\* $p < 0.0005$ , \*\*\*\* $p < 0.00005$ ), with all error bars representing SEM,  $n=3$ .

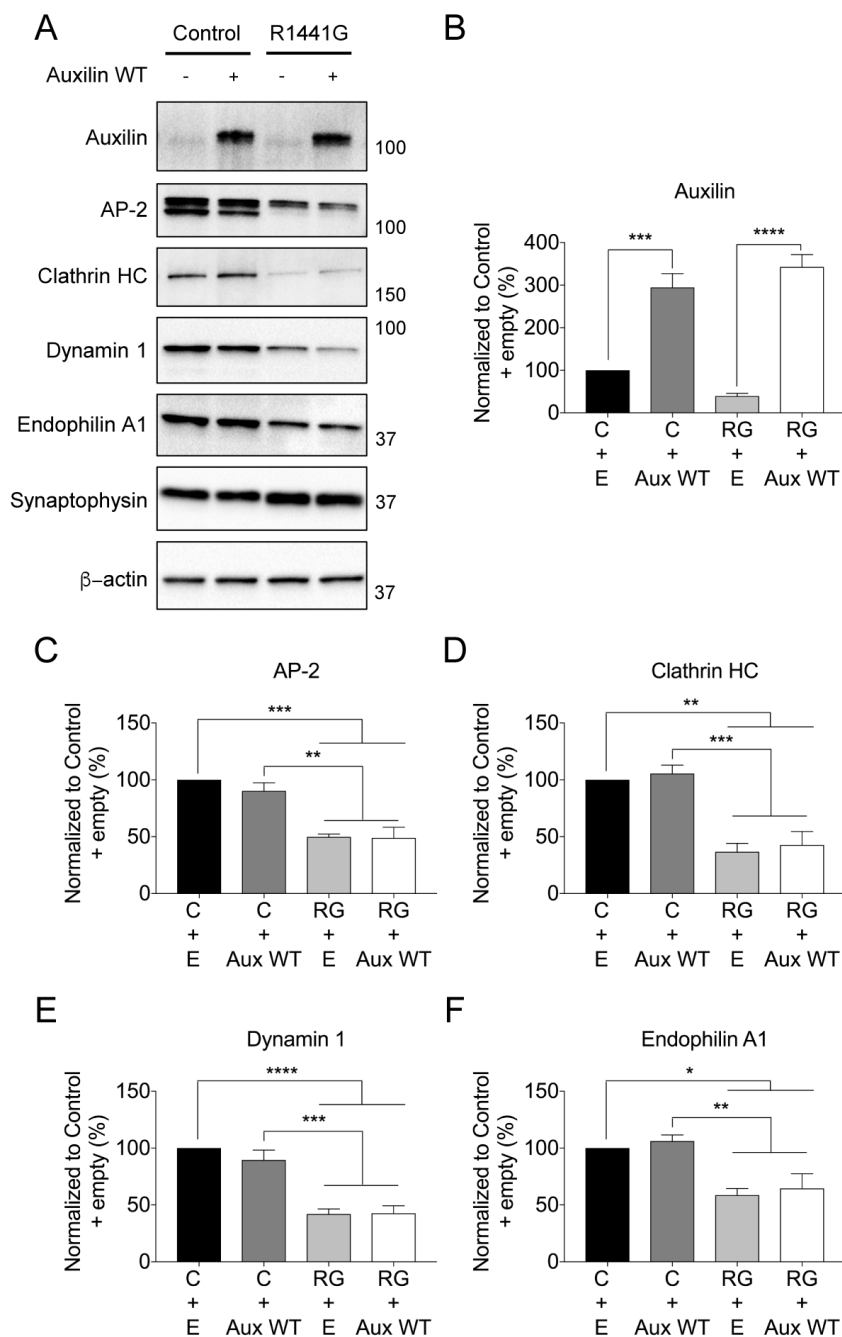


**Figure 18. Synaptic protein expression following wild-type auxilin transduction in human dopaminergic neurons.** (A) Western blot analysis of control and LRRK2 R1441G dopaminergic neurons transduced with either empty (E) or wild-type (WT) auxilin and day 100 post-differentiation. The Western blot was probed with auxilin, adaptor protein 2 (AP-2), clathrin heavy chain (HC), dynamin 1, and endophilin A1. Synaptophysin and  $\beta$ -Actin were used as loading controls. (B-F) Quantification of Western blots in (A), normalized to both synaptophysin and  $\beta$ -Actin protein signals. The results were analyzed using one-way ANOVA (\* $p < 0.05$ , \*\* $p < 0.005$ , \*\*\* $p < 0.0005$ , \*\*\*\* $p < 0.00005$ ), with all error bars representing SEM,  $n=3$ .

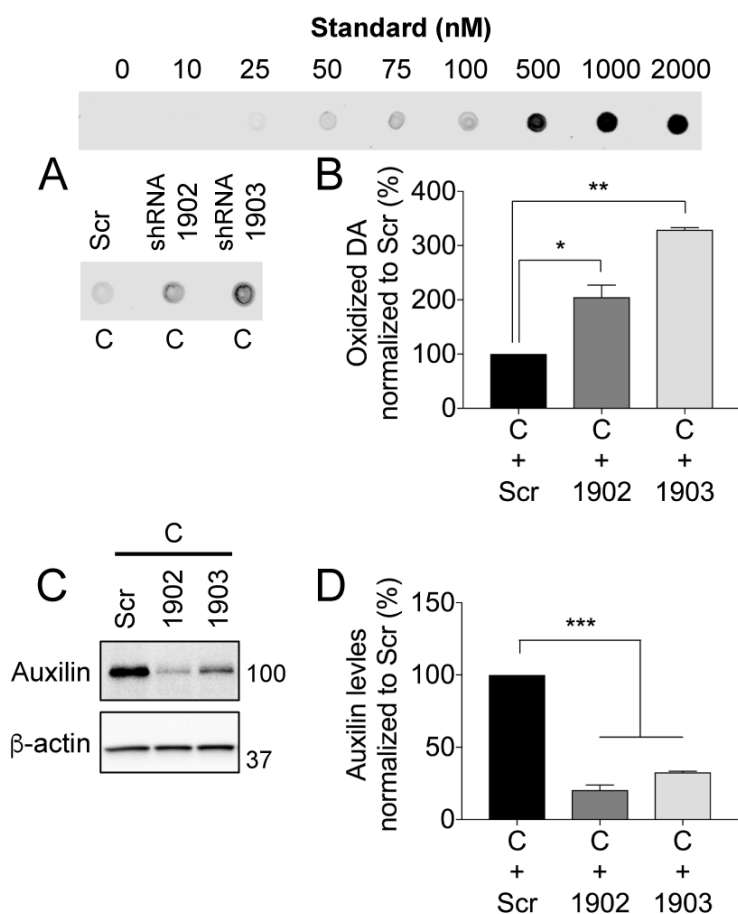


**Figure 19. Lentiviral shRNA-mediated auxilin knockdown leads to the accumulation of oxidized DA in control dopaminergic neurons.** (A) nIRF analysis of mutant LRRK2 dopaminergic neurons at day 100 following transduction with two independent auxilin shRNA (1902 and 1903) for 30 days, starting at day 70 post-differentiation. (B) Quantification of oxidized DA levels in (A). (C) Western blot analysis of dopaminergic neurons following transduction with auxilin shRNA at day 100. The blot was probed with auxilin and  $\beta$ -actin antibodies. (D) Quantification of (C). The results were analyzed using one-way ANOVA (\* $p < 0.05$ , \*\* $p < 0.005$ , \*\*\* $p < 0.0005$ ), with all error bars representing SEM,  $n=2$ .

## Conclusions

Mutations in *SYNJI* (synaptojanin 1) also lead to early-onset parkinsonism (Kirola et al., 2016; Krebs et al., 2013; Olgiati et al., 2014; Quadri et al., 2013), and loss of either endophilin A1 or synaptojanin 1 in knockout mouse models result in defective SVE (Cao et al., 2014; Kim et al., 2002; Milosevic et al., 2011). In line with this, we found that dopaminergic neurons derived from LRRK2 R1441G patients had decreased levels of SVE proteins, including auxilin, AP-2, endophilin A1, synaptojanin 1, and dynamin 1, as well as decreased activity-dependent endocytic capacity implying that SVE is impaired.

Using TEM, we also observed decreased synaptic vesicle density in presynaptic terminals of LRRK2 R1441C dopaminergic neurons indicative of defective SVE. This data is consistent with studies of knockout mouse models for endophilin A1, synaptojanin 1, dynamin 1, or auxilin (Cao et al., 2014; Ferguson et al., 2007; Kim et al., 2002; Milosevic et al., 2011; Yim et al., 2010). Additionally, auxilin knockout mouse models display an increased presence of membraneless clathrin cages, a unique structural feature that results from delays in SVE due to loss of auxilin function (Hirst et al., 2008; Yim et al., 2010). We observed a similar structural feature in LRRK2 R1441C dopaminergic nerve terminals suggesting that synaptic defects in mutant LRRK2 neurons are mediated through auxilin loss of function. In addition to this, several studies have found that delays in SVE result in enlarged endosomal-like structures which we similarly observed in LRRK2 R1441C dopaminergic neurons (Jakobsson et al., 2008; Zhang et al., 1998), providing further support that SVE is impaired through loss of auxilin function by PD-linked mutations in LRRK2.

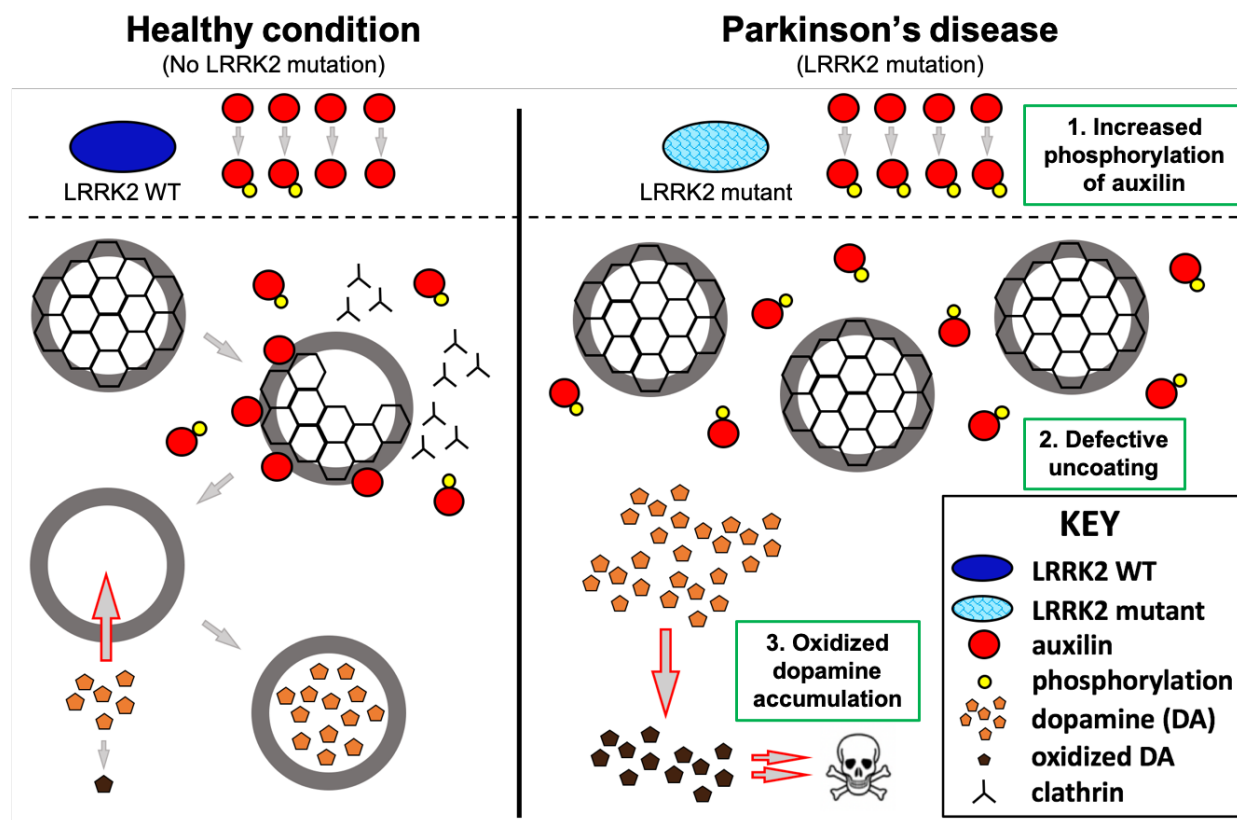


**Figure 20. Summary diagram highlighting LRRK2's involvement in synaptic dysfunction and Parkinson's disease pathogenesis.** Under normal, healthy conditions, wild-type LRRK2 phosphorylates auxilin at homeostatic levels. The balance between phosphorylated and unphosphorylated states allows auxilin to interact with clathrin-coated synaptic vesicles budding from the plasma membrane. Once the clathrin coat is removed, newly synthesized dopamine (DA) can be packaged into synaptic vesicles, thereby reducing the levels of cytosolic DA and consequently the levels of oxidized DA. In LRRK2 mutant conditions, which lead to increased kinase activity, auxilin is hyperphosphorylated preventing it from interacting with clathrin on newly budding vesicles. As a result, the clathrin coat cannot be removed and cytosolic and subsequently oxidized DA accumulates within the cell. High levels of oxidized DA can lead to  $\alpha$ Synuclein accumulation and decreased GCase activity resulting in dopaminergic neuron degeneration.

Our recent data showed that dopamine plays an important role in dysfunction and degeneration of midbrain dopaminergic neurons (Burbulla et al., 2017). In the nerve terminal, DA is rapidly packaged into an incoming population of regenerated synaptic vesicles. Efficient vesicular function and storage of DA is critical for maintaining low levels of cytosolic DA (**Figure 20**) (Lotharius & Brundin, 2002; Vergo, Johansen, Leist, & Lotharius, 2007). As cytosolic DA can be rapidly oxidized (Lotharius & Brundin, 2002), we observed increased levels of oxidized DA in

LRRK2 R1441C/G and G2019S dopaminergic neurons indicative of increased cytosolic DA levels. We also previously showed that increased oxidized DA can modulate GCase at a cysteine residue within its active domain and that increased  $\alpha$ Syn levels correlate with decreased GCase activity (Burbulla et al., 2017; Mazzulli et al., 2011). Consistent with this, we also found decreased GCase activity and increased  $\alpha$ Syn levels in mutant LRRK2 dopaminergic neurons. Importantly, by expressing wild-type auxilin but not phosphomutant auxilin S627A or S627D, the levels of oxidized DA could be reduced, and downstream DA-mediated effects attenuated, highlighting the importance of mutant LRRK2-mediated auxilin dysfunction in the generation of toxic oxidized DA following defective SVE.

In conclusion, we find that LRRK2 kinase activity regulates the phosphorylation state of auxilin, an important mediator of SVE linked to juvenile and early-onset forms of atypical parkinsonism (Edvardson et al., 2012; Koroglu et al., 2013; Olgiati et al., 2016), resulting in disrupted SVE in LRRK2 patient-derived dopaminergic neurons. Moreover, these defects in synaptic function may further contribute to DA-mediated toxicity and ultimately drive dopaminergic neurodegeneration in LRRK2-linked PD.

## CHAPTER 4.

### DISCUSSION

#### Summary

SVE is controlled by a class of structurally distinct proteins, termed dephosphins, that are regulated through phosphorylation–dephosphorylation events (Cousin & Robinson, 2001). This term was originally used to refer to a list of less than 10 proteins (Cousin & Robinson, 2001). However, new evidence revealed that more synaptic proteins involved in synaptic vesicle recycling are regulated by kinases, but whether they are also regulated by the  $\text{Ca}^{2+}$ -dependent phosphatase, calcineurin, remains to be determined. Our results indicate that auxilin is highly phosphorylated within its PTEN-like and clathrin-binding domains (**Figure 4A and Figure 8A**). As previous studies have also identified phosphosites on endophilin A1 and synaptojanin 1, our results and others indicate that these proteins can be phosphoregulated during SVE (Ambroso et al., 2014; Islam et al., 2016; Matta et al., 2012; Pan et al., 2017). In addition, our unbiased phosphoanalysis of wild-type auxilin also identified many additional phosphorylation sites not regulated by LRRK2 (data not shown). Therefore, future studies should focus on identifying additional kinases that may regulate SVE, either through auxilin or other key proteins involved in this process.

In this study, our results indicate that LRRK2, a PD-linked gene (Funayama et al., 2002; Zimprich et al., 2004), encodes an important kinase that is involved in regulatory posttranslational modifications of synaptic proteins involved in SVE. It was previously shown that LRRK2 phosphorylates both endophilin A1 and synaptojanin 1 (Ambroso et al., 2014; Islam et al., 2016; Matta et al., 2012; Pan et al., 2017), two independent synaptic proteins with distinct roles in SVE (Saheki & De Camilli, 2012). Here, we show that LRRK2 also phosphorylates auxilin (Nguyen &

Krainc, 2018), which is involved in the removal of the clathrin-coat (Eisenberg & Greene, 2007; Greener et al., 2001; Ma et al., 2002; Massol, Boll, Griffin, & Kirchhausen, 2006; Morgan et al., 2001; Rapoport et al., 2008). Importantly, we show that LRRK2 phosphorylates auxilin in the clathrin-binding domain at Ser627 and that posttranslational modification of this site leads to altered auxilin binding to clathrin (**Figure 7A-F**). As mutations in LRRK2 lead to an increase in kinase activity (Steger et al., 2016), we conclude that enhancing the ratio of phosphorylated to unphosphorylated auxilin at position Ser627 results in loss of auxilin function in SVE (**Figure 20**). Interestingly, loss of function mutations in *DNAJC6*, the gene encoding auxilin, are linked to juvenile or early atypical parkinsonism independently of LRRK2 mutations (Edvardson et al., 2012; Koroglu et al., 2013; Olgiati et al., 2016), suggesting that LRRK2 may act upstream of auxilin.

Our work identifies a new mechanistic convergence between two PD-linked genes at the synapse, specifically in SVE. This highlights the importance of using genetics to discover novel disease mechanisms that may contribute to PD pathogenesis. For example, endophilin A1 knockout mice displayed a significant increase in the E3 ubiquitin ligase parkin levels (Cao et al., 2014). This study found that parkin is responsible for ubiquitinating endophilin A1 and its interaction partners (Cao et al., 2014). Although canonical E3 ubiquitin ligase activity targets proteins for degradation by the proteasome (Riley et al., 2013; Yoshii et al., 2011), several new lines of evidence suggest that ubiquitination may also facilitate interactions between SVE proteins (Cao et al., 2014; Fallon et al., 2006; Oldham, Mohny, Miller, Hanes, & O'Bryan, 2002; Stamenova et al., 2007; Trempe et al., 2009). As recent studies have independently linked several non-synaptic PD genes to SVE dysfunction (Inoshita et al., 2017; Kyung et al., 2018), future studies should focus on identifying the non-canonical functions of PD-linked genes, such as *VPS35* and *PRKN*, in SVE.

We generated iPSC-derived dopaminergic neurons from LRRK2 patients harboring either the R1441C/G or G2019S mutations, both of which are the most common pathogenic mutations in LRRK2 (Funayama et al., 2002; Zimprich et al., 2004). LRRK2 mutant dopaminergic neurons displayed synaptic defects such as decreased SVE protein levels (auxilin, endophilin A1, dynamin 1, and AP-2) and endocytic capacity (**Figure 11A-H**). These defects further led to decreased synaptic vesicle density and an increase in the levels of enlarged vesicles and membraneless clathrin cages reminiscent of those described in auxilin knockout mouse models (**Figure 12A-D**) (Hirst et al., 2008; Yim et al., 2010). Together, this indicates that mutant LRRK2 regulation of auxilin at Ser627 results in a loss of auxilin function during SVE.

Furthermore, as functional SVE is important for the generation of synaptic vesicles to package newly synthesized DA that is generated in the cell (Lotharius & Brundin, 2002), disruptions in SVE potentially negatively affect DA neurotransmitter synthesis. As a result of SVE dysfunction, cytosolic DA accumulates within the cell and a subset of that cytosolic DA becomes oxidized or is metabolized by monoamine oxidase (MAO) (Meiser, Weindl, & Hiller, 2013). We show that cytosolic DA is increased in LRRK2 mutant neurons through the increase in oxidized DA levels (**Figure 13A-C and Figure 15A, B**). Additionally, accumulation of oxidized DA further led to downstream toxic events such as  $\alpha$ Syn accumulation and decreased GCase activity (**Figure 13D-F and Figure 15C-E**). Importantly, these phenotypes observed in the LRRK2 mutant dopaminergic neurons were attenuated when wild-type auxilin was overexpressed (**Figure 17A-E**). However, overexpression of phosphodeficient (S627A) or phosphomimetic auxilin (S627D) were unable to reverse the phenotypes observed (**Figure 16A-H**). We conclude that the dynamic exchange between phosphorylated and desphosphorylated auxilin is necessary for its proper function. Therefore, preventing auxilin phosphorylation or desphosphorylation would exacerbate any mutant LRRK2-mediated loss of auxilin function in SVE.

### ***Synaptic vesicle endocytosis dysfunction in dopaminergic neurodegeneration***

As SVE is not unique to dopaminergic neurons of the ventral midbrain, the specific vulnerability of this neuronal population in PD to deficits in SVE has not been clear. PD-linked *SYNJ1* R258Q mouse models revealed delays in SVE and marked changes in dopaminergic axon terminals in the dorsal striatum, highlighting a region-specific vulnerability of these neurons to synaptojanin 1 dysfunction (Cao et al., 2017). Additionally, decreased synaptic densities and an accumulation of CCVs, specifically in dopaminergic neurons, were also reported in *SYNJ1* heterozygous knockout and *LRRK2* G2019S transgenic mice leading to dystrophic axons and selective degeneration of these neurons (Pan et al., 2017).

One possibility may be the sensitivity of dopaminergic neurons to the accumulation of cytosolic dopamine (DA). Acute overexpression of human  $\alpha$ Syn, which was previously linked to SVE dysfunction, in a rat model led to the specific degeneration of striatal terminals in the absence of nigral cell death (Busch et al., 2014; Medeiros, Soll, Tessari, Bubacco, & Morgan, 2017; Phan et al., 2017; Vargas et al., 2014). This may be due in part to  $\alpha$ Syn-induced dopamine leakage from synaptic vesicles (Plotegher et al., 2017; Ysselstein et al., 2015). DA is packaged into synaptic vesicles regenerated from SVE using a proton gradient created by vATPases located on the membrane surface of synaptic vesicles (Eiden, Schafer, Weihe, & Schutz, 2004). In contrast to previous work suggesting that synaptic vesicle acidification is needed for removal of the clathrin-coat, a recent study found that acidification of the vesicle could not occur while the clathrin-coat was retained (Farsi et al., 2018). Specifically, vATPase activity is sterically inhibited by the clathrin-coat and is restored once the coat is removed through the function of auxilin (Farsi et al., 2018). This result suggests that a delay in SVE could lead to improper packaging of DA into vesicles leading to increased cytosolic DA, ultimately contributing to dopaminergic

neurodegeneration beginning at the axon terminals. In line with this, we show that knockdown of auxilin in control dopaminergic neurons led to the accumulation of oxidized DA (**Figure 19**).

Moreover, SNc dopaminergic neurons are subject to increased levels of oxidative stress resulting from the high metabolic activity that is required to support their extensive axonal arborization (Giguere et al., 2018; Pacelli et al., 2015). As a consequence of oxidative phosphorylation, toxic reactive oxygen species (ROS) including oxygen radicals, semiquinones, quinones, and H<sub>2</sub>O<sub>2</sub> are produced and collectively contribute to oxidative stress (Zaichick et al., 2017). These ROS can react with cytosolic DA, leading to the formation of highly reactive dopamine quinones (Dias, Junn, & Mouradian, 2013; Jana et al., 2011). In addition, cytosolic DA metabolized by monoamine oxidase (MAO) located in the outer mitochondrial membrane also produces H<sub>2</sub>O<sub>2</sub> byproducts, thus further exacerbating accumulation of ROS and toxic dopamine quinones (Meiser et al., 2013). Nigral dopaminergic neurons also employ protective mechanisms such as the formation of neuromelanin and sequestration of DA into synaptic vesicles to minimize DA oxidation (Sulzer et al., 2000). We recently showed that PD patient neurons carrying mutations in *DJ-1* which lead to loss of mitochondrial antioxidant function exhibit increased levels of oxidized DA, which further result in downstream toxic effects including lysosomal dysfunction and  $\alpha$ Syn accumulation (Burbulla et al., 2017). Specifically, oxidized DA was also found to modify the lysosomal enzyme glucocerebrosidase on a critical cysteine residue leading to a decrease in its enzymatic activity (Burbulla et al., 2017). We thus hypothesized that delays in SVE can lead to increased levels of unpackaged, cytosolic DA that is then subject to oxidation. Indeed, mutant LRRK2-mediated auxilin dysfunction resulted in increased levels of oxidized DA in patient-derived dopaminergic neurons that was partially rescued by expression of auxilin (Nguyen & Krainc, 2018). Taken together, these studies highlight a connection between synaptic,

mitochondrial, and lysosomal function and suggest that defects in these pathways may synergize to contribute to PD pathogenesis (**Figure 21**).

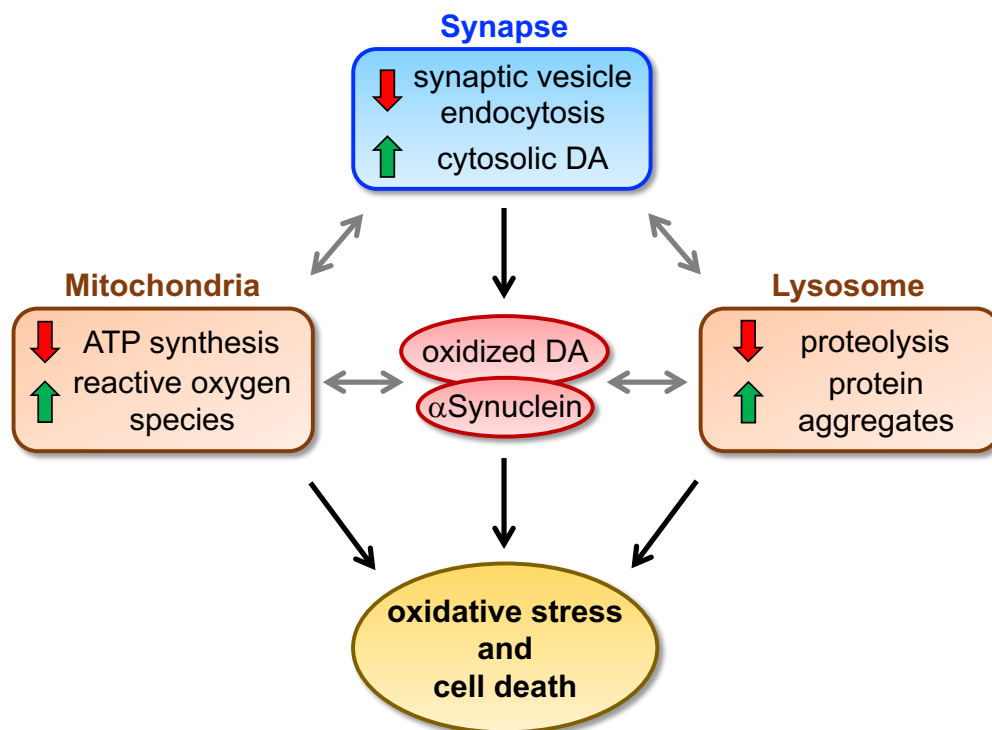


**Figure 21. Deficits in synaptic vesicle endocytosis potentially mediate dopaminergic neurodegeneration through intersections with mitochondrial and lysosomal dysfunction.** Our recent work has identified a pathway for cytosolic oxidized dopamine (DA) and  $\alpha$ Synuclein accumulation due to dysfunction in synaptic vesicle endocytosis in human-derived dopaminergic neurons. These byproducts can further inhibit mitochondrial function by impairing ATP production, and also increase reactive oxygen species production via mitochondrial-mediated metabolism of cytosolic DA. In addition, they can also contribute to lysosomal dysfunction which may further involve defective proteolytic turnover of synaptic proteins and the accumulation of insoluble protein aggregates. Ultimately, the convergence of synaptic, mitochondrial and lysosomal dysfunction may together exacerbate cytosolic DA and  $\alpha$ Synuclein accumulation, and ultimately result in cell death in PD.

Another possibility for the selective vulnerability of nigral dopaminergic neurons to SVE deficits is their pacemaking function, which modulates the sustained release of dopamine to targeted brain regions such as the striatum (Guzman et al., 2009). Pacemaking activity leads to large influxes of  $\text{Ca}^{2+}$  into the neuron which can stimulate the  $\text{Ca}^{2+}$ -dependent calcineurin to initiate endocytosis of synaptic vesicles (Cousin & Robinson, 2001). Mitochondria located at the

synapse also contribute to the maintenance of pacemaker activity by buffering  $\text{Ca}^{2+}$  when cytosolic levels are high (Zaichick et al., 2017). Of note, increased mitochondrial calcium stores have been shown to lead to mitochondrial dysfunction, suggesting that excessive cytosolic DA, ROS accumulation, and  $\text{Ca}^{2+}$  buffering by mitochondria may together compromise nigral dopaminergic function (Meiser et al., 2013; Zaichick et al., 2017).

### ***Dysfunction of mitochondria and autophagy at the synapse***

Mitochondria perform crucial energetic roles for active neurons by providing ATP to power SVE, which replenishes synaptic vesicles to sustain repeated release of neurotransmitters (Rangaraju, Calloway, & Ryan, 2014; Reeve et al., 2018; Sobieski, Fitzpatrick, & Mennerick, 2017). In agreement with this, oligomycin-treatment of cells to block mitochondrial ATP synthesis led to complete cessation of SVE following sustained high-frequency stimulation (Pathak et al., 2015). Furthermore, inhibition of mitochondrial fission, which reduces mitochondrial mass in axon terminals, led to the preferential degeneration of nigral dopaminergic neurons in mice (Berthet et al., 2014). This degeneration initiated at presynaptic terminals through the loss of striatal tyrosine hydroxylase (TH) signal while ~65% of TH-positive neurons in the SNc remained (Berthet et al., 2014).

Aside from the regulation of SVE at the synapse, several endocytic genes have also been identified as critical modulators of synaptic autophagy, a pathway for maintaining synaptic protein homeostasis and turnover via the lysosome following neurotransmission (Soukup, Vanhauwaert, & Verstreken, 2018). Altered synaptojanin 1 function blocked autophagosome maturation in presynaptic terminals through the accumulation of Atg18a, an autophagy-related protein, in *SYNJI* R258Q patient-derived dopaminergic neurons (Vanhauwaert et al., 2017). This dysfunction ultimately led to dopaminergic neuron loss in the *SYNJI* R258Q *Drosophila* model (Vanhauwaert

et al., 2017). Another study demonstrated that endophilin A1 function is required for synaptic autophagy through its recruitment of Atg3 to vesicular membranes upon LRRK2-mediated phosphorylation (Soukup et al., 2016). We have shown that one consequence of defective SVE is the accumulation of oxidized DA in human derived dopaminergic neurons (Burbulla et al., 2017; Nguyen & Krainc, 2018). Lysosomes may contribute to synaptic integrity by degrading oxidized DA adducts through the synaptic autophagy pathway, although the exact mechanisms are unclear (Dias et al., 2013; Soukup et al., 2018). Therefore, turnover of synaptic proteins and the elimination of damaged mitochondria and oxidized DA by lysosomes via synaptic autophagy is critical for maintaining dopaminergic synapses (Ashrafi, Schlehe, LaVoie, & Schwarz, 2014; Soukup et al., 2018).

Lastly, we recently identified the dynamic formation of inter-organelle mitochondria-lysosome contact sites, which were distinct from mitophagy or lysosomal engulfment of mitochondria (Wong et al., 2018). These contact sites may further mediate mitochondrial and lysosomal dysfunction in PD, in addition to other previously identified contacts such as ER-mitochondria contacts (Hirabayashi et al., 2017; Wu et al., 2017). Together, these contacts may regulate synaptic  $\text{Ca}^{2+}$  buffering and exchange and additionally regulate SVE by modulating  $\text{Ca}^{2+}$ -dependent calcineurin activity during SVE (Cottrell et al., 2016; Cousin & Robinson, 2001; Marland, Hasel, Bonnycastle, & Cousin, 2016; X. S. Wu et al., 2014). Thus, synaptic, mitochondrial, and lysosomal dysfunction may synergize during PD pathogenesis.

## **Conclusions**

A major hurdle to the development of neuroprotective therapies for PD is an incomplete understanding of key pathways and targets for therapeutic development. The recent emergence of genetic forms of PD has highlighted the importance of major molecular pathways in the pathogenesis of disease, including synaptic, mitochondrial and lysosomal dysfunction. Despite this new evidence, there remain significant gaps in our understanding of the consequences of synaptic dysregulation and how deficits in this pathway are connected to other pathogenic processes such as mitochondrial and lysosomal dysfunction. In addition, there remains a need to better understand the link between deficits in synaptic, mitochondrial, and lysosomal dysfunction and the selective vulnerability of SNc dopaminergic neurons in PD. Ultimately, further investigation of these molecular pathways will be necessary to identify key targets for therapeutic intervention.

## REFERENCES

- Alcalay, R. N., Levy, O. A., Wolf, P., Oliva, P., Zhang, X. K., Waters, C. H., . . . Gan-Or, Z. (2016). SCARB2 variants and glucocerebrosidase activity in Parkinson's disease. *NPJ Parkinsons Dis*, 2. doi:10.1038/npjparkd.2016.4
- Ambroso, M. R., Hegde, B. G., & Langen, R. (2014). Endophilin A1 induces different membrane shapes using a conformational switch that is regulated by phosphorylation. *Proc Natl Acad Sci U S A*, 111(19), 6982-6987. doi:10.1073/pnas.1402233111
- Arranz, A. M., Delbroek, L., Van Kolen, K., Guimaraes, M. R., Mandemakers, W., Daneels, G., . . . Moechars, D. (2015). LRRK2 functions in synaptic vesicle endocytosis through a kinase-dependent mechanism. *J Cell Sci*, 128(3), 541-552. doi:10.1242/jcs.158196
- Ashrafi, G., Schlehe, J. S., LaVoie, M. J., & Schwarz, T. L. (2014). Mitophagy of damaged mitochondria occurs locally in distal neuronal axons and requires PINK1 and Parkin. *J Cell Biol*, 206(5), 655-670. doi:10.1083/jcb.201401070
- Barodia, S. K., Creed, R. B., & Goldberg, M. S. (2017). Parkin and PINK1 functions in oxidative stress and neurodegeneration. *Brain Res Bull*, 133, 51-59. doi:10.1016/j.brainresbull.2016.12.004
- Beilina, A., Rudenko, I. N., Kaganovich, A., Civiero, L., Chau, H., Kalia, S. K., . . . Cookson, M. R. (2014). Unbiased screen for interactors of leucine-rich repeat kinase 2 supports a common pathway for sporadic and familial Parkinson disease. *Proc Natl Acad Sci U S A*, 111(7), 2626-2631. doi:10.1073/pnas.1318306111
- Belluzzi, E., Gonnelli, A., Cirnaru, M. D., Marte, A., Plotegher, N., Russo, I., . . . Greggio, E. (2016). LRRK2 phosphorylates pre-synaptic N-ethylmaleimide sensitive fusion (NSF) protein enhancing its ATPase activity and SNARE complex disassembling rate. *Mol Neurodegener*, 11, 1. doi:10.1186/s13024-015-0066-z
- Berthet, A., Margolis, E. B., Zhang, J., Hsieh, I., Zhang, J., Hnasko, T. S., . . . Nakamura, K. (2014). Loss of mitochondrial fission depletes axonal mitochondria in midbrain dopamine neurons. *J Neurosci*, 34(43), 14304-14317. doi:10.1523/JNEUROSCI.0930-14.2014
- Biskup, S., Moore, D. J., Celsi, F., Higashi, S., West, A. B., Andrabi, S. A., . . . Dawson, V. L. (2006). Localization of LRRK2 to membranous and vesicular structures in mammalian brain. *Ann Neurol*, 60(5), 557-569. doi:10.1002/ana.21019
- Blesa, J., Trigo-Damas, I., Quiroga-Varela, A., & Jackson-Lewis, V. R. (2015). Oxidative stress and Parkinson's disease. *Front Neuroanat*, 9, 91. doi:10.3389/fnana.2015.00091

- Burbulla, L. F., Song, P., Mazzulli, J. R., Zampese, E., Wong, Y. C., Jeon, S., . . . Krainc, D. (2017). Dopamine oxidation mediates mitochondrial and lysosomal dysfunction in Parkinson's disease. *Science*, *357*(6357), 1255-1261. doi:10.1126/science.aam9080
- Burd, C., & Cullen, P. J. (2014). Retromer: a master conductor of endosome sorting. *Cold Spring Harb Perspect Biol*, *6*(2). doi:10.1101/cshperspect.a016774
- Busch, D. J., Oliphint, P. A., Walsh, R. B., Banks, S. M., Woods, W. S., George, J. M., & Morgan, J. R. (2014). Acute increase of alpha-synuclein inhibits synaptic vesicle recycling evoked during intense stimulation. *Mol Biol Cell*, *25*(24), 3926-3941. doi:10.1091/mbc.E14-02-0708
- Byers, B., Cord, B., Nguyen, H. N., Schule, B., Fenno, L., Lee, P. C., . . . Palmer, T. D. (2011). SNCA triplication Parkinson's patient's iPSC-derived DA neurons accumulate alpha-synuclein and are susceptible to oxidative stress. *PLoS One*, *6*(11), e26159. doi:10.1371/journal.pone.0026159
- Cao, M., Milosevic, I., Giovedi, S., & De Camilli, P. (2014). Upregulation of Parkin in endophilin mutant mice. *J Neurosci*, *34*(49), 16544-16549. doi:10.1523/JNEUROSCI.1710-14.2014
- Cao, M., Wu, Y., Ashrafi, G., McCartney, A. J., Wheeler, H., Bushong, E. A., . . . De Camilli, P. (2017). Parkinson Sac Domain Mutation in Synaptojanin 1 Impairs Clathrin Uncoating at Synapses and Triggers Dystrophic Changes in Dopaminergic Axons. *Neuron*, *93*(4), 882-896 e885. doi:10.1016/j.neuron.2017.01.019
- Chang, D., Nalls, M. A., Hallgrimsdottir, I. B., Hunkapiller, J., van der Brug, M., Cai, F., . . . Graham, R. R. (2017). A meta-analysis of genome-wide association studies identifies 17 new Parkinson's disease risk loci. *Nat Genet*, *49*(10), 1511-1516. doi:10.1038/ng.3955
- Chartier-Harlin, M. C., Kachergus, J., Roumier, C., Mouroux, V., Douay, X., Lincoln, S., . . . Destee, A. (2004). Alpha-synuclein locus duplication as a cause of familial Parkinson's disease. *Lancet*, *364*(9440), 1167-1169. doi:10.1016/S0140-6736(04)17103-1
- Chen, C. K., Bregere, C., Paluch, J., Lu, J. F., Dickman, D. K., & Chang, K. T. (2014). Activity-dependent facilitation of Synaptojanin and synaptic vesicle recycling by the Minibrain kinase. *Nat Commun*, *5*, 4246. doi:10.1038/ncomms5246
- Chen, E. I., McClatchy, D., Park, S. K., & Yates, J. R., 3rd. (2008). Comparisons of mass spectrometry compatible surfactants for global analysis of the mammalian brain proteome. *Anal Chem*, *80*(22), 8694-8701. doi:10.1021/ac800606w
- Chen, Y., & Dorn, G. W., 2nd. (2013). PINK1-phosphorylated mitofusin 2 is a Parkin receptor for culling damaged mitochondria. *Science*, *340*(6131), 471-475. doi:10.1126/science.1231031

- Cociorva, D., D. L. T., & Yates, J. R. (2007). Validation of tandem mass spectrometry database search results using DTASelect. *Curr Protoc Bioinformatics, Chapter 13*, Unit 13 14. doi:10.1002/0471250953.bi1304s16
- Cooper, A. A., Gitler, A. D., Cashikar, A., Haynes, C. M., Hill, K. J., Bhullar, B., . . . Lindquist, S. (2006). Alpha-synuclein blocks ER-Golgi traffic and Rab1 rescues neuron loss in Parkinson's models. *Science, 313*(5785), 324-328. doi:10.1126/science.1129462
- Cottrell, J. R., Li, B., Kyung, J. W., Ashford, C. J., Mann, J. J., Horvath, T. L., . . . Gerber, D. J. (2016). Calcineurin Agamma is a Functional Phosphatase That Modulates Synaptic Vesicle Endocytosis. *J Biol Chem, 291*(4), 1948-1956. doi:10.1074/jbc.M115.705319
- Cousin, M. A. (2017). Integration of Synaptic Vesicle Cargo Retrieval with Endocytosis at Central Nerve Terminals. *Front Cell Neurosci, 11*, 234. doi:10.3389/fncel.2017.00234
- Cousin, M. A., & Robinson, P. J. (2001). The dephosphins: dephosphorylation by calcineurin triggers synaptic vesicle endocytosis. *Trends Neurosci, 24*(11), 659-665.
- Cremona, O., Di Paolo, G., Wenk, M. R., Luthi, A., Kim, W. T., Takei, K., . . . De Camilli, P. (1999). Essential role of phosphoinositide metabolism in synaptic vesicle recycling. *Cell, 99*(2), 179-188.
- Crosiers, D., Ceulemans, B., Meeus, B., Nuytemans, K., Pals, P., Van Broeckhoven, C., . . . Theuns, J. (2011). Juvenile dystonia-parkinsonism and dementia caused by a novel ATP13A2 frameshift mutation. *Parkinsonism Relat Disord, 17*(2), 135-138. doi:10.1016/j.parkreldis.2010.10.011
- Crosiers, D., Verstraeten, A., Wauters, E., Engelborghs, S., Peeters, K., Mattheijssens, M., . . . Cras, P. (2016). Mutations in glucocerebrosidase are a major genetic risk factor for Parkinson's disease and increase susceptibility to dementia in a Flanders-Belgian cohort. *Neurosci Lett, 629*, 160-164. doi:10.1016/j.neulet.2016.07.008
- Dehay, B., Ramirez, A., Martinez-Vicente, M., Perier, C., Canron, M. H., Doudnikoff, E., . . . Bezard, E. (2012). Loss of P-type ATPase ATP13A2/PARK9 function induces general lysosomal deficiency and leads to Parkinson disease neurodegeneration. *Proc Natl Acad Sci U S A, 109*(24), 9611-9616. doi:10.1073/pnas.1112368109
- Devi, L., Raghavendran, V., Prabhu, B. M., Avadhani, N. G., & Anandatheerthavarada, H. K. (2008). Mitochondrial import and accumulation of alpha-synuclein impair complex I in human dopaminergic neuronal cultures and Parkinson disease brain. *J Biol Chem, 283*(14), 9089-9100. doi:10.1074/jbc.M710012200
- Di Fonzo, A., Chien, H. F., Socal, M., Giraudo, S., Tassorelli, C., Illiceto, G., . . . Bonifati, V. (2007). ATP13A2 missense mutations in juvenile parkinsonism and young onset Parkinson disease. *Neurology, 68*(19), 1557-1562. doi:10.1212/01.wnl.0000260963.08711.08

- Di Fonzo, A., Rohe, C. F., Ferreira, J., Chien, H. F., Vacca, L., Stocchi, F., . . . Italian Parkinson Genetics, N. (2005). A frequent LRRK2 gene mutation associated with autosomal dominant Parkinson's disease. *Lancet*, *365*(9457), 412-415. doi:10.1016/S0140-6736(05)17829-5
- Dias, V., Junn, E., & Mouradian, M. M. (2013). The role of oxidative stress in Parkinson's disease. *J Parkinsons Dis*, *3*(4), 461-491. doi:10.3233/JPD-130230
- Do, C. B., Tung, J. Y., Dorfman, E., Kiefer, A. K., Drabant, E. M., Francke, U., . . . Eriksson, N. (2011). Web-based genome-wide association study identifies two novel loci and a substantial genetic component for Parkinson's disease. *PLoS Genet*, *7*(6), e1002141. doi:10.1371/journal.pgen.1002141
- Edvardson, S., Cinnamon, Y., Ta-Shma, A., Shaag, A., Yim, Y. I., Zenvirt, S., . . . Elpeleg, O. (2012). A deleterious mutation in DNAJC6 encoding the neuronal-specific clathrin-uncoating co-chaperone auxilin, is associated with juvenile parkinsonism. *PLoS One*, *7*(5), e36458. doi:10.1371/journal.pone.0036458
- Eiden, L. E., Schafer, M. K., Weihe, E., & Schutz, B. (2004). The vesicular amine transporter family (SLC18): amine/proton antiporters required for vesicular accumulation and regulated exocytotic secretion of monoamines and acetylcholine. *Pflugers Arch*, *447*(5), 636-640. doi:10.1007/s00424-003-1100-5
- Eisenberg, E., & Greene, L. E. (2007). Multiple roles of auxilin and hsc70 in clathrin-mediated endocytosis. *Traffic*, *8*(6), 640-646. doi:10.1111/j.1600-0854.2007.00568.x
- Eng, J. K., McCormack, A. L., & Yates, J. R. (1994). An approach to correlate tandem mass spectral data of peptides with amino acid sequences in a protein database. *J Am Soc Mass Spectrom*, *5*(11), 976-989. doi:10.1016/1044-0305(94)80016-2
- Fallon, L., Belanger, C. M., Corera, A. T., Kontogianna, M., Regan-Klapisz, E., Moreau, F., . . . Fon, E. A. (2006). A regulated interaction with the UIM protein Eps15 implicates parkin in EGF receptor trafficking and PI(3)K-Akt signalling. *Nat Cell Biol*, *8*(8), 834-842. doi:10.1038/ncb1441
- Farsi, Z., Gowrisankaran, S., Krunic, M., Rammner, B., Woehler, A., Lafer, E. M., . . . Milosevic, I. (2018). Clathrin coat controls synaptic vesicle acidification by blocking vacuolar ATPase activity. *Elife*, *7*. doi:10.7554/eLife.32569
- Fedorow, H., Tribl, F., Halliday, G., Gerlach, M., Riederer, P., & Double, K. L. (2005). Neuromelanin in human dopamine neurons: comparison with peripheral melanins and relevance to Parkinson's disease. *Prog Neurobiol*, *75*(2), 109-124. doi:10.1016/j.pneurobio.2005.02.001
- Ferguson, S. M., Brasnjo, G., Hayashi, M., Wolfel, M., Collesi, C., Giovedi, S., . . . De Camilli, P. (2007). A selective activity-dependent requirement for dynamin 1 in synaptic vesicle endocytosis. *Science*, *316*(5824), 570-574. doi:10.1126/science.1140621

- Follett, J., Norwood, S. J., Hamilton, N. A., Mohan, M., Kovtun, O., Tay, S., . . . Teasdale, R. D. (2014). The Vps35 D620N mutation linked to Parkinson's disease disrupts the cargo sorting function of retromer. *Traffic*, *15*(2), 230-244. doi:10.1111/tra.12136
- Funayama, M., Hasegawa, K., Kowa, H., Saito, M., Tsuji, S., & Obata, F. (2002). A new locus for Parkinson's disease (PARK8) maps to chromosome 12p11.2-q13.1. *Ann Neurol*, *51*(3), 296-301.
- Geng, J., Wang, L., Lee, J. Y., Chen, C. K., & Chang, K. T. (2016). Phosphorylation of Synaptojanin Differentially Regulates Endocytosis of Functionally Distinct Synaptic Vesicle Pools. *J Neurosci*, *36*(34), 8882-8894. doi:10.1523/JNEUROSCI.1470-16.2016
- Giguere, N., Pacelli, C., Saumure, C., Bourque, M. J., Matheoud, D., Levesque, D., . . . Trudeau, L. E. (2018). Comparative analysis of Parkinson's disease-associated genes in mice reveals altered survival and bioenergetics of Parkin-deficient dopamine neurons. *J Biol Chem*, *293*(25), 9580-9593. doi:10.1074/jbc.RA117.000499
- Gilks, W. P., Abou-Sleiman, P. M., Gandhi, S., Jain, S., Singleton, A., Lees, A. J., . . . Wood, N. W. (2005). A common LRRK2 mutation in idiopathic Parkinson's disease. *Lancet*, *365*(9457), 415-416. doi:10.1016/S0140-6736(05)17830-1
- Goker-Alpan, O., Giasson, B. I., Eblan, M. J., Nguyen, J., Hurtig, H. I., Lee, V. M., . . . Sidransky, E. (2006). Glucocerebrosidase mutations are an important risk factor for Lewy body disorders. *Neurology*, *67*(5), 908-910. doi:10.1212/01.wnl.0000230215.41296.18
- Gomez-Suaga, P., Rivero-Rios, P., Fdez, E., Blanca Ramirez, M., Ferrer, I., Aiastui, A., . . . Hilfiker, S. (2014). LRRK2 delays degradative receptor trafficking by impeding late endosomal budding through decreasing Rab7 activity. *Hum Mol Genet*, *23*(25), 6779-6796. doi:10.1093/hmg/ddu395
- Graham, D. G. (1978). Oxidative pathways for catecholamines in the genesis of neuromelanin and cytotoxic quinones. *Mol Pharmacol*, *14*(4), 633-643.
- Greener, T., Grant, B., Zhang, Y., Wu, X., Greene, L. E., Hirsh, D., & Eisenberg, E. (2001). *Caenorhabditis elegans* auxilin: a J-domain protein essential for clathrin-mediated endocytosis in vivo. *Nat Cell Biol*, *3*(2), 215-219. doi:10.1038/35055137
- Greener, T., Zhao, X., Nojima, H., Eisenberg, E., & Greene, L. E. (2000). Role of cyclin G-associated kinase in uncoating clathrin-coated vesicles from non-neuronal cells. *J Biol Chem*, *275*(2), 1365-1370.
- Greggio, E. (2012). Role of LRRK2 kinase activity in the pathogenesis of Parkinson's disease. *Biochem Soc Trans*, *40*(5), 1058-1062. doi:10.1042/BST20120054

- Guan, R., Dai, H., Harrison, S. C., & Kirchhausen, T. (2010). Structure of the PTEN-like region of auxilin, a detector of clathrin-coated vesicle budding. *Structure*, *18*(9), 1191-1198. doi:10.1016/j.str.2010.06.016
- Guzman, J. N., Sanchez-Padilla, J., Chan, C. S., & Surmeier, D. J. (2009). Robust pacemaking in substantia nigra dopaminergic neurons. *J Neurosci*, *29*(35), 11011-11019. doi:10.1523/JNEUROSCI.2519-09.2009
- Hastings, T. G., Lewis, D. A., & Zigmond, M. J. (1996). Role of oxidation in the neurotoxic effects of intrastriatal dopamine injections. *Proc Natl Acad Sci U S A*, *93*(5), 1956-1961.
- He, L., Diedrich, J., Chu, Y. Y., & Yates, J. R., 3rd. (2015). Extracting Accurate Precursor Information for Tandem Mass Spectra by RawConverter. *Anal Chem*, *87*(22), 11361-11367. doi:10.1021/acs.analchem.5b02721
- Henry, A. G., Aghamohammadzadeh, S., Samaroo, H., Chen, Y., Mou, K., Needle, E., & Hirst, W. D. (2015). Pathogenic LRRK2 mutations, through increased kinase activity, produce enlarged lysosomes with reduced degradative capacity and increase ATP13A2 expression. *Hum Mol Genet*, *24*(21), 6013-6028. doi:10.1093/hmg/ddv314
- Hernandez, D. G., Reed, X., & Singleton, A. B. (2016). Genetics in Parkinson disease: Mendelian versus non-Mendelian inheritance. *J Neurochem*, *139 Suppl 1*, 59-74. doi:10.1111/jnc.13593
- Hill, E., van Der Kaay, J., Downes, C. P., & Smythe, E. (2001). The role of dynamin and its binding partners in coated pit invagination and scission. *J Cell Biol*, *152*(2), 309-323.
- Hinkle, K. M., Yue, M., Behrouz, B., Dachselt, J. C., Lincoln, S. J., Bowles, E. E., . . . Melrose, H. L. (2012). LRRK2 knockout mice have an intact dopaminergic system but display alterations in exploratory and motor co-ordination behaviors. *Mol Neurodegener*, *7*, 25. doi:10.1186/1750-1326-7-25
- Hirabayashi, Y., Kwon, S. K., Paek, H., Pernice, W. M., Paul, M. A., Lee, J., . . . Polleux, F. (2017). ER-mitochondria tethering by PDZD8 regulates Ca(2+) dynamics in mammalian neurons. *Science*, *358*(6363), 623-630. doi:10.1126/science.aan6009
- Hirst, J., Sahlender, D. A., Li, S., Lubben, N. B., Borner, G. H., & Robinson, M. S. (2008). Auxilin depletion causes self-assembly of clathrin into membraneless cages in vivo. *Traffic*, *9*(8), 1354-1371. doi:10.1111/j.1600-0854.2008.00764.x
- Hopfner, F., Schulte, E. C., Mollenhauer, B., Bereznai, B., Knauf, F., Lichtner, P., . . . Winkelmann, J. (2013). The role of SCARB2 as susceptibility factor in Parkinson's disease. *Mov Disord*, *28*(4), 538-540. doi:10.1002/mds.25349
- Hutagalung, A. H., & Novick, P. J. (2011). Role of Rab GTPases in membrane traffic and cell physiology. *Physiol Rev*, *91*(1), 119-149. doi:10.1152/physrev.00059.2009

- Inoshita, T., Arano, T., Hosaka, Y., Meng, H., Umezaki, Y., Kosugi, S., . . . Hattori, N. (2017). Vps35 in cooperation with LRRK2 regulates synaptic vesicle endocytosis through the endosomal pathway in *Drosophila*. *Hum Mol Genet*, *26*(15), 2933-2948. doi:10.1093/hmg/ddx179
- Islam, M. S., Nolte, H., Jacob, W., Ziegler, A. B., Putz, S., Grosjean, Y., . . . Kruger, M. (2016). Human R1441C LRRK2 regulates the synaptic vesicle proteome and phosphoproteome in a *Drosophila* model of Parkinson's disease. *Hum Mol Genet*. doi:10.1093/hmg/ddw352
- Jakobsson, J., Gad, H., Andersson, F., Low, P., Shupliakov, O., & Brodin, L. (2008). Role of epsin 1 in synaptic vesicle endocytosis. *Proc Natl Acad Sci U S A*, *105*(17), 6445-6450. doi:10.1073/pnas.0710267105
- Jana, S., Sinha, M., Chanda, D., Roy, T., Banerjee, K., Munshi, S., . . . Chakrabarti, S. (2011). Mitochondrial dysfunction mediated by quinone oxidation products of dopamine: Implications in dopamine cytotoxicity and pathogenesis of Parkinson's disease. *Biochim Biophys Acta*, *1812*(6), 663-673. doi:10.1016/j.bbadis.2011.02.013
- Kim, W. T., Chang, S., Daniell, L., Cremona, O., Di Paolo, G., & De Camilli, P. (2002). Delayed reentry of recycling vesicles into the fusion-competent synaptic vesicle pool in synaptotagmin 1 knockout mice. *Proc Natl Acad Sci U S A*, *99*(26), 17143-17148. doi:10.1073/pnas.222657399
- Kirola, L., Behari, M., Shishir, C., & Thelma, B. K. (2016). Identification of a novel homozygous mutation Arg459Pro in SYNJ1 gene of an Indian family with autosomal recessive juvenile Parkinsonism. *Parkinsonism Relat Disord*, *31*, 124-128. doi:10.1016/j.parkreldis.2016.07.014
- Kitada, T., Asakawa, S., Hattori, N., Matsumine, H., Yamamura, Y., Minoshima, S., . . . Shimizu, N. (1998). Mutations in the parkin gene cause autosomal recessive juvenile parkinsonism. *Nature*, *392*(6676), 605-608. doi:10.1038/33416
- Koroglu, C., Baysal, L., Cetinkaya, M., Karasoy, H., & Tolun, A. (2013). DNAJC6 is responsible for juvenile parkinsonism with phenotypic variability. *Parkinsonism Relat Disord*, *19*(3), 320-324. doi:10.1016/j.parkreldis.2012.11.006
- Krebs, C. E., Karkheiran, S., Powell, J. C., Cao, M., Makarov, V., Darvish, H., . . . Paisan-Ruiz, C. (2013). The Sac1 domain of SYNJ1 identified mutated in a family with early-onset progressive Parkinsonism with generalized seizures. *Hum Mutat*, *34*(9), 1200-1207. doi:10.1002/humu.22372
- Kriks, S., Shim, J. W., Piao, J., Ganat, Y. M., Wakeman, D. R., Xie, Z., . . . Studer, L. (2011). Dopamine neurons derived from human ES cells efficiently engraft in animal models of Parkinson's disease. *Nature*, *480*(7378), 547-551. doi:10.1038/nature10648

- Kyung, J. W., Kim, J. M., Lee, W., Ha, T. Y., Cha, S. H., Chung, K. H., . . . Park, S. M. (2018). DJ-1 deficiency impairs synaptic vesicle endocytosis and reavailability at nerve terminals. *Proc Natl Acad Sci U S A*, *115*(7), 1629-1634. doi:10.1073/pnas.1708754115
- Lee, S. Y., Wenk, M. R., Kim, Y., Nairn, A. C., & De Camilli, P. (2004). Regulation of synaptotagmin 1 by cyclin-dependent kinase 5 at synapses. *Proc Natl Acad Sci U S A*, *101*(2), 546-551. doi:10.1073/pnas.0307813100
- Lemmon, S. K. (2001). Clathrin uncoating: Auxilin comes to life. *Curr Biol*, *11*(2), R49-52.
- Lesage, S., Durr, A., Tazir, M., Lohmann, E., Leutenegger, A. L., Janin, S., . . . French Parkinson's Disease Genetics Study, G. (2006). LRRK2 G2019S as a cause of Parkinson's disease in North African Arabs. *N Engl J Med*, *354*(4), 422-423. doi:10.1056/NEJMc055540
- Lewis, P. A., Greggio, E., Beilina, A., Jain, S., Baker, A., & Cookson, M. R. (2007). The R1441C mutation of LRRK2 disrupts GTP hydrolysis. *Biochem Biophys Res Commun*, *357*(3), 668-671. doi:10.1016/j.bbrc.2007.04.006
- Lotharius, J., & Brundin, P. (2002). Pathogenesis of Parkinson's disease: dopamine, vesicles and alpha-synuclein. *Nat Rev Neurosci*, *3*(12), 932-942. doi:10.1038/nrn983
- Ma, Y., Greener, T., Pacold, M. E., Kaushal, S., Greene, L. E., & Eisenberg, E. (2002). Identification of domain required for catalytic activity of auxilin in supporting clathrin uncoating by Hsc70. *J Biol Chem*, *277*(51), 49267-49274. doi:10.1074/jbc.M203695200
- Marland, J. R., Hasel, P., Bonnycastle, K., & Cousin, M. A. (2016). Mitochondrial Calcium Uptake Modulates Synaptic Vesicle Endocytosis in Central Nerve Terminals. *J Biol Chem*, *291*(5), 2080-2086. doi:10.1074/jbc.M115.686956
- Marras, C., Beck, J. C., Bower, J. H., Roberts, E., Ritz, B., Ross, G. W., . . . Parkinson's Foundation, P. G. (2018). Prevalence of Parkinson's disease across North America. *NPJ Parkinsons Dis*, *4*, 21. doi:10.1038/s41531-018-0058-0
- Massol, R. H., Boll, W., Griffin, A. M., & Kirchhausen, T. (2006). A burst of auxilin recruitment determines the onset of clathrin-coated vesicle uncoating. *Proc Natl Acad Sci U S A*, *103*(27), 10265-10270. doi:10.1073/pnas.0603369103
- Matta, S., Van Kolen, K., da Cunha, R., van den Bogaart, G., Mandemakers, W., Miskiewicz, K., . . . Verstreken, P. (2012). LRRK2 controls an EndoA phosphorylation cycle in synaptic endocytosis. *Neuron*, *75*(6), 1008-1021. doi:10.1016/j.neuron.2012.08.022
- Mazzulli, J. R., Burbulla, L. F., Krainc, D., & Ischiropoulos, H. (2016). Detection of Free and Protein-Bound ortho-Quinones by Near-Infrared Fluorescence. *Anal Chem*, *88*(4), 2399-2405. doi:10.1021/acs.analchem.5b04420

- Mazzulli, J. R., Xu, Y. H., Sun, Y., Knight, A. L., McLean, P. J., Caldwell, G. A., . . . Krainc, D. (2011). Gaucher disease glucocerebrosidase and alpha-synuclein form a bidirectional pathogenic loop in synucleinopathies. *Cell*, *146*(1), 37-52. doi:10.1016/j.cell.2011.06.001
- McCoy, M. K., & Cookson, M. R. (2011). DJ-1 regulation of mitochondrial function and autophagy through oxidative stress. *Autophagy*, *7*(5), 531-532.
- Medeiros, A. T., Soll, L. G., Tessari, I., Bubacco, L., & Morgan, J. R. (2017). alpha-Synuclein Dimers Impair Vesicle Fission during Clathrin-Mediated Synaptic Vesicle Recycling. *Front Cell Neurosci*, *11*, 388. doi:10.3389/fncel.2017.00388
- Meiser, J., Weindl, D., & Hiller, K. (2013). Complexity of dopamine metabolism. *Cell Commun Signal*, *11*(1), 34. doi:10.1186/1478-811X-11-34
- Milosevic, I. (2018). Revisiting the Role of Clathrin-Mediated Endocytosis in Synaptic Vesicle Recycling. *Front Cell Neurosci*, *12*, 27. doi:10.3389/fncel.2018.00027
- Milosevic, I., Giovedi, S., Lou, X., Raimondi, A., Collesi, C., Shen, H., . . . De Camilli, P. (2011). Recruitment of endophilin to clathrin-coated pit necks is required for efficient vesicle uncoating after fission. *Neuron*, *72*(4), 587-601. doi:10.1016/j.neuron.2011.08.029
- Mir, R., Tonelli, F., Lis, P., Macartney, T., Polinski, N. K., Martinez, T. N., . . . Alessi, D. R. (2018). The Parkinson's disease VPS35[D620N] mutation enhances LRRK2-mediated Rab protein phosphorylation in mouse and human. *Biochem J*, *475*(11), 1861-1883. doi:10.1042/BCJ20180248
- Morgan, J. R., Prasad, K., Jin, S., Augustine, G. J., & Lafer, E. M. (2001). Uncoating of clathrin-coated vesicles in presynaptic terminals: roles for Hsc70 and auxilin. *Neuron*, *32*(2), 289-300.
- Nagle, M. W., Latourelle, J. C., Labadorf, A., Dumitriu, A., Hadzi, T. C., Beach, T. G., & Myers, R. H. (2016). The 4p16.3 Parkinson Disease Risk Locus Is Associated with GAK Expression and Genes Involved with the Synaptic Vesicle Membrane. *PLoS One*, *11*(8), e0160925. doi:10.1371/journal.pone.0160925
- Nalls, M. A., Pankratz, N., Lill, C. M., Do, C. B., Hernandez, D. G., Saad, M., . . . Singleton, A. B. (2014). Large-scale meta-analysis of genome-wide association data identifies six new risk loci for Parkinson's disease. *Nat Genet*, *46*(9), 989-993. doi:10.1038/ng.3043
- Narendra, D. P., Jin, S. M., Tanaka, A., Suen, D. F., Gautier, C. A., Shen, J., . . . Youle, R. J. (2010). PINK1 is selectively stabilized on impaired mitochondria to activate Parkin. *PLoS Biol*, *8*(1), e1000298. doi:10.1371/journal.pbio.1000298
- Nguyen, M., & Krainc, D. (2018). LRRK2 phosphorylation of auxilin mediates synaptic defects in dopaminergic neurons from patients with Parkinson's disease. *Proc Natl Acad Sci U S A*, *115*(21), 5576-5581. doi:10.1073/pnas.1717590115

- Oldham, C. E., Mohny, R. P., Miller, S. L., Hanes, R. N., & O'Bryan, J. P. (2002). The ubiquitin-interacting motifs target the endocytic adaptor protein epsin for ubiquitination. *Curr Biol*, *12*(13), 1112-1116.
- Olgiati, S., De Rosa, A., Quadri, M., Criscuolo, C., Breedveld, G. J., Picillo, M., . . . Bonifati, V. (2014). PARK20 caused by SYNJ1 homozygous Arg258Gln mutation in a new Italian family. *Neurogenetics*, *15*(3), 183-188. doi:10.1007/s10048-014-0406-0
- Olgiati, S., Quadri, M., Fang, M., Rood, J. P., Saute, J. A., Chien, H. F., . . . Bonifati, V. (2016). DNAJC6 Mutations Associated With Early-Onset Parkinson's Disease. *Ann Neurol*, *79*(2), 244-256. doi:10.1002/ana.24553
- Ozelius, L. J., Senthil, G., Saunders-Pullman, R., Ohmann, E., Deligtisch, A., Tagliati, M., . . . Bressman, S. B. (2006). LRRK2 G2019S as a cause of Parkinson's disease in Ashkenazi Jews. *N Engl J Med*, *354*(4), 424-425. doi:10.1056/NEJMc055509
- Pacelli, C., Giguere, N., Bourque, M. J., Levesque, M., Slack, R. S., & Trudeau, L. E. (2015). Elevated Mitochondrial Bioenergetics and Axonal Arborization Size Are Key Contributors to the Vulnerability of Dopamine Neurons. *Curr Biol*, *25*(18), 2349-2360. doi:10.1016/j.cub.2015.07.050
- Pan, P. Y., Li, X., Wang, J., Powell, J., Wang, Q., Zhang, Y., . . . Yue, Z. (2017). Parkinson's Disease-Associated LRRK2 Hyperactive Kinase Mutant Disrupts Synaptic Vesicle Trafficking in Ventral Midbrain Neurons. *J Neurosci*, *37*(47), 11366-11376. doi:10.1523/JNEUROSCI.0964-17.2017
- Park, B. C., Yim, Y. I., Zhao, X., Olszewski, M. B., Eisenberg, E., & Greene, L. E. (2015). The clathrin-binding and J-domains of GAK support the uncoating and chaperoning of clathrin by Hsc70 in the brain. *J Cell Sci*, *128*(20), 3811-3821. doi:10.1242/jcs.171058
- Pathak, D., Shields, L. Y., Mendelsohn, B. A., Haddad, D., Lin, W., Gerencser, A. A., . . . Nakamura, K. (2015). The role of mitochondrially derived ATP in synaptic vesicle recycling. *J Biol Chem*, *290*(37), 22325-22336. doi:10.1074/jbc.M115.656405
- Pechstein, A., Gerth, F., Milosevic, I., Japel, M., Eichhorn-Grunig, M., Vorontsova, O., . . . Haucke, V. (2015). Vesicle uncoating regulated by SH3-SH3 domain-mediated complex formation between endophilin and intersectin at synapses. *EMBO Rep*, *16*(2), 232-239. doi:10.15252/embr.201439260
- Phan, J. A., Stokholm, K., Zareba-Paslawska, J., Jakobsen, S., Vang, K., Gjedde, A., . . . Romero-Ramos, M. (2017). Early synaptic dysfunction induced by alpha-synuclein in a rat model of Parkinson's disease. *Sci Rep*, *7*(1), 6363. doi:10.1038/s41598-017-06724-9
- Plotegher, N., Berti, G., Ferrari, E., Tessari, I., Zanetti, M., Lunelli, L., . . . Bubacco, L. (2017). DOPAL derived alpha-synuclein oligomers impair synaptic vesicles physiological function. *Sci Rep*, *7*, 40699. doi:10.1038/srep40699

- Polymeropoulos, M. H., Lavedan, C., Leroy, E., Ide, S. E., Dehejia, A., Dutra, A., . . . Nussbaum, R. L. (1997). Mutation in the alpha-synuclein gene identified in families with Parkinson's disease. *Science*, *276*(5321), 2045-2047.
- Quadri, M., Fang, M., Picillo, M., Olgiati, S., Breedveld, G. J., Graafland, J., . . . Bonifati, V. (2013). Mutation in the SYNJ1 gene associated with autosomal recessive, early-onset Parkinsonism. *Hum Mutat*, *34*(9), 1208-1215. doi:10.1002/humu.22373
- Rangaraju, V., Calloway, N., & Ryan, T. A. (2014). Activity-driven local ATP synthesis is required for synaptic function. *Cell*, *156*(4), 825-835. doi:10.1016/j.cell.2013.12.042
- Rapoport, I., Boll, W., Yu, A., Bocking, T., & Kirchhausen, T. (2008). A motif in the clathrin heavy chain required for the Hsc70/auxilin uncoating reaction. *Mol Biol Cell*, *19*(1), 405-413. doi:10.1091/mbc.E07-09-0870
- Ray, S., Bender, S., Kang, S., Lin, R., Glicksman, M. A., & Liu, M. (2014). The Parkinson disease-linked LRRK2 protein mutation I2020T stabilizes an active state conformation leading to increased kinase activity. *J Biol Chem*, *289*(19), 13042-13053. doi:10.1074/jbc.M113.537811
- Reeve, A. K., Grady, J. P., Cosgrave, E. M., Bennison, E., Chen, C., Hepplewhite, P. D., & Morris, C. M. (2018). Mitochondrial dysfunction within the synapses of substantia nigra neurons in Parkinson's disease. *NPJ Parkinsons Dis*, *4*, 9. doi:10.1038/s41531-018-0044-6
- Reith, A. D., Bamborough, P., Jandu, K., Andreotti, D., Mensah, L., Dossang, P., . . . Gray, N. S. (2012). GSK2578215A; a potent and highly selective 2-arylmethoxy-5-substituent-N-arylbzamide LRRK2 kinase inhibitor. *Bioorg Med Chem Lett*, *22*(17), 5625-5629. doi:10.1016/j.bmcl.2012.06.104
- Rhodes, S. L., Sinsheimer, J. S., Bordelon, Y., Bronstein, J. M., & Ritz, B. (2011). Replication of GWAS associations for GAK and MAPT in Parkinson's disease. *Ann Hum Genet*, *75*(2), 195-200. doi:10.1111/j.1469-1809.2010.00616.x
- Riley, B. E., Loughheed, J. C., Callaway, K., Velasquez, M., Brecht, E., Nguyen, L., . . . Johnston, J. A. (2013). Structure and function of Parkin E3 ubiquitin ligase reveals aspects of RING and HECT ligases. *Nat Commun*, *4*, 1982. doi:10.1038/ncomms2982
- Rothaug, M., Zunke, F., Mazzulli, J. R., Schweizer, M., Altmeyen, H., Lullmann-Rauch, R., . . . Blanz, J. (2014). LIMP-2 expression is critical for beta-glucocerebrosidase activity and alpha-synuclein clearance. *Proc Natl Acad Sci U S A*, *111*(43), 15573-15578. doi:10.1073/pnas.1405700111
- Saheki, Y., & De Camilli, P. (2012). Synaptic vesicle endocytosis. *Cold Spring Harb Perspect Biol*, *4*(9), a005645. doi:10.1101/cshperspect.a005645
- Scheele, U., Alves, J., Frank, R., Duwel, M., Kalthoff, C., & Ungewickell, E. (2003). Molecular and functional characterization of clathrin- and AP-2-binding determinants within a

- disordered domain of auxilin. *J Biol Chem*, 278(28), 25357-25368. doi:10.1074/jbc.M303738200
- Schuske, K. R., Richmond, J. E., Matthies, D. S., Davis, W. S., Runz, S., Rube, D. A., . . . Jorgensen, E. M. (2003). Endophilin is required for synaptic vesicle endocytosis by localizing synaptojanin. *Neuron*, 40(4), 749-762.
- Sheng, Z., Zhang, S., Bustos, D., Kleinheinz, T., Le Pichon, C. E., Dominguez, S. L., . . . Zhu, H. (2012). Ser1292 autophosphorylation is an indicator of LRRK2 kinase activity and contributes to the cellular effects of PD mutations. *Sci Transl Med*, 4(164), 164ra161. doi:10.1126/scitranslmed.3004485
- Shin, N., Jeong, H., Kwon, J., Heo, H. Y., Kwon, J. J., Yun, H. J., . . . Seol, W. (2008). LRRK2 regulates synaptic vesicle endocytosis. *Exp Cell Res*, 314(10), 2055-2065. doi:10.1016/j.yexcr.2008.02.015
- Sobieski, C., Fitzpatrick, M. J., & Mennerick, S. J. (2017). Differential Presynaptic ATP Supply for Basal and High-Demand Transmission. *J Neurosci*, 37(7), 1888-1899. doi:10.1523/JNEUROSCI.2712-16.2017
- Song, L., He, Y., Ou, J., Zhao, Y., Li, R., Cheng, J., . . . Ho, M. S. (2017). Auxilin Underlies Progressive Locomotor Deficits and Dopaminergic Neuron Loss in a Drosophila Model of Parkinson's Disease. *Cell Rep*, 18(5), 1132-1143. doi:10.1016/j.celrep.2017.01.005
- Song, W., & Zinsmaier, K. E. (2003). Endophilin and synaptojanin hook up to promote synaptic vesicle endocytosis. *Neuron*, 40(4), 665-667.
- Soukup, S. F., Kuenen, S., Vanhauwaert, R., Manetsberger, J., Hernandez-Diaz, S., Swerts, J., . . . Verstreken, P. (2016). A LRRK2-Dependent EndophilinA Phosphoswitch Is Critical for Macroautophagy at Presynaptic Terminals. *Neuron*, 92(4), 829-844. doi:10.1016/j.neuron.2016.09.037
- Soukup, S. F., Vanhauwaert, R., & Verstreken, P. (2018). Parkinson's disease: convergence on synaptic homeostasis. *EMBO J*. doi:10.15252/embj.201898960
- Stafa, K., Tsika, E., Moser, R., Musso, A., Glauser, L., Jones, A., . . . Moore, D. J. (2014). Functional interaction of Parkinson's disease-associated LRRK2 with members of the dynamin GTPase superfamily. *Hum Mol Genet*, 23(8), 2055-2077. doi:10.1093/hmg/ddt600
- Stamenova, S. D., French, M. E., He, Y., Francis, S. A., Kramer, Z. B., & Hicke, L. (2007). Ubiquitin binds to and regulates a subset of SH3 domains. *Mol Cell*, 25(2), 273-284. doi:10.1016/j.molcel.2006.12.016
- Steger, M., Tonelli, F., Ito, G., Davies, P., Trost, M., Vetter, M., . . . Mann, M. (2016). Phosphoproteomics reveals that Parkinson's disease kinase LRRK2 regulates a subset of Rab GTPases. *Elife*, 5. doi:10.7554/eLife.12813

- Sulzer, D., Bogulavsky, J., Larsen, K. E., Behr, G., Karatekin, E., Kleinman, M. H., . . . Zecca, L. (2000). Neuromelanin biosynthesis is driven by excess cytosolic catecholamines not accumulated by synaptic vesicles. *Proc Natl Acad Sci U S A*, *97*(22), 11869-11874. doi:10.1073/pnas.97.22.11869
- Sundborger, A., Soderblom, C., Vorontsova, O., Evergren, E., Hinshaw, J. E., & Shupliakov, O. (2011). An endophilin-dynamin complex promotes budding of clathrin-coated vesicles during synaptic vesicle recycling. *J Cell Sci*, *124*(Pt 1), 133-143. doi:10.1242/jcs.072686
- Tabb, D. L., McDonald, W. H., & Yates, J. R., 3rd. (2002). DTASelect and Contrast: tools for assembling and comparing protein identifications from shotgun proteomics. *J Proteome Res*, *1*(1), 21-26.
- Takahashi, K., & Yamanaka, S. (2006). Induction of pluripotent stem cells from mouse embryonic and adult fibroblast cultures by defined factors. *Cell*, *126*(4), 663-676. doi:10.1016/j.cell.2006.07.024
- Tan, T. C., Valova, V. A., Malladi, C. S., Graham, M. E., Berven, L. A., Jupp, O. J., . . . Robinson, P. J. (2003). Cdk5 is essential for synaptic vesicle endocytosis. *Nat Cell Biol*, *5*(8), 701-710. doi:10.1038/ncb1020
- Thomas, K. J., McCoy, M. K., Blackinton, J., Beilina, A., van der Brug, M., Sandebring, A., . . . Cookson, M. R. (2011). DJ-1 acts in parallel to the PINK1/parkin pathway to control mitochondrial function and autophagy. *Hum Mol Genet*, *20*(1), 40-50. doi:10.1093/hmg/ddq430
- Tong, Y., Pisani, A., Martella, G., Karouani, M., Yamaguchi, H., Pothos, E. N., & Shen, J. (2009). R1441C mutation in LRRK2 impairs dopaminergic neurotransmission in mice. *Proc Natl Acad Sci U S A*, *106*(34), 14622-14627. doi:10.1073/pnas.0906334106
- Trempe, J. F., Chen, C. X., Grenier, K., Camacho, E. M., Kozlov, G., McPherson, P. S., . . . Fon, E. A. (2009). SH3 domains from a subset of BAR proteins define a Ubl-binding domain and implicate parkin in synaptic ubiquitination. *Mol Cell*, *36*(6), 1034-1047. doi:10.1016/j.molcel.2009.11.021
- Tsunemi, T., & Krainc, D. (2014). Zn(2)(+) dyshomeostasis caused by loss of ATP13A2/PARK9 leads to lysosomal dysfunction and alpha-synuclein accumulation. *Hum Mol Genet*, *23*(11), 2791-2801. doi:10.1093/hmg/ddt572
- Tysnes, O. B., & Storstein, A. (2017). Epidemiology of Parkinson's disease. *J Neural Transm (Vienna)*, *124*(8), 901-905. doi:10.1007/s00702-017-1686-y
- van Veen, S., Sorensen, D. M., Holemans, T., Holen, H. W., Palmgren, M. G., & Vangheluwe, P. (2014). Cellular function and pathological role of ATP13A2 and related P-type transport ATPases in Parkinson's disease and other neurological disorders. *Front Mol Neurosci*, *7*, 48. doi:10.3389/fnmol.2014.00048

- Vanhouwaert, R., Kuenen, S., Masius, R., Bademosi, A., Manetsberger, J., Schoovaerts, N., . . . Verstrecken, P. (2017). The SAC1 domain in synaptojanin is required for autophagosome maturation at presynaptic terminals. *EMBO J*, 36(10), 1392-1411. doi:10.15252/emj.201695773
- Vargas, K. J., Makani, S., Davis, T., Westphal, C. H., Castillo, P. E., & Chandra, S. S. (2014). Synucleins regulate the kinetics of synaptic vesicle endocytosis. *J Neurosci*, 34(28), 9364-9376. doi:10.1523/JNEUROSCI.4787-13.2014
- Vergo, S., Johansen, J. L., Leist, M., & Lotharius, J. (2007). Vesicular monoamine transporter 2 regulates the sensitivity of rat dopaminergic neurons to disturbed cytosolic dopamine levels. *Brain Res*, 1185, 18-32. doi:10.1016/j.brainres.2007.09.028
- Verma, M., Callio, J., Otero, P. A., Sekler, I., Wills, Z. P., & Chu, C. T. (2017). Mitochondrial Calcium Dysregulation Contributes to Dendrite Degeneration Mediated by PD/LBD-Associated LRRK2 Mutants. *J Neurosci*, 37(46), 11151-11165. doi:10.1523/JNEUROSCI.3791-16.2017
- Verstreken, P., Koh, T. W., Schulze, K. L., Zhai, R. G., Hiesinger, P. R., Zhou, Y., . . . Bellen, H. J. (2003). Synaptojanin is recruited by endophilin to promote synaptic vesicle uncoating. *Neuron*, 40(4), 733-748.
- Wang, X., Petrie, T. G., Liu, Y., Liu, J., Fujioka, H., & Zhu, X. (2012). Parkinson's disease-associated DJ-1 mutations impair mitochondrial dynamics and cause mitochondrial dysfunction. *J Neurochem*, 121(5), 830-839. doi:10.1111/j.1471-4159.2012.07734.x
- Wang, Y., Nartiss, Y., Steipe, B., McQuibban, G. A., & Kim, P. K. (2012). ROS-induced mitochondrial depolarization initiates PARK2/PARKIN-dependent mitochondrial degradation by autophagy. *Autophagy*, 8(10), 1462-1476. doi:10.4161/auto.21211
- Watanabe, S., Mamer, L. E., Raychaudhuri, S., Luvsanjav, D., Eisen, J., Trimbuch, T., . . . Jorgensen, E. M. (2018). Synaptojanin and Endophilin Mediate Neck Formation during Ultrafast Endocytosis. *Neuron*, 98(6), 1184-1197 e1186. doi:10.1016/j.neuron.2018.06.005
- Webber, P. J., Smith, A. D., Sen, S., Renfrow, M. B., Mobley, J. A., & West, A. B. (2011). Autophosphorylation in the leucine-rich repeat kinase 2 (LRRK2) GTPase domain modifies kinase and GTP-binding activities. *J Mol Biol*, 412(1), 94-110. doi:10.1016/j.jmb.2011.07.033
- West, A. B., Moore, D. J., Choi, C., Andrabi, S. A., Li, X., Dikeman, D., . . . Dawson, T. M. (2007). Parkinson's disease-associated mutations in LRRK2 link enhanced GTP-binding and kinase activities to neuronal toxicity. *Hum Mol Genet*, 16(2), 223-232. doi:10.1093/hmg/ddl471

- Wong, Y. C., Ysselstein, D., & Krainc, D. (2018). Mitochondria-lysosome contacts regulate mitochondrial fission via RAB7 GTP hydrolysis. *Nature*, *554*(7692), 382-386. doi:10.1038/nature25486
- Wu, X. S., Zhang, Z., Zhao, W. D., Wang, D., Luo, F., & Wu, L. G. (2014). Calcineurin is universally involved in vesicle endocytosis at neuronal and nonneuronal secretory cells. *Cell Rep*, *7*(4), 982-988. doi:10.1016/j.celrep.2014.04.020
- Wu, Y., O'Toole, E. T., Girard, M., Ritter, B., Messa, M., Liu, X., . . . De Camilli, P. (2014). A dynamin 1-, dynamin 3- and clathrin-independent pathway of synaptic vesicle recycling mediated by bulk endocytosis. *Elife*, *3*, e01621. doi:10.7554/eLife.01621
- Wu, Y., Whiteus, C., Xu, C. S., Hayworth, K. J., Weinberg, R. J., Hess, H. F., & De Camilli, P. (2017). Contacts between the endoplasmic reticulum and other membranes in neurons. *Proc Natl Acad Sci U S A*, *114*(24), E4859-E4867. doi:10.1073/pnas.1701078114
- Xiao, B., Goh, J. Y., Xiao, L., Xian, H., Lim, K. L., & Liou, Y. C. (2017). Reactive oxygen species trigger Parkin/PINK1 pathway-dependent mitophagy by inducing mitochondrial recruitment of Parkin. *J Biol Chem*, *292*(40), 16697-16708. doi:10.1074/jbc.M117.787739
- Xiao, J., Kim, L. S., & Graham, T. R. (2006). Dissection of Swa2p/auxilin domain requirements for cochaperoning Hsp70 clathrin-uncoating activity in vivo. *Mol Biol Cell*, *17*(7), 3281-3290. doi:10.1091/mbc.E06-02-0106
- Xiong, Y., Neifert, S., Karuppagounder, S. S., Liu, Q., Stankowski, J. N., Lee, B. D., . . . Dawson, V. L. (2018). Robust kinase- and age-dependent dopaminergic and norepinephrine neurodegeneration in LRRK2 G2019S transgenic mice. *Proc Natl Acad Sci U S A*, *115*(7), 1635-1640. doi:10.1073/pnas.1712648115
- Xu, T., Park, S. K., Venable, J. D., Wohlschlegel, J. A., Diedrich, J. K., Cociorva, D., . . . Yates, J. R., 3rd. (2015). ProLuCID: An improved SEQUEST-like algorithm with enhanced sensitivity and specificity. *J Proteomics*, *129*, 16-24. doi:10.1016/j.jprot.2015.07.001
- Yim, Y. I., Sun, T., Wu, L. G., Raimondi, A., De Camilli, P., Eisenberg, E., & Greene, L. E. (2010). Endocytosis and clathrin-uncoating defects at synapses of auxilin knockout mice. *Proc Natl Acad Sci U S A*, *107*(9), 4412-4417. doi:10.1073/pnas.1000738107
- Yoshii, S. R., Kishi, C., Ishihara, N., & Mizushima, N. (2011). Parkin mediates proteasome-dependent protein degradation and rupture of the outer mitochondrial membrane. *J Biol Chem*, *286*(22), 19630-19640. doi:10.1074/jbc.M110.209338
- Ysselstein, D., Joshi, M., Mishra, V., Griggs, A. M., Asiago, J. M., McCabe, G. P., . . . Rochet, J. C. (2015). Effects of impaired membrane interactions on alpha-synuclein aggregation and neurotoxicity. *Neurobiol Dis*, *79*, 150-163. doi:10.1016/j.nbd.2015.04.007

- Yun, H. J., Kim, H., Ga, I., Oh, H., Ho, D. H., Kim, J., . . . Seol, W. (2015). An early endosome regulator, Rab5b, is an LRRK2 kinase substrate. *J Biochem*, *157*(6), 485-495. doi:10.1093/jb/mvv005
- Zaichick, S. V., McGrath, K. M., & Caraveo, G. (2017). The role of Ca(2+) signaling in Parkinson's disease. *Dis Model Mech*, *10*(5), 519-535. doi:10.1242/dmm.028738
- Zhang, B., Koh, Y. H., Beckstead, R. B., Budnik, V., Ganetzky, B., & Bellen, H. J. (1998). Synaptic vesicle size and number are regulated by a clathrin adaptor protein required for endocytosis. *Neuron*, *21*(6), 1465-1475.
- Zimprich, A., Biskup, S., Leitner, P., Lichtner, P., Farrer, M., Lincoln, S., . . . Gasser, T. (2004). Mutations in LRRK2 cause autosomal-dominant parkinsonism with pleomorphic pathology. *Neuron*, *44*(4), 601-607. doi:10.1016/j.neuron.2004.11.005

# CURRICULUM VITAE of

## MARIA NGUYEN

Northwestern University  
303 E Chicago Ave  
Chicago, IL 60611

Department of Neurology  
maria.nguyen@u.northwestern.edu  
Tel (503) 740-1280

### EDUCATION

**Northwestern University**, Chicago, IL GPA: 3.4  
*PhD Candidate*, Neuroscience *In progress*

**Oregon State University**, Corvallis, OR GPA: 3.6  
*Bachelor of Science*, Biochemistry & Biophysics June 2013

### MAJOR PROJECTS & POSITIONS

- 03/2014 – Present** **Dr. Dimitri Krainc Laboratory, Northwestern University**, Chicago, IL  
*Neuroscience PhD Candidate/Graduate Student*
- Topics include the characterization of Parkinson's disease linked LRRK2 mutations in iPSCs
  - Research mainly focuses on identifying interactions between LRRK2 and other PD like genes with an emphasis on its role at the synapse
- 01/2014 – 03/2014** **Dr. Richard Miller Laboratory, Northwestern University**, Chicago, IL  
*Neuroscience PhD Rotation Student*
- Studied the use of lipopolysaccharides (LPS) to potentiate seizures in mouse models
  - Used kainic acid to induce seizures in mice that mimic febrile seizures experienced by young children
  - Treated mice prematurely with LPS to see if the severity of induced-seizures would be increased
- 07/2013 – 12/2013** **Dr. Yongchao Ma Laboratory, Northwestern University**, Chicago, IL  
*Neuroscience PhD Rotation Student*
- Investigated motor axon transport in mouse models of spinal muscular atrophy (SMA)
  - Focused on cdk5 regulation of tau phosphorylation and the transport of mitochondria in primary neuronal axons
  - Other work also included the co-culturing of primary neurons with astrocytes from wild-type and mutant SMA mice to discern the role that unhealthy astrocytes played in disease progression

- 09/2012 – 06/2013 **Dr. Debbie Mustacich Laboratory, Oregon State University, Corvallis, OR**  
*Undergraduate Researcher*
- Tested the efficacy of cisplatin on spinal cord injury rat models
  - Work included the generation of spinal cord injury/ovarian cancer rat models and treatment with cisplatin supplemented with alpha-tocopherol to increase recovery outcome
- 06/2012 – 09/2012 **Dr. Joseph Gleeson Laboratory, University of California, SD, La Jolla, CA**  
*Howard Hughes Medical Institute (HHMI) Capstone Intern*
- Identified and characterized a potentially druggable protein target for patients with mutations in ADPRHL2 that cause a lethal epilepsy syndrome
  - Work mainly involved the treatment of patient cells (fibroblasts and iPSC-derived neurons) with PARP inhibitors and repurposed FDA-approved drugs
- 06/2011 – 09/2011 **Dr. Joseph Gleeson Laboratory, University of California, SD, La Jolla, CA**  
*Howard Hughes Medical Institute (HHMI) EXROP Intern*
- Discerned significant morphological differences in neurons belonging to patients diagnosed with epilepsy, a neurodevelopmental disorder
  - Research was focused on the development process of dendritic spines in mice and how perturbations during development could lead to epileptic like phenotypes as the mice aged
- 06/2010 – 09/2010 **Dr. Julie Greenwood Laboratory, Oregon State University, Corvallis, OR**  
*Howard Hughes Medical Institute (HHMI) Summer Intern*
- Explored how glioblastoma cells invade in the human brain by elucidating molecular mechanisms involved
  - Studied and identified major underlying proteins involved in the invasion process, specifically protein kinase B and its regulation by calpain-2
- 10/2009 – 09/2012 **Dr. Julie Greenwood Laboratory, Oregon State University, Corvallis, OR**  
*Undergraduate Researcher*
- Investigated the mechanisms of glioblastoma invasion, specifically focusing on cellular mechanisms and phosphorylation events between protein players previously identified in the lab

## **HONORS & AWARDS**

- 11/2018 **Society for Neuroscience, Trainee Professional Development Award**  
11/2018 Northwestern University, the Graduate School Conference Travel Award  
7/2018 Northwestern University Interdepartmental Neuroscience Student Travel Award  
09/2011 – 09/2012 Ray, Frances, and Dale Cripps Student Support Fund  
09/2010 – 06/2011 Jesse Hanson Scholarship  
09/2010 – 09/2011 Dale Krueger Scholarship  
09/2009 – 09/2012 Diversity Achievement Scholarship  
09/2009 – 06/2013 Early Admission to Pharmacy School Recipient

## PRESENTATIONS

### Oral

- 2018 LRRK2 phosphorylation of auxilin mediates synaptic defects in dopaminergic neurons from patients with Parkinson's disease. **MAD T32 Training Day**, Chicago, IL.
- 2018 LRRK2 phosphorylation of auxilin mediates synaptic defects in dopaminergic neurons from patients with Parkinson's disease. **MAD T32 Research in Progress**, Chicago, IL.
- 2017 Implications for LRRK2 and auxilin in Parkinson's disease pathogenesis. **Society for Neuroscience Annual Meeting**, Washington, D.C. *Selected to present in Nanosymposium.*
- 2017 Implications for LRRK2 and auxilin in Parkinson's disease pathogenesis. **MAD T32 Training Day**, Chicago, IL.
- 2017 Implications for LRRK2 and auxilin in Parkinson's disease pathogenesis. **MAD T32 Research in Progress**, Chicago, IL.
- 2012 Using PARP inhibitors to treat epilepsy syndrome. **HHMI Undergraduate Summer Research Symposium**, Corvallis, OR.
- 2011 Effects of mutations in FMN2 leading to rare forms of intellectual disability. **HHMI Undergraduate Summer Research Symposium**, Corvallis, OR. *Received Top Speaker Award.*
- 2011 Effects of mutations in FMN2 leading to rare forms of intellectual disability. **University of California, San Diego Research Conference**, La Jolla, CA.
- 2010 Calpain 2 regulates Akt in glioblastoma cell invasion. **HHMI Undergraduate Summer Research Symposium**, Corvallis, OR.

### Posters

- 2018 LRRK2 phosphorylation of auxilin mediates synaptic defects in dopaminergic neurons from patients with Parkinson's disease. **Society for Neuroscience Annual Meeting**, San Diego, CA. *Received Trainee Professional Development Award.*
- 2018 LRRK2 phosphorylation of auxilin mediates synaptic defects in dopaminergic neurons from patients with Parkinson's disease. **Keystone Symposia – Mechanisms of Neurodegeneration**, Keystone, CO.
- 2017 Implications for LRRK2 and auxilin in Parkinson's disease pathogenesis. **Chicago Society for Neuroscience Conference**, Chicago, IL. *Best Graduate Student Poster – Second place.*
- 2014 Dysregulation of mitochondrial trafficking in spinal muscular atrophy (SMA). **NUIN Recruitment Event**, Chicago, IL.
- 2013 Testing the efficacy of cisplatin on spinal cord injury models in rat. **Diet and Optimum Health Conference**, Corvallis, OR.
- 2013 Using PARP inhibitors to treat epilepsy syndrome. **Celebrating Undergraduate Excellence**, Corvallis, OR.
- 2012 Mutations in FMN2 cause intellectual disability. **HHMI ExROP National Meeting**, Chevy Chase, MD.
- 2011 Mutations in FMN2 cause intellectual disability. **Celebrating Undergraduate Excellence**, Corvallis, OR. *Awarded Best HHMI Poster.*
- 2010 Calpain 2 regulates Akt in glioblastoma cell invasion. **Celebrating Undergraduate Excellence**, Corvallis, OR.

## PROFESSIONAL MEMBERSHIPS

09/2015 – Present      **Society for Neuroscience**

## TEACHING AND MENTORSHIP

10/2016 – 09/2017      **Northwestern University / Mentor for Undergraduate Neuron Program**

- 03/2015 – 06/2015 Mentoring students interested in pursuing research beyond university, specifically by advising and assisting with professional development of young researchers.  
**Northwestern University / Teaching Assistant for Anatomy of Vertebrates**  
 Oversaw and led discussions and laboratory dissections  
 Graded homework, in-class lab assignments and exams
- 03/2013 – 06/2013 **Oregon State University / Teaching Assistant for Introduction to Biochemistry**  
 Held open office hours to mentor and tutor students with coursework  
 Graded assignments and exams

### RESEARCH SUPPORT

- 10/1/2016 – 9/30/2018 **National Institutes of Health T32 Training Grant (2T32AG020506-16)**  
*Mechanisms of Aging and Dementia*
- 10/1/2016 – 9/30/2018 **Michael J. Fox Foundation Grant**  
*LRRK2 and GBA in PD pathogenesis*
- 6/10/2012 – 8/31/2012 **HHMI Capstone Summer Research Fellowship**  
*Role of ADPRHL2 in lethal epilepsy syndrome*
- 6/10/2011 – 8/31/2011 **HHMI ExROP Summer Research Fellowship**  
*Role of FMN2 in intellectual disability*
- 1/1/2011 – 3/31/2011 **Undergraduate Research, Innovation, Scholarship and Creativity Award**  
*Calpain 2 regulation of Akt*
- 9/30/2010 – 6/10/2011 **Cripps Undergraduate Research Award (CURE)**  
*Calpain 2 regulation of Akt*
- 6/10/2010 – 9/30/2010 **HHMI Summer Research Fellowship**  
*Mechanisms of glioblastoma cell invasion*

### ACADEMIC AFFILIATIONS

- 10/2016 – Present **NUIN Student Advisory Committee (NSAC), Representative**  
 Responsible for meeting with NUIN leadership to represent and advocate for the views of students in the NUIN program.
- 03/2015 – Present **Northwestern University Brain Awareness Outreach (NUBAO) Program, Volunteer**  
 Participates in educating K-12 students on the different functions of the brain. Duties include: volunteering in the Brain Awareness Fair held once a year.
- 09/2011 – 06/2013 **Sigma Delta Omega, Sister**  
 Member of a unique science sorority only found at Oregon State University. Duties include: volunteering in the local community, attending weekly Chapter meetings and holding academic study sessions.
- 05/2011 – 06/2013 **Mortar Board National Honorary Society, President and Secretary**  
 Responsibilities include managing meeting notes, tracking of member participation hours, volunteering within the community, and assisting with any member concerns.  
**Textbook Scholarship Committee, Chair head**  
 Organizing and communicating with committee members to make sure the selections process runs smoothly.
- 04/2010 – 06/2013 **College of Science, Ambassador**  
 Meeting and greeting prospect students, informing them of programs offered at Oregon State and guiding students through tours.

## LIST OF PUBLICATIONS

**Nguyen M**, Wong YC, Ysselstein D, Severino A, Krainc D (2018) Synaptic, mitochondrial, and lysosomal dysfunction in Parkinson's disease, *Trends in Neurosciences*, **S0166-2236**(18): 30282-0.

**Nguyen M**, Krainc D (2018) LRRK2 phosphorylation of auxilin mediates synaptic defects in dopaminergic neurons from patients with Parkinson's disease, *PNAS*, **115**(21): 5576-5581.

Law R, Dixon-Salazar T, Jerber J, Cai N, Abbasi A, Zaki M, Mittal K, Gabriel S, Rafiq MA, Khan V, **Nguyen M**, Ali G, Copeland B, Scott E, Vasli N, Mikhailov A, Khan MN, Andrade D, Ayaz M, Ansar M, Ayub M, Vincent J, Gleeson J (2014). Biallelic truncating mutations in FMN2, encoding the actin-regulatory protein formin 2, causes nonsyndromic autosomal-recessive intellectual disability. *American Journal of Human Genetics*, **95**(6): 721-728.